Novel Biopsy Needle and Assisted Robotic System Design for Prostate Biopsy Procedure under MRI

by

Davut Ibrahim Mahcicek

BSc, Electrical and Electronics Engineering, Bilkent University, 2007

MSc, Biomedical Engineering, Swiss Federal Institute of Technology, ETH-Zurich, 2009

Submitted to the Institute of Biomedical Engineering
in partial fulfillment of the requirements
for the degree of
Doctor
of
Philosophy

Boğaziçi University
2021

ACKNOWLEDGMENTS

I would like to express my sincere gratitude and appreciation to my thesis advisor Prof. Özgür Kocatürk for his continuous support and guidance during my PhD study. Without his support I would not be able to finalize this thesis and probably gave up at early stages of my study. There is no way for me to thank enough for his positive attitude, his solution oriented thinking and backing up against all kind of challenges that I faced in this journey.

I would like to thank Prof. Can Yucesoy and Prof. Cengizhan Ozturk for their rich discussions, valuable comments and guidance as a member of my thesis committee. Thanks to their contribution our study has been steered in the right way and reached to the desired target.

I would like to send my special thanks to Ahmet Turan Talas, my dear Ahmet Abi, for his endless support, guidance and his brotherhood during my thesis. His excellence and creativity in technical processes paved the way for overcoming challenging technical tasks and brought fantastic results.

I used to owe a happy life, an adorable son to my dear wife, Senem, and now I also owe a PhD degree. In this journey, she never let me down under difficult circumstances and she kept motivating me. Her mentorship and expert touches eased the way to reach this important milestone in my life. Thanks to this I recognised how lucky is her own students are.

Lastly, I would like express my sincere gratitude to my father and mother. I felt their support and encouragement at every stage.

ACADEMIC ETHICS AND INTEGRITY STATEMENT

I, Davut Ibrahim Mahcicek, hereby certify that I am aware of the Academic Ethics and Integrity Policy issued by the Council of Higher Education (YÖK) and I fully acknowledge all the consequences due to its violation by plagiarism or any other way.

Name : Signature:

Date:

ABSTRACT

Novel Biopsy Needle and Assisted Robotic System Design for Prostate Biopsy Procedure under MRI

Prostate cancer (PCa) is one of the most common cancer type among men. The mortality rate for prostate cancer is significantly high compared to other common cancer types which makes it even more concerning for elderly males. For this reason the early and accurate diagnosis of PCa is vital to avoid deaths caused by PCa. In clinical practice, PCa is diagnosed with ultrasound guided biopsy procedure (TRUS-guided biopsy) after observing signs of PCa with different pre-screening methods. However, diagnosing PCa with the TRUS-guided prostate biopsy is controversial mainly because US imaging is not able to provide contrast difference between healthy tissue and lesion. For this reason, biopsy samples are taken statistically from different regions of the prostate. On the other hand, magnetic resonance imaging (MRI) can help to distinguish lesions from healthy tissues. Therefore, the optimal way to perform prostate biopsy is to perform it under MRI guidance in order to eliminate accuracy concerns. In this thesis, a novel hydraulic needle delivery system that is designed for performing MRI-guided prostate biopsy procedure is proposed. The needle delivery system is composed of the main robotic unit, control unit, hydraulic actuator, biopsy gun and biopsy needle. All of these components were designed, manufactured and assembled in the scope of this thesis. The feasibility of the overall system was evaluated through in-vitro phantom experiments under an MRI guidance. The in vitro experiments performed using a certified prostate phantom (incorporating MRI visible lesions). MRI experiments showed that overall hydraulic biopsy needle delivery system has excellent MRI compatibility (SNR Loss $< 3\%$), provides acceptable targeting accuracy (average 2.05 ± 0.46 mm) and procedure time (average 40 minutes).

Keywords: Image Guided Intervention, Minimally Invasive Devices, MRI compatible robotics, Prostate Biopsy, Hydraulic Actuation, Biopsy Needle.

ÖZET

MRG Altında Prostat Biyopsi İşlemi için Yenilikçi Biyopsi İğnesi ve Yardımcı Robotik Sistem Tasarımı

Prostat kanseri, erkekler arasında en sık görülen kanser türlerinden biridir. Prostat kanseri için ölüm oranı, diğer yaygın kanser türlerine kıyasla önemli ölçüde yüksektir ve bu durum prostat kanserini yaşlı erkekler için daha da önemli hale getirmektedir. Bu nedenle prostat kanserinin neden olduğu ölümleri önlemek için prostat kanserinin erken ve doğru teşhisi hayati önem şımaktadır. Klinik pratikte prostat kanserine, farklı ön tarama yöntemleri ile prostat kanseri belirtileri gözlemlendikten sonra ultrason eşliğinde biyopsi prosedürü (TRUS kılavuzluğunda biyopsi) ile teşhis konulur. Bununla birlikte, TRUS kılavuzluğunda prostat biyopsisi ile prostat kanseri teşhisi, esas olarak ultrason görüntülemesinin sağlıklı doku ve lezyon arasında kontrast farkı sağlayamaması nedeniyle tartışmalıdır. Bu nedenle prostatın farklı bölgelerinden istatistiksel olarak biyopsi örnekleri alınır.Öte yandan, manyetik rezonans görüntüleme (MRG), lezyonları sağlıklı dokulardan ayırt etmeye yardımcı olabilir. Bu nedenle, bu tür endişeleri ortadan kaldırmak için prostat biyopsisi yapmanın en uygun yolu, MRG rehberliğinde yapmaktır. Bu tezde, transperineal yaklaşımla MRG eşliğinde prostat biyopsisi işlemini gerçekleştirmek için tasarlanmış yeni bir hidrolik iğne iletim sistemi önerilmiştir. İğne iletim sistemi, ana robotik ünite, kontrol ünitesi, hidrolik aktüatör, biyopsi tabancası ve biyopsi iğnesinden oluşur. Bu bileşenlerin tamamı bu tez kapsamında tasarlanmış, üretilmiş ve montajı yapılmıştır. Tasarlanan sistemin fizibilitesi, MRG rehberliği altında in vitro fantom deneyleriyle değerlendirilmiştir. Gerçekleştirilen in vitro MRG deneyleri hidrolik biyopsi iğnesi iletim sisteminin mükemmel MRI uyumluluğuna (SNR Kaybı $< 3\%$), yeteri derecede güvenilir hedefleme doğruluğuna (ortalama 2.05 ± 0.46 mm) ve kabul edilebilir işlem süresine (ortalama 40 dakika) sahip olduğunu göstermiştir.

Keywords: Görüntü Kılavuzlu Müdahale, Minimal İnvaziv Cihazlar, MRG uyumlu robotik, Prostat Biyopsisi, Hidrolik Aktüatör, Biyopsi İğnesi.

TABLE OF CONTENTS

LIST OF FIGURES

LIST OF TABLES

LIST OF SYMBOLS

Fe_2O_3	Iron Oxide
R_1	First rotation axis
R_2	Second rotation axis
L	Insertion axis

LIST OF ABBREVIATIONS

PCa	Prostate Cancer
MRI	Magnetic Resonance Imaging
PSA	Prostate Specific Antigen
DRE	Digital Rectal Examination
DCE	Dynamic Contrast Enhancement
DWI	Diffusion Weighted Imaging
MD	Mean Diffusion
FA	Fractional Anisotropy
ADC	Apparent Diffusion Coefficient
RF	Radio Frequency
DOF	Degree Of Freedom
SNR	Signal to Noise Ratio
ABS	Acrylonitrile Butadiene Styrene
MRS	Magnetic Resonance Spectroscopy
Nd:YAG	YAG neodymium-doped Yttrium Aluminum Garnet
PVD	Physical Vapor Deposition
SE	Spin Echo
PDW	Proton Density Weighted
T1	T1 Weighted
T2	T2 Weighted
GRE	Gradient Echo
SSFP	Steady-state free precession
GRASS	Gradient Recalled Acquisition in Steady State
FISP	Fast Imaging with Steady state Precession
FLASH	Fast Low Angle Shot
IR	Inversion Recovery
STIR	Short Tau Inversion Recovery
FLAIR	Fluid-Attenuated Inversion Recovery

DIR	Double Inversion Recovery
DWI	Diffusion Weighted Imaging
ADC	Apparent Diffusion Coefficient
DT	Diffusion Tensor
PWI	Perfusion Weighted Imaging
DSC	Dynamic Susceptibility Contrast
DCE	Dynamic contrast enhanced
fMRI	Functional MRI
MRA	Magnetic Resonance Angiography
TOF	Time-of-Flight
SWI	Susceptibility Weighted Imaging

1. INTRODUCTION

1.1 Prostate Cancer

The prostate is a small gland that is located at the base of the bladder and encircles the water pipe (urethra) that transports urine from the bladder to the penis. The prostate gland's function is to produce substances that aid in the passage of sperm. In young men, the prostate gland is about the size of a walnut. However, it may grow larger as you age, and for most men, this is a completely harmless process. Prostate cancer (PCa) affects a moderate percentage of men.

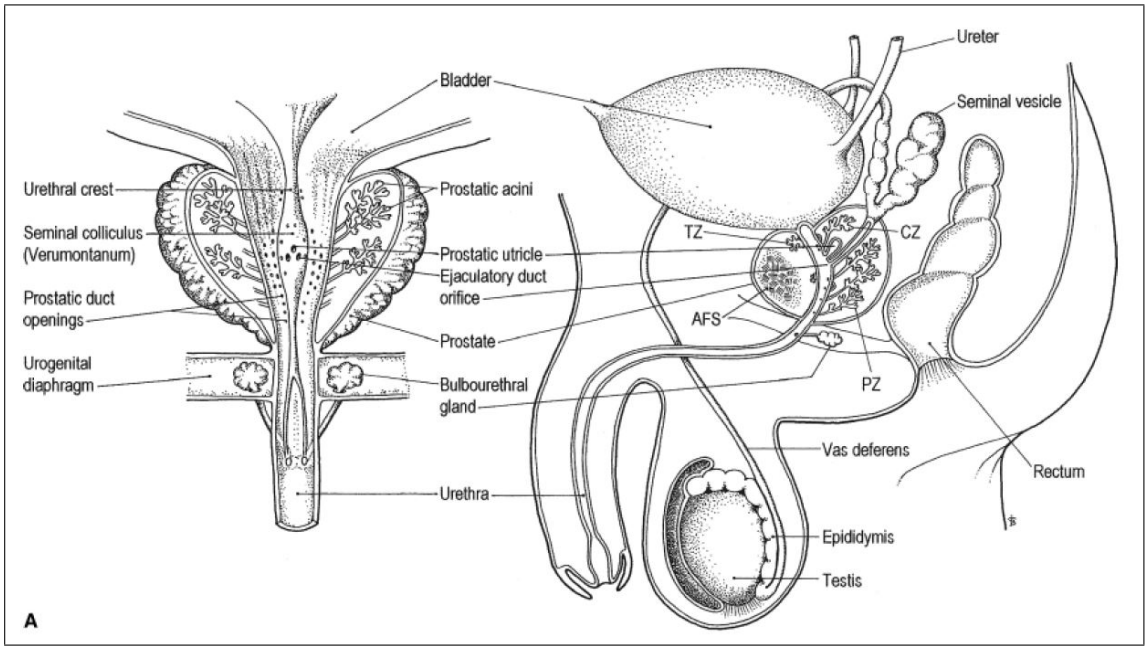

Figure 1.1 Anatomy of Prostate [1]

Prostate cancer (PCa) is one of the most common cancer type among men. In 2020, approximately 1.4 million new PCa diagnose and more than 375.000 deaths due to PCa were reported globally [25]. With these figures PCa is the second most common cancer type and fifth highest cause of cancer death among men. The diagnosis of PCa

is possible with pathological examination after obtaining biopsy samples. The biopsy procedure is performed after screening the elevated prostate-specific antigen (PSA) level or after getting abnormal digital rectal examination (DRE)results [26]. However, PSA show rather low specificity (37%) [27] and DRE is an insensitive examination (36%) [28] for PCa detection.

1.2 Methods to Perform Prostate Biopsy Procedure

1.2.1 Transrectal Ultrasound Guided Prostate Biopsy

In clinical practice, the most common prostate biopsy procedure is transrectal ultrasound (TRUS)-biopsy procedure. The first TRUS prostate biopsy procedure was proposed by Takahashi et. al after the introduction of US imaging technologies in clinical applications [29]. Although, at early stages the image qualities were poor but with the advancements in US imaging technologies the efficacy of the TRUS biopsy was improved significantly. For instance, with US imaging the detection of small tissues was not straightforward and image resolution was poor in early days but advanced features such as color, power Doppler, contrast-enhancement, harmonic and flash replenishment imaging, and elastography helped to detect the cancer in early stages [30]. As a result of these enhancements, in clinical routine TRUS-biopsy became as the most preferred biopsy procedure to diagnose PCa [31].

It is estimated that annually over 1 million TRUS-biopsy operations are performed in the USA and the European Union [32]. Although the TRUS-biopsy procedure is the current gold standard for prostate cancer diagnosis, it has some drawbacks and limitations from patient and clinician standpoint. For instance, with the TRUS biopsy 23% false-negative results [33] and a minimum detection rate of 33.3% [34] were reported which show that the reliability of TRUS-biopsy is questionable. In clinics, the TRUS-biopsy is performed by taking 10-12 biopsy samples from statistically-defined regions without leveraging visual guidance about location of the target tissue. The statistical approach causes inherent sampling errors. Therefore, cancer detection accuracy is

controversial because of the variations of the size and location of the target tissues. Furthermore, TRUS-biopsy is an uncomfortable procedure for the patients due to its nature and taking large number of samples (e.g. 10-12 samples) results in prolonged procedure time. Besides, TRUS-biopsy is an invasive procedure and carries high risk of infection due to the contamination of biopsy needles during multiple transrectal insertions. Therefore, taking large number of samples during prostate biopsy is not desirable.

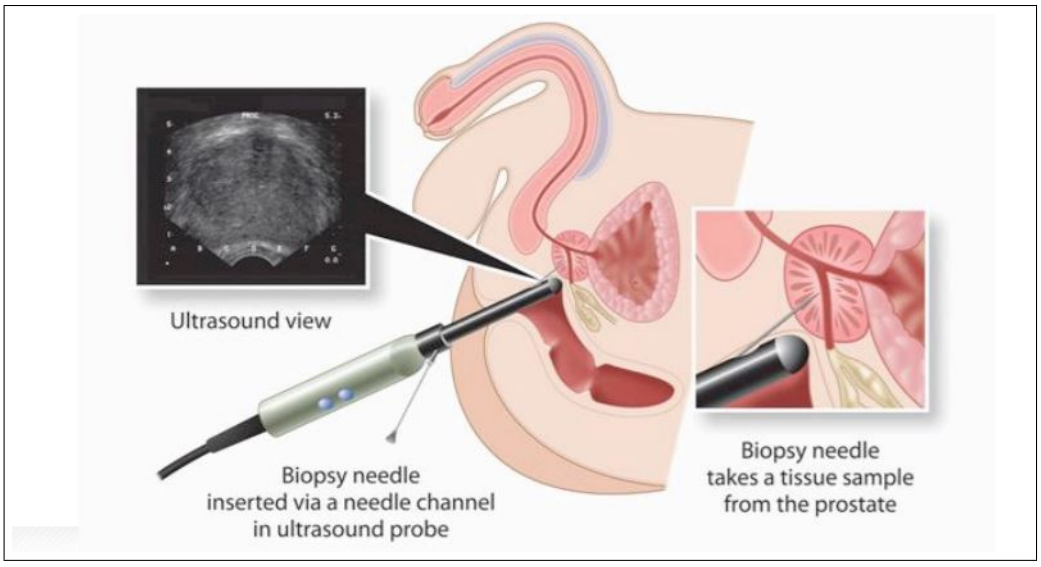

Figure 1.2 Illustration of TRUS Biopsy Procedure

1.2.2 MRI-Fused and TRUS Guided Prostate Biopsy Procedure

Prostate biopsy is the only standardized biopsy procedure which does not utilize any visual information prior to the biopsy procedure as a guidance. Recent studies report that Magnetic Resonance Imaging (MRI) fused TRUS-biopsy increased PCa detection rate by 32% compared to the traditional TRUS-biopsy [35]. In this procedure, MRI images of the prostate are obtained prior to the biopsy procedure. After obtaining the MRI images target locations are defined and with advanced tools the MRI images are registered to the US images during the procedure. In this way the biopsy samples are taken from pre-defined target locations with certain accuracy [36].

Additionally, registration of MRI images with US images resulted in reduction of the total number of biopsy samples. It was shown that reducing the number of biopsy samples during prostate biopsy procedure reduces the number of low-risk cancer diagnosis [36] and also minimize patient discomfort and risk of infection. Although the MRI-fused TRUS-biopsy decreases the number of unnecessary prostate biopsies and improves the reliability of the biopsy procedure, real-time images are limited by the TRUS technology which bring inadequate resolution and soft tissue contrast during the procedure. Additionally, the registration of MRI images with US images is usually complicated, time consuming [35] and require expensive devices. Therefore, a better solution to improve the diagnostic quality of the prostate biopsy to perform the biopsy procedure under MRI guidance.

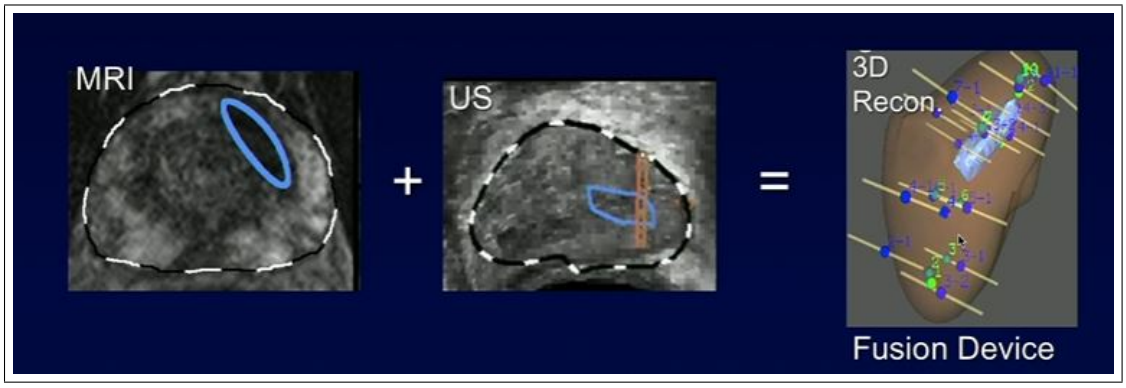

Figure 1.3 MR/US Image Fusion for Targeted Biopsy

1.2.3 Prostate Biopsy Procedure Under MRI

1.2.3.1 Prostate Cancer Imaging with Magnetic Resonance. MRI is a non-invasive imaging modality that employs the absorption and emission of radio frequency energy as well as the systematic manipulation of magnetic fields along three axes. The basic principle is leveraging the interaction of nuclear spins (usually from water and fat) with the externally applied magnetic fields and measuring the various impacts of external magnetic fields on nuclear spins. MRI offers multi-dimensional images from multiple planes and without the necessity of repositioning the object.

In MRI the signal to noise (SNR) depends on various factors such nuclear spin density, size and location of the target object. Prostate is rather located in the center of the body and it is small in size (means less nuclear spins) which result in limited SNR for conventional imaging. Furthermore, it is encased in a lipid pool. Given the prevalence of PCa in the peripheral zone [37], additional precautions must be taken to avoid the negative consequences of chemical shift interference, particularly for vulnerable modalities like magnetic resonance spectroscopy (MRS). Several solutions have been developed to address these issues. Combining phased array coils with endorectal coils is a typical approach for increasing SNR to acceptable levels. It has been shown that this solution offers better detection of PCa with DWI technique [38].

T2 weighted imaging is a fundamental MRI sequence which is based on T2 relaxation differences between different tissues. The degree of difference between healthy and diseased tissue is a limiting factor in detecting tumorous tissue in the prostate. T2 weighted images have been found to have limited accuracy for this purpose because the characteristics of malignant prostate tissue can be confused with those of other disorders [39]. It has been shown that the performance of DWI in detection of PCa is more reliable than that of T2 weighted images. T2 weighted imaging, on the other hand, is still used in prostate imaging methods because of its capacity to offer high-resolution morphological anatomy. Standard T1 and T2 weighted sequences and additional functional parameters such as dynamic contrast enhancement (DCE), diffusion-weighted imaging (DWI) may be used to determine high-risk regions for PCa [26]-[36].

In DWI the contrast is obtained from the microscopic movements of water molecules in certain directions. Diffusion generating gradients are applied in several directions and the diffusion properties of each voxel are modeled as a tensor [40]. Various parameters, such as mean diffusion (MD), fractional anisotropy (FA) and apparent diffusion coefficient (ADC) maps, are derived using these tensors [41]. In peripheral PCa, DWI has been reported to be efficient way in distinguishing malign tissues [38]-[42].

DCE imaging is a type of magnetic resonance imaging (MRI) technology that uses contrast chemicals to better define malignancies and vascular networks [53]. Image reconstruction takes advantage that dynamic changes are observed only in a specific parts of the data, allowing for quick and efficient collections. DCE has been reported to be an effective technique for the detection and grading of early PCa [43].

To summarize, MRI is an advanced imaging tool for reliable diagnosis and grading of PCa because to its excellent soft tissue contrasts, high spatial resolution, non-ionizing radiation, non-invasive nature and flexible target localization to capture images in multiple planes.

Table 1.1: MRI Sequences

Sequence Group	Sequence Type	Physics	Clinical Features	Example Image
Spin Echo (SE)	T1 Weighted (T1)	In T1 Weighted imaging short TR and TE are used. T1 sequence relies on the relaxation of the longitudinal relaxation (spin-lattice) of the tissueâs magnetization	-Fat produces high signal and appears bright in MR images. -Water produces low signal and appears dark in MRI images. -Contrast agents and paramagnetic materials produce high signal and appears bright. -Muscle produces intermediate signal intensity. -Brain white matter produces intermediate signal intensity and grey matter produces hyper-intense signal intensity.	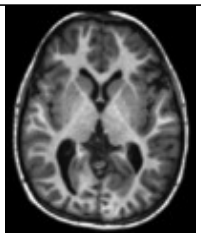

Continued on next page

continued from previous page

Sequence Group	Sequence Type	Physics	Clinical Features	Example Image
Spin Echo (SE)	T2 weighted (T2)	In T2 Weighed imaging long TR and TE are used to measure transverse (spin-spin) relaxation.	-Water produces high signal and appears bright in MRI images. -Fat produces low-intermediate signal intensity in conventional Spin Echo (SE). However, it produces high signal in advanced sequences like Turbo Spin Echo (TSE) and Fast Spin Echo (FSE) and appears bright in MR images. -Contrast agents and paramagnetic materials produce low signal intensity. -Muscle produces intermediate signal intensity. - Brain white matter produces hypo-intense signal intensity, grey matter produces intermediate signal intensity.	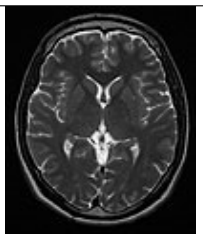

Continued on next page

continued from previous page

Sequence Group	Sequence Type	Physics	Clinical Features	Example Image
Spin Echo (SE)	Proton density weighted (PD)	In PD Weighed imaging long TR and short TE are used to measure proton density.	-PD weighted sequences used to be preferred for brain imaging but replaced by other modern imaging sequences. PD sequences offer good contrast difference between fluid and hyaline/fibro cartilage which makes PD sequences ideal in the imaging of joints. -Water produces high signal and appears bright in MRI images. -Fat produces high signal intensity -Muscle produces intermediate signal intensity. -Hyaline cartilage produces intermediate signal intensity. -Fibrocartilage produces low signal intensity.	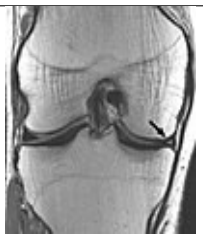
Gradient Echo (GRE)	Steady-state free precession (SSFP)	In SSFP imaging transverse magnetization is maintained between successive cycles.	This sequence is mainly used assessment of dynamic cardiac functions.	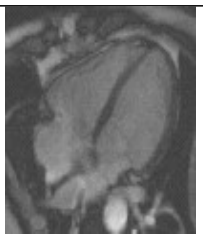

Continued on next page

continued from previous page

Sequence Group	Sequence Type	Physics	Clinical Features	Example Image
Gradient Echo (GRE)		-T2* -Gradient Recalled Acquisition in Steady State GRASS -Fast Imaging with Steady state Precession (FISP) -Fast Low Angle Shot (FLASH)	GRASS and FISP offer less image contrast compared to FLASH. GRASS and FISP and are ideal when there is no time limitation for acquisition and can offer better SNR compared to FLASH with short TR times.	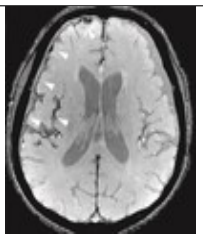
Inversion Recovery (IR)	Short tau inversion recovery (STIR)	STIR sequence is used to suppress fat in MR images.	Initially, Inversion Recovery sequences are developed to obtain T1 weighted images. In current practice they are used to suppress certain type of material. (e.g. fat, fluid etc.). In order to distinguish different tissues, the T1s should be different. Materials that are shortening T1 (e.g. gadolinium) cannot be used with STIR.	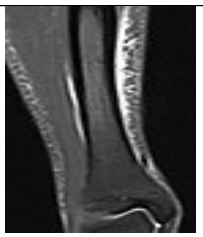
Inversion Recovery (IR)	Fluid-attenuated inversion recovery (FLAIR)	FLAIR sequence is used to suppress fluid in MR images.	FLAIR sequence is particularly used for brain imaging. It has been tested for various studies for central nervous system (CNS) diseases such as: multiple sclerosis, subarachnoid hemorrhage, infarction and head injuries.	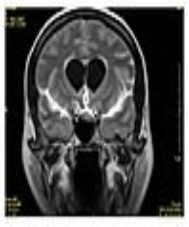

Continued on next page

continued from previous page

Sequence Group	Sequence Type	Physics	Clinical Features	Example Image
Inversion Recovery (IR)	Double inversion recovery (DIR)	DIR sequence is used to suppress fluid in MR images.	Double Inversion Recovery sequence is mainly used for neuro-imaging and cardiovascular imaging.	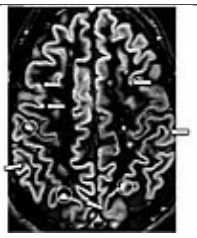
Diffusion Weighted Imaging (DWI)	Conventional	DWI sequence is used to measure diffusion of water and diffusion characteristic of tissues.	DWI sequence is used for various clinical needs such as: Early identification of cerebral infarction, chronic vs acute stroke differentiation.	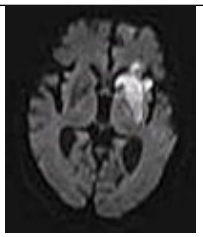
Diffusion Weighted Imaging (DWI)	Apparent diffusion coefficient (ADC)	ADC is a measure of water diffusion and it is used to determine abnormal diffusion restricted tissues.	ADC sequence has similar use cases with conventional DWI.	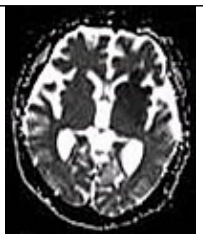
Diffusion Weighted Imaging (DWI)	Diffusion tensor (DT)	The diffusivity of water molecules differs between tissues and axon fascicles in favor of axon fascicles. This is measured to determine axonal organization.	DT sequence is mainly used for diagnosis of CNS diseases such as alzheimer, schizophrenia or white matte deformation due to tumors.	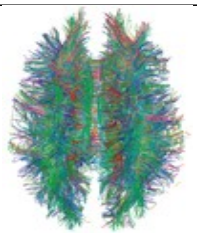
Perfusion Weighted Imaging (PWI)	Dynamic susceptibility contrast (DSC)	DSC sequence is based on the susceptibility related signal loss to due contrast agent injection.	With PWI color coded images can be created to assess the perfusion of the tissues.	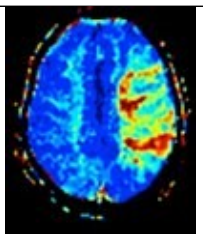

Continued on next page

continued from previous page

Sequence Group	Sequence Type	Physics	Clinical Features	Example Image
Perfusion Weighted Imaging (PWI)	Dynamic contrast enhanced (DCE)	DCE sequence is used to calculate perfusion related parameters by measuring the contrast agent related T1 shortening.	With PWI color coded images can be created to assess the perfusion of the tissues.	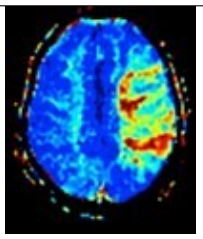
Functional MRI (fMRI)	Functional MRI (fMRI)	fMRI sequence relies on changes in blood flow in response to actions or stimuli.	fMRI provides functional information by assessing the activity of cortex.	
Magnetic resonance angiography (MRA)	Time-of-flight (TOF)	TOF sequences are used to detect flow within vessels leveraging the enhancement of spins that are entering into the slice.	MRA is used to detect vascular structures from any part of human body. It is used an replacement of conventional or CT angiography and avoids ionizing radiation.	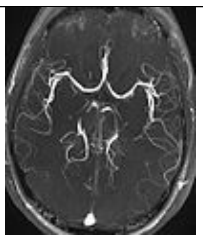
Susceptibility-weighted Imaging (SWI)	Susceptibility-weighted Imaging (SWI)	SWI sequence leverages the particles that distort the main magnetic field.	SWI is mainly used to determine calcium or hemorrhage that is not visible with other MRI sequences.	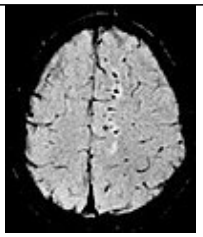

1.2.3.2 Challenges for MRI Guided Applications . Although, MRI is an excellent imaging tool for the diagnosis of several diseases lately it has been used as a part of a therapy tool during some interventional procedures [44]-[45]-[46]. However, performing interventional procedures under MRI is usually not straightforward because the MRI environment brings some technical limitations such as:

a.) The high-frequency and high-power magnetic field (RF field) may couple with the conductive materials and generate inductive surface current which may cause excessive heating and serious burns if get in contact with the patients. It has been reported that the temperature increase might be up 34at the tip of the conductive wire which shows that RF heating should be considered as a big safety threat for such MRI applications [47]. Besides, such eddy currents may degrade the image SNR significantly.
b.) Ferromagnetic materials such as iron, cobalt and nickel that disturb the homogeneity of the static magnetic field may degrade the MRI signal and image quality. Therefore, such material should be avoided in the close proximity of MRI bore.
c.) In order to use conventional electronic devices within MRI environment proper sealing of these devices against electromagnetic interference is required even if these devices are made of MRI-Conditional or MRI-Compatible materials. Otherwise, the electronic devices may couple electromagnetic field induced current and as as result may fail to function or do not function as expected. Therefore, the number of electromagnetic devices that can be used inside the MRI room is very limited and specially designed and sealed devices must be designed for MRI applications.
d.) The physical dimensions of the MRI instrument also bring a challenge for the clinicians. In clinical practice the MRI bores are usually 60 cm 70 cm in diameter which does not leave sufficient space to insert and manipulate therapy tools. Therefore, it is not easy for clinicians to navigate the biopsy needle while patients are lying inside the MRI bore [48]. This is a serious limitation on the activities of clinicians which brings necessity for the MRI-compatible biopsy needle and delivery systems for the clinical procedures.

1.2.3.3 Biopsy Needle Visualization Under MRI . MRI-visibility of interventional tools is still in important topic for researchers. In order to track interventional procedures in real time under MRI specially designed tools are required. These tools should be designed such that they should be able to create sufficient signal to track the pose and position of the devices under MRI but at the same time should not distort the anatomical signals and images significantly. There are different approaches to ensure

MRI-visibility of the tools. Some of these approaches are usually less complicated but offer reduce tracking precision and some approaches require complex hardware but can offer high precision tracking. The tracking methods can be grouped as follows:

1. Encoder Tracking

   In this tracking method, encoders are used to monitor the movements of the individual components (e.g. needle, robot arms etc.) of the robotic system [49]-[50]-[51]. The movements are tracked by the encoders that are placed on the robotic system's joints. In this way any movement in each joint is captured by the encoders and the exact position of each arm can be calculated. In this method, the robotic system should be anchored to the MRI scanner table with rigid mounting elements and the system should be calibrated with respect to the MRI scannerâs coordinate system before each procedure.

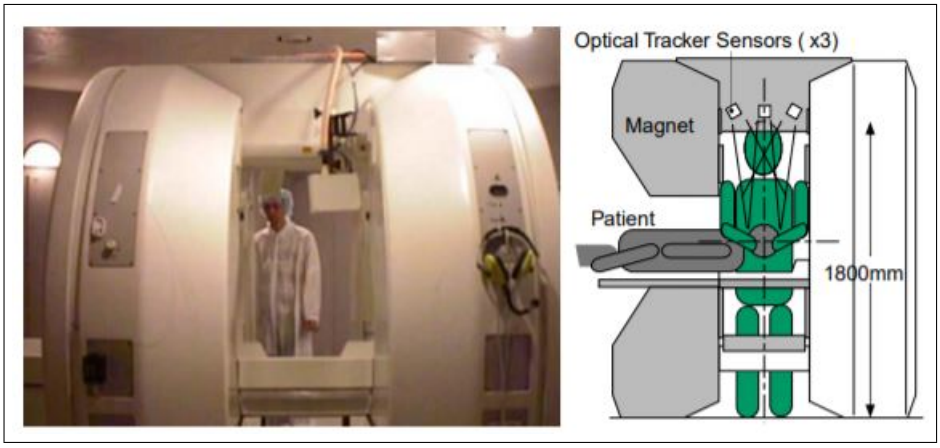

Figure 1.4 The intraoperative MR scanner and the sensors of the tracking device [2]

2. Passive Tracking

   In this tracking method, the exact posture and position of the robotic system's components are determined by imaging the passive markers under MRI. The passive markers are placed within the robotic systemâs components using specially designed holes or structures. Susil et al. proposed a prostate brachytherapy device to operate under MRI [52]-[3]. The holes within the device were filled with contrast material and the system was imaged under MRI before the procedure

using conventional T1 or T2 weighted images. As a contrast material a surgical lubricant (Surgilube, NY, USA) was chosen to provide high strength MRI signal with T1=1850 ms and T2=240 ms and to ease insertion of the catheter. In this study, the contrast materials was measured with SE and FSE sequences. Therefore, contrast material should be chosen from high T1 and high T2 materials in order to obtain bright images with T1 weighted and T2 weighted sequences. As it is seen in figure 1.5 regularly designed patterns are easily seen in the MRI image and can be used to register robotic system with the MR coordinate system. Two holes were used to determine the x coordinate axis and other two were used to determine y coordinate axis. In order to prevent inaccuracies due to the resolution and spacing of the holes, the tracking of the system is supported with the endorectal guide. The endocrectal guide was also covered with a tube (6 cm long and 0.125" diameter tube) which was filled with the same contrast material to enhance MRI visibility. Beyersdorff et al. utilized fiducial markers to track biopsy needle for MRI-guided prostate biopsy procedure [53].

3. Optical Tracking

   In this tracking method, the exact posture and position of the robotic system's components is measured by a tracking system that relies on optical principles. In this approach, there should be optical visibility between the robotic system and optical components (camera etc.) in order to calibrate the robotics systemâs position with the MRI scannerâs coordinate system. In order to track the components of the robotic system there should be optical targets or LEDs fixed to the robotic system. DiMaio et al. proposed an optical tracking system that used to register and track a robotic system with an open MRI scanner [4].

4. Gradient Field Tracking

   In this tracking method, the posture and the position of the robotic system's components is determined by magnetic sensors that are fixed to the robotic system. The magnetic sensors are used to sense the gradient fields of the MRI scanner. Hushek et al. employed a commercially available tracking system, EndoScout (Robin Medical Systems, USA), in an MRI application [54]. In this approach, the magnetic sensors should be positioned close to the isocenter of the

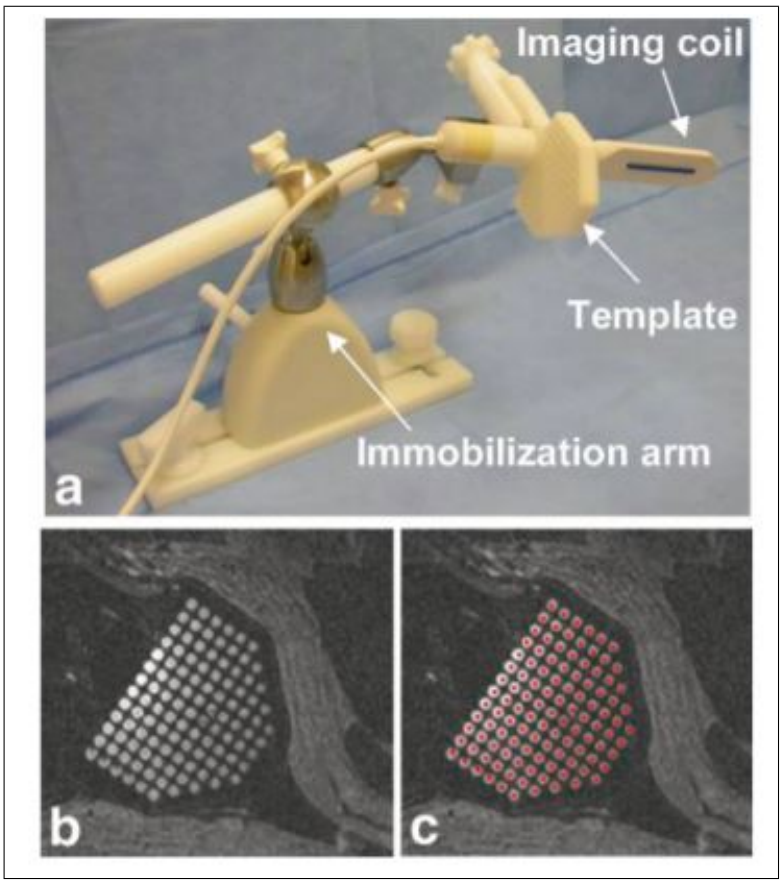

Figure 1.5 Needle placement device. a) The needle-guiding template and endorectal imaging coil. b) The template holes, filled with surgical lubricant, are easily visualized in MR images. c) After registration of the position and orientation of the needle-guiding template. Visualization of the template allows for easy verification of this registration. [3]

MRI scanner's magnet and precise calibration is required should be performed for the entire ROI in each MRI application.

5. Active Tracking with Micro Coils

   In this tracking method, the posture and the position of the robotic system's components is determined by micro coils which are either embedded of surface coated to the robotic system. The micro coils are electronically connected to the MRI scanner to measure signals coming from the micro coils and constructing the MRI images. In this approach customized MRI sequences are used to track these micro coils under MRI. Firstly, the active tracking approach with micro coils is proposed by Dumoilin et al. to track 6-DOF system under MRI [55]. Yildirim et al. proposed a novel method to surface coat needles and robotic component to create surface micro coils which are used for precise tracking [5].

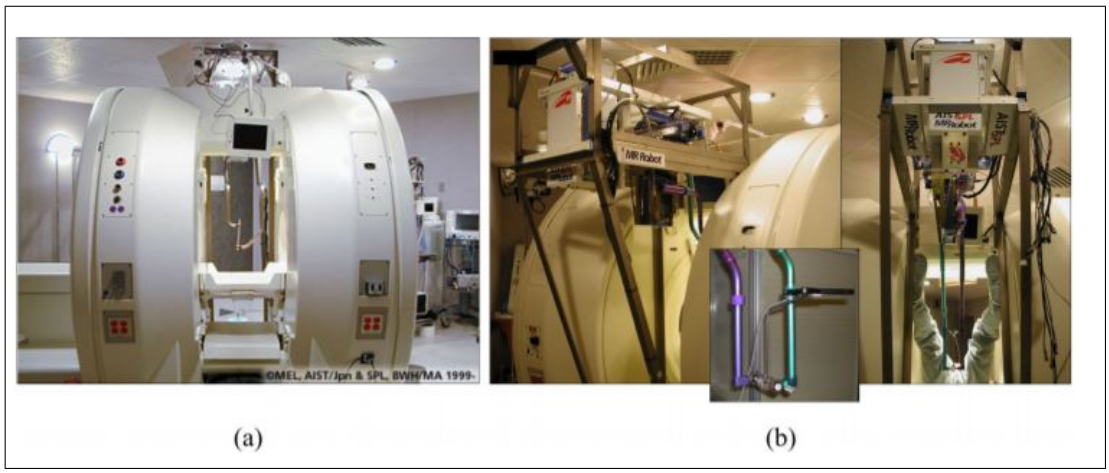

Figure 1.6 a) Open-MRI scanner b) 5-DOF MR-compatible robot which equipped with an optical tracking (inset) [4]

Yaras et al. employed an opto-acoustic coupled active micro coil for real time

Figure 1.7 Surface Coated Active Coils [5]

device tracking under MRI [6]. The opto-acoustic markers helped to reduce the micro coil induced RF heating significantly.

Krieger et al. reported a hybrid tracking method which utilized active and passive tracking approaches in the same design [7]. The active tracking coils are used for imaging and the passive markers are used for real time tracking the device components.

The active tracking method offers accurate and fast tracking without requiring pre-calibration. However, the active tracking requires electronic components to connect micro coils to the MRI scanner and channels dedicated for the micro coils are needed which increase the complexity of the system. Also, customized MRI sequences may limit the clinical deployment since this approach requires special MRI sequences.

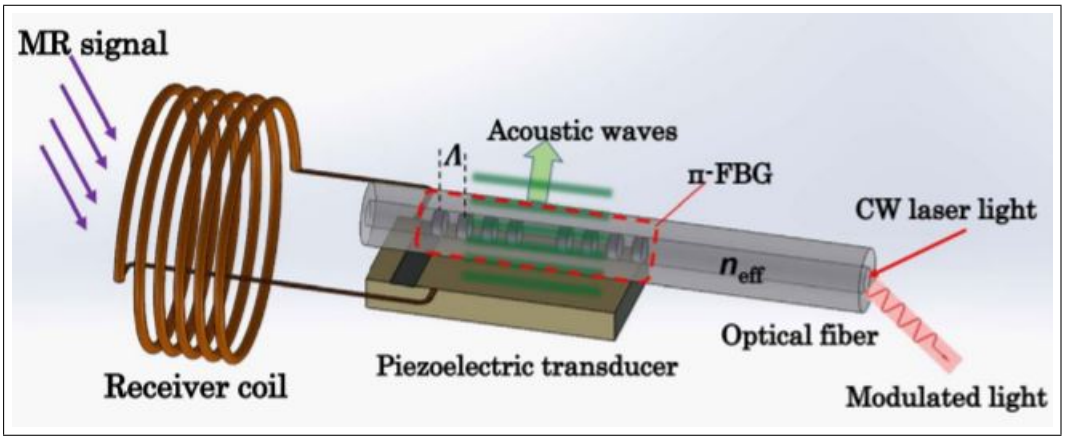

Figure 1.8 Opto-acoustic Active Tracking [6]

Table 1.2: Comparison of Tracking Methods

Tracking Method	Advantages	Disadvantages
Encoder Tracking	-Commercially available tools can be used (e.g optical encoders etc.). -Optical encoders are usually MRI-compatible and do not bring additional issues.	-Requires mechanical stiffness and anchoring mechanism for fixing the robotic system to the MRI scannerâs table. -Precise calibration is required before each procedure with respect to the MRI scannerâs coordinate system.
Passive Tracking	-It is possible to develop customized designs depending on the robotic systemâs design and application. -Easy to implement and does not require expensive tools. -Does not require pre-calibration.	-Requires image based registration and real time image based calculations. -The excitation is less controlled compared to active tracking.
Optical Tracking	-Commercially available optical sensors or LEDs can be used. -Optical components usually do not bring MRI compatibility issues.	-Requires optical visibility within MRI environment which brings additional physical limitations.

Continued on next page

continued from previous page

Tracking Method	Advantages	Disadvantages
Gradient Field Tracking	-Commercially available magnetic sensors can be used. -3D tracking is practical thanks to the 3D magnetic sensors.	-Magnetic sensors might distort the MRI images if not positioned properly. -Precise pre-calibration is required for the whole volume of interest.
Active Tracking	-Offers the best tracking accuracy. -Offers fast tracking for real-time applications. -Does not require pre-calibration. -The excitation is more controlled compared to passive tracking. - Can be combined with other technologies to eliminate RF heating concerns.	-Requires complex processes to produce micro-coils or other tracking technologies. -Might bring RF heating concerns. -Dedicated MRI channels are required for the micro-coils.

1.2.3.4 MRI Compatible Robotic Systems for Prostate Biopsy Procedure.

In order to cope with the limitations of working under MRI, remote controlled MRI-compatible robotic assist devices are proposed for various interventional applications e.g. prostate biopsy and brachytherapy, brain biopsy, breast biopsy and bone biopsy etc. More than 25% of the literature published in the last decade concentrates on prostate biopsy, which makes it the most popular application [56].

Fischer et al. developed a pneumatically actuated prostate biopsy robot with 8 degrees of freedom (DOF) [8]. Custom-made pneumatic cylinders were controlled with precise stepper motors and a transperineal approach was preferred for the biopsy operation.

Elhawary et al. proposed a transrectal robot with 5-DOF control where piezoceramic motors were used to actuate robotic arms [57]. Song et al. reported a pneumatically actuated 4-DOF needle delivery system for prostate biopsy with a transperineal approach [58]. Van den Bosch et al. developed a 5 DOF device where needle insertion was performed with the pneumatic tapping principle [59]. Seifebadi et al., Su et al.

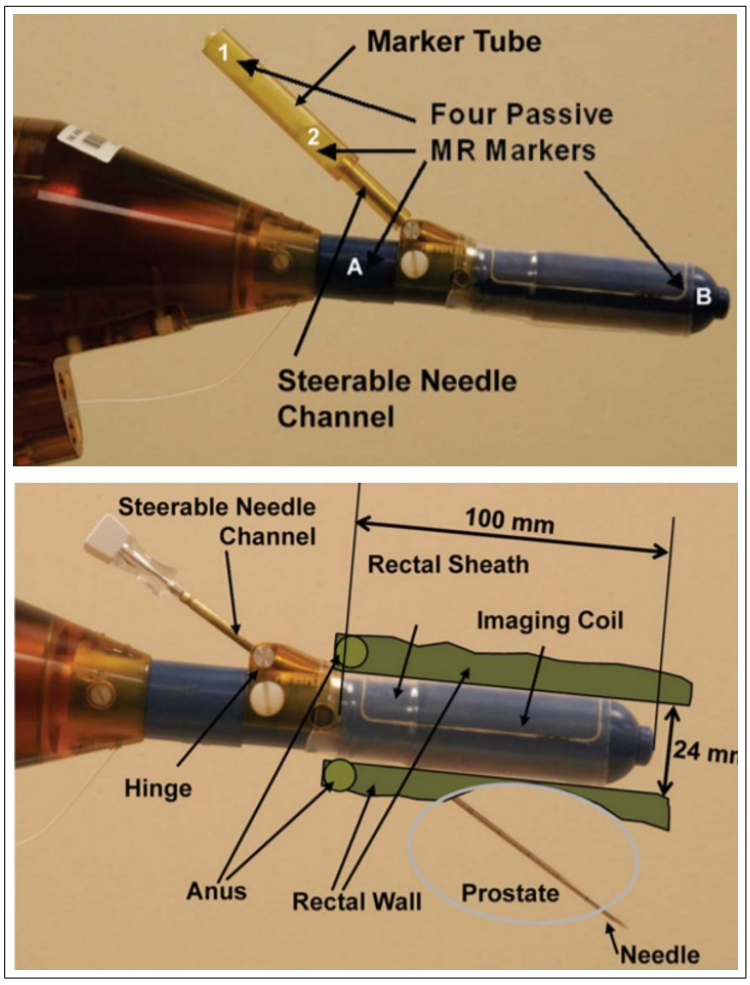

Figure 1.9 Hybrid Tracking Approach [7]

and Eslami et al. proposed a prostate biopsy device with a transperineal approach and preferred piezoelectric motors for remote actuation [9]-[20]-[10].

Yakar et al., reported a pneumatically actuated 5-DOF robotic system where for inserting needle guide and biopsy needle transrectal approach was preferred [60]. A needle delivery design was utilized by Krieger et al. and Stoianovici et al. as a part of a robotic prostate biopsy system where Krieger et al. preferred piezoelectric motors and Stoianovici et al. used custom-made pneumatic motors to actuate robotic arms [12]-[11].

In this design, the endorectal guide and the biopsy needle were designed to be visible under MRI. The biopsy needle and the guide incorporate passive markers to

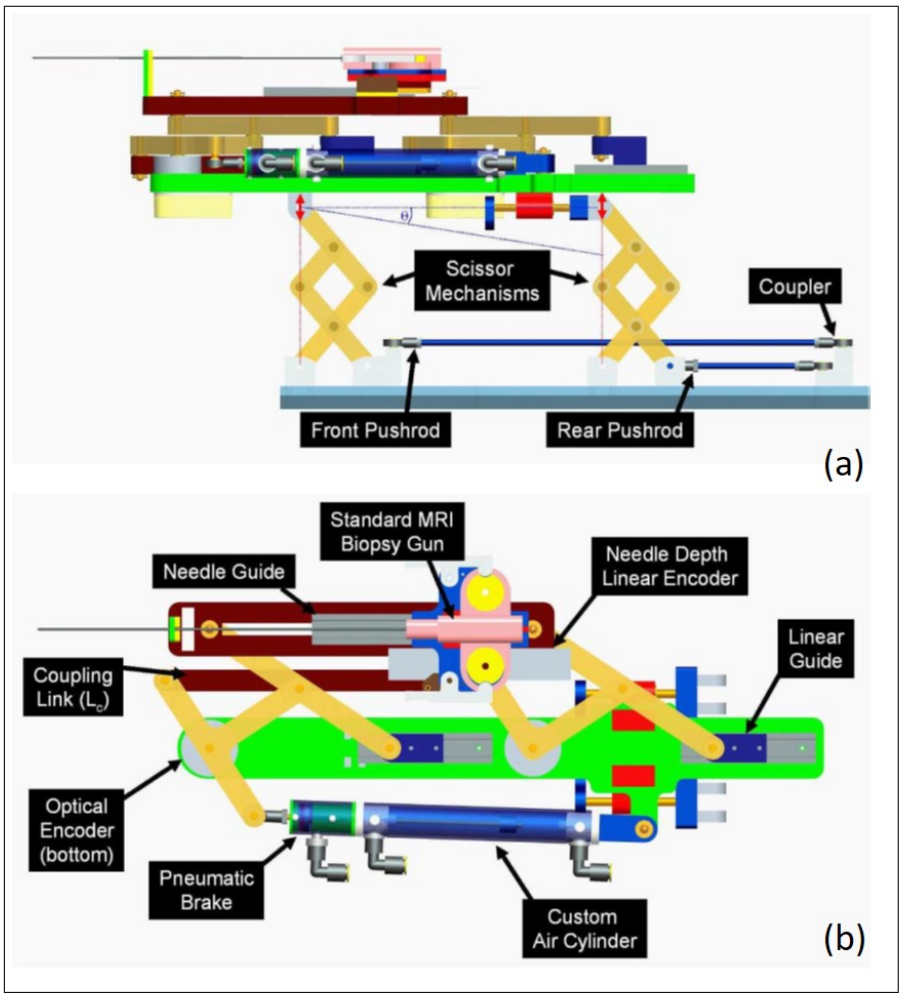

Figure 1.10 Pneumatic Prostate Biopsy Robot a)Horizontal View b) Vertical View [8]

make them visible under MRI guidance. Patel et al. proposed a modular transperineal prostate biopsy system with 4-DOF which were actuated using piezoelectric actuators [13]. The previous MRI-guided prostate biopsy studies were summarized in table 1.3 in terms of number of DOF, actuator type, signal to noise ratio (SNR), targeting accuracy and clinical approach.

There are also commercially available solutions that are designed to perform prostate biopsy procedure under MRI. For instance, Philips Dynatrim Solution (Philips Healthcare, Netherlands) offers a stage for targeted transrectal prostate biopsy. The stage is used to to target the lesions inside the prostate with 3 DOF. However, the adjustment of the stage is done manually with high accuracy adjustment knobs. The solution offers MRI visible transrectal guide which is partially filled with a liquid that is visible under the MRI. In this was, the stage to patient registration is done within the system.

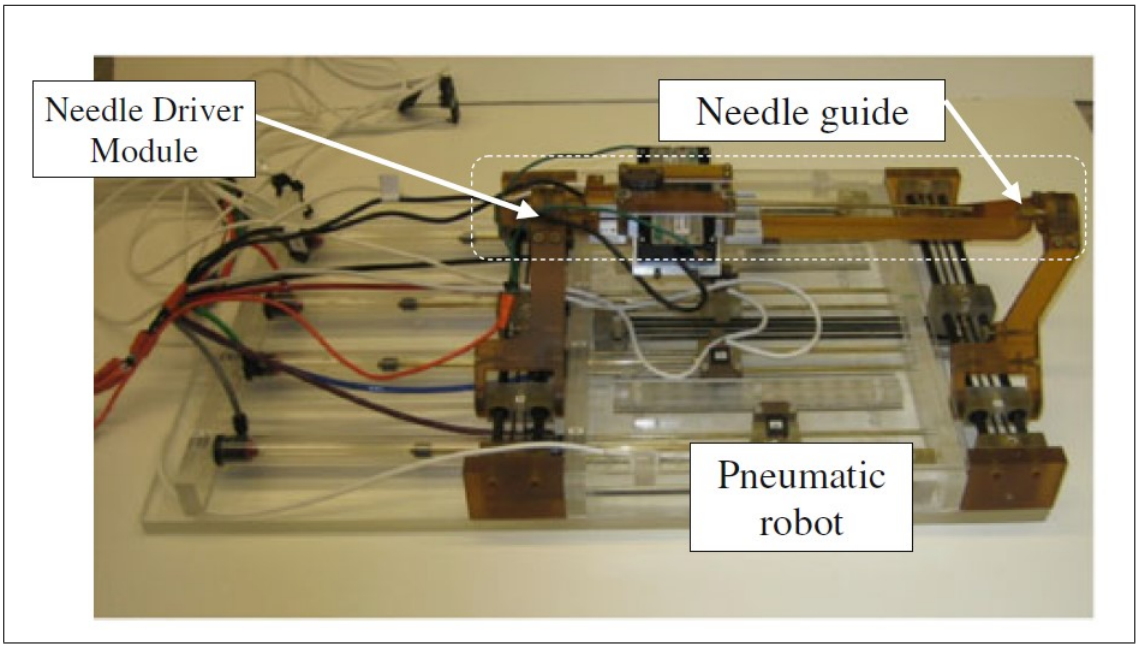

Figure 1.11 Pneumatic Prostate Biopsy Robot [9]

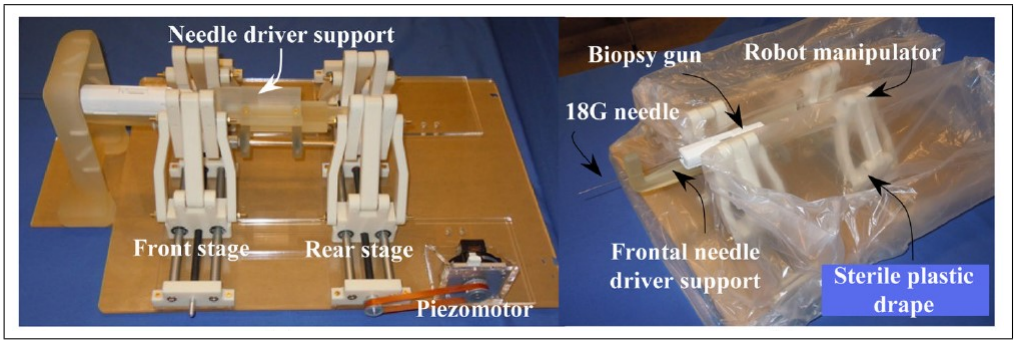

Figure 1.12 Piezoelectric Prostate Biopsy Robot [10]

Besides, the solution offers a navigation tool which can calculate the required manipulation of the DOFs after acquiring the patient image. The system works with standard biopsy guns and nitinol biopsy needles. Therefore, the visibility of the biopsy needle is poor and this bring practical challenges during the procedure.

As shown in table 1.3, in existing literature various actuator types were used to perform prostate biopsy procedure under MRI. However, in none of these studies hydraulic actuators were used. In the proposed design the tele-operated arms are controlled with the custom-made master-slave type hydraulic actuators to isolate the MRI incompatible system components such as stepper motors and controllers from MRI room. The hydraulic actuators helped to minimize RF signal interference and distortions on the

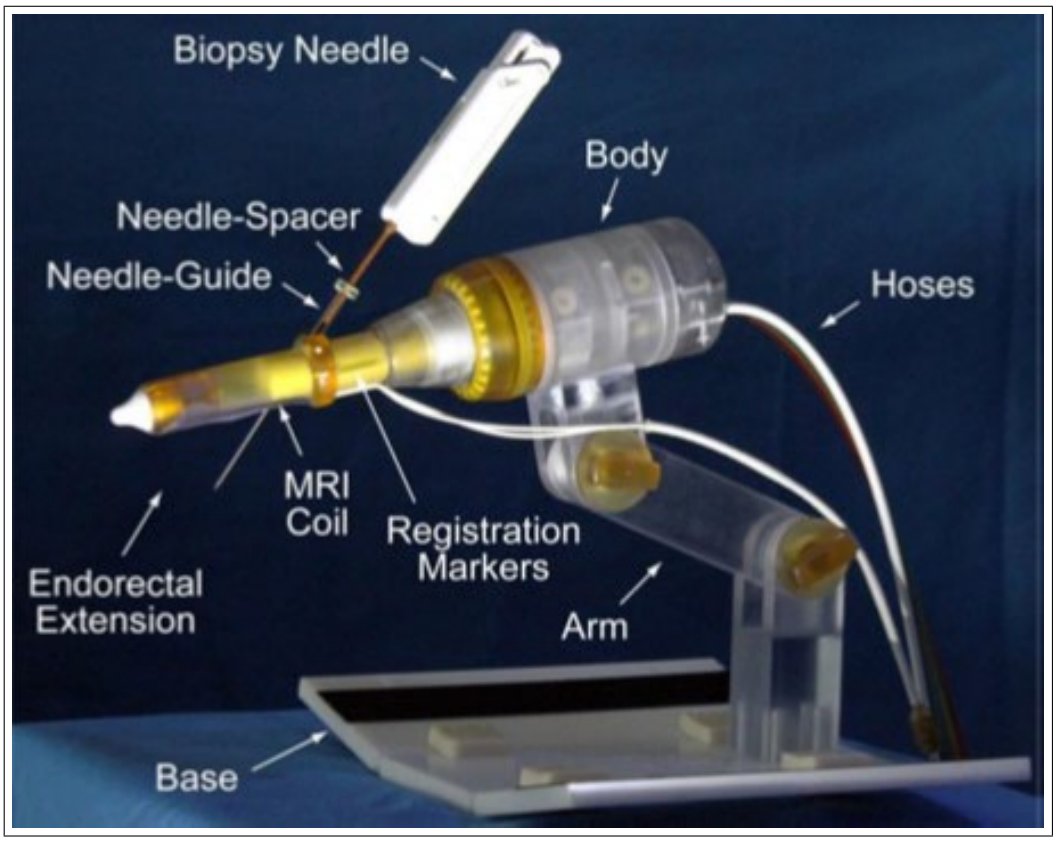

Figure 1.13 Custom-made Pneumatic Prostate Biopsy Robot [11]

MRI images. As seen in table 1.3, the hydraulic actuators offer significant improvement in terms of SNR loss when compared with ultrasonic and piezoelectric actuators, Similarly, our hydraulically-actuated design offers better accuracy compared to pneumatic actuators since pneumatic systems suffer from maintaining acceptable accuracy between cases due to the compressibility of gasses. Furthermore, the proposed design uses rolling diaphragm cylinders against the conventional diaphragm cylinders for driving the biopsy needle which also reduces the complexity of the design and enables a low friction, compact, master-slave type of actuation. As depicted in table 1.3, in most of the previous studies either transrectal or transperineal approach was preferred. The proposed hydraulic based needle delivery system is designed to perform the prostate biopsy procedure using transperineal approach. However, it is supported with a transrectal (endorectal) guide. The endorectal guide is enabled to have a more robust kinematics, since it is used to fix the position of the needle delivery system with respect to the prostate phantom which is mimicking an average patientâs anatomy. Besides, the tip of the endorectal guide is designed to be visible under MRI and it is used

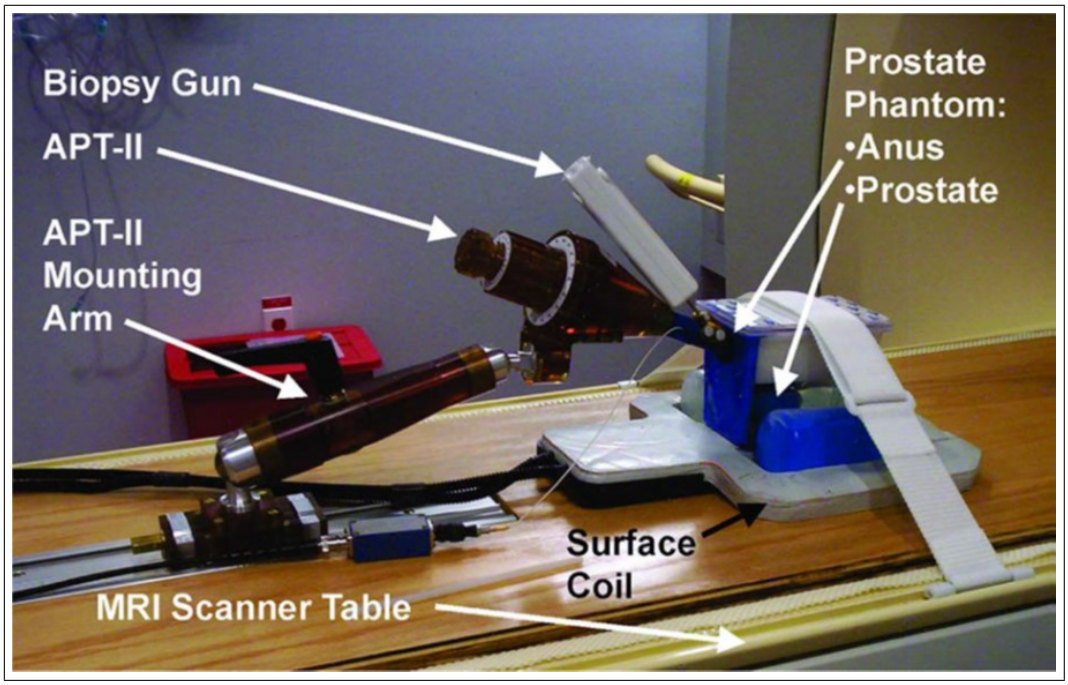

Figure 1.14 Piezoelectric Prostate Biopsy Robot [12]

to register the MRI image with the coordinate system of the needle delivery unit. The prostate biopsy needles are also designed and fabricated using shape memory (medical grade) nitinol tubes in order to have the least amount of deviation from the targeted trajectory during needle-tissue interaction and needle insertion. The biopsy needles incorporated with equidistantly spaced Fe_2O_3 strips to improve the MRI visibility of the needles. The biopsy gun is designed to be MRI compatible and it is enabled for tele-operation with a hydraulic actuator.

Table 1.3: MRI-Guided prostate biopsy applications

Year	Authors	DOF	Actuator Type	SNR Loss	Accuracy	Clinical Design	MRI Visibility
Continued on next page							

continued from previous page

Year	Authors	DOF	Actuator Type	SNR Loss	Accuracy	Clinical Design	MRI Visibility
2008	Fischer et al.[8]	8	Pneumatic Cylinders were used together with Proportional Pressure Regulators	5%	0.94 mm rms per axis measured with phantom studies)	Transperineal	No enhancement for MRI Visibility
2010	Elhawary et al.[57]	5	Piezoceramic Motors and linear slides were used	1.1%	min:1.97 mm, max:2.72 mm, ave:2.3 mm, in phantom	Transrectal	Fiducial markers are inserted for passive tracking and RF Coil is used for active tracking
2010	Van den Bosch et al.[59]	5	Pneumatic tapping	-	-	Transperineal	No enhancement for MRI Visibility
2011	Yakar et al.[60]	5	Pneumatic motors	-	-	Transrectal	No additional enhancement for MRI Visibility
2012	Seifebadi et al.[9]	5	Piezoelectric motors and Pneumatic actuators	-	2.50 mm (in phantom)	Transperineal	No enhancement for MRI Visibility
2011	Su et al.[20]	6	Piezoelectric actuators	No significant signal degradation	-	Transperineal	Fiducial frame for passive tracking

Continued on next page

continued from previous page

Year	Authors	DOF	Actuator Type	SNR Loss	Accuracy	Clinical Design	MRI Visibility
2013	Song et al.[58]	4	Ultrasonic motors	44% and 0.4% with and without motor respectively	ave:0.94 mm (in phantom)	Transperineal	No enhancement for MRI Visibility
2012	Krieger et al.[12]	8	Piezoelectric motors	80% and 40-60% with and without motor respectively	ave: 2.40 mm, max: 3.70 mm (in phantom)	Transperineal with a transrectal guide	Hybrid Tracking
2016	Eslami et al.[10]	4	Piezoelectric motors	6.37%	0.50 mm(in air)	Transperineal	No enhancement for MRI Visibility
2013	Stoianovici et al.[11]	3	Pneumatic motors	No significant SNR Loss	2.09 mm (in phantom), 2.58 mm (animal)	Transperineal with a transrectal guide	Passive markers and Active RF Coil for imaging
2019	Patel et al.[13]	4	Piezoelectric	15.35%	1.5 mm (in phantom), 3.7-4.0 mm (clinical)	Transperineal	No enhancement for MRI visibility

1.3 Actuation Principles for MRI Biopsy Applications

The actuation principles that are used in MRI biopsy applications can be categorized in three main groups from MRI compatibility and patient/medical staff safety standpoint:

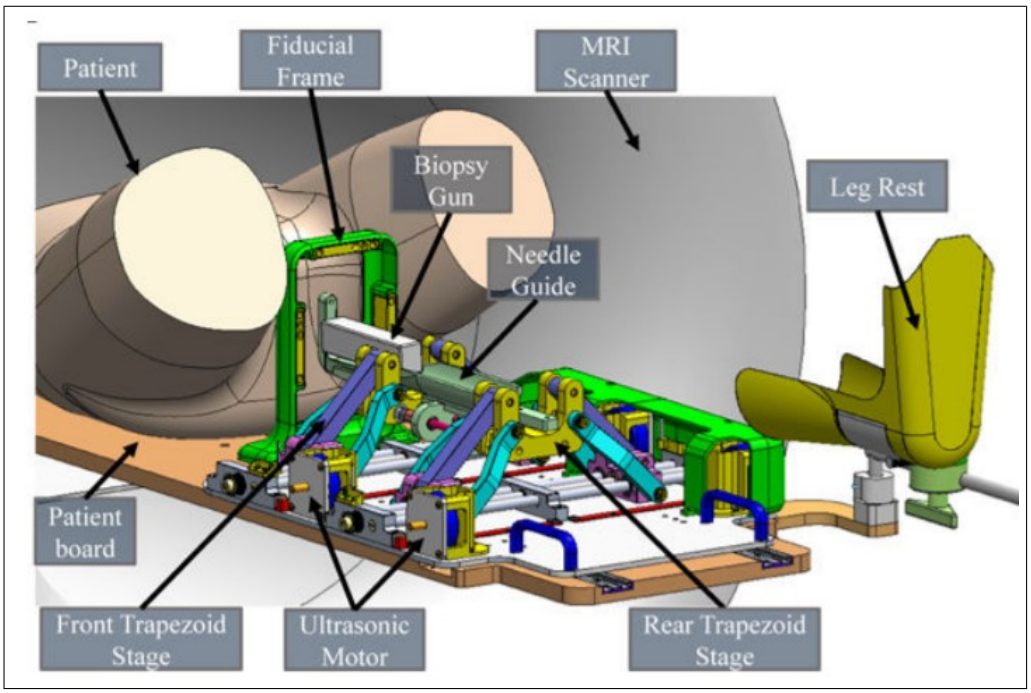

Figure 1.15 Piezoelectric Prostate Biopsy Robot [13]

1. Actuation methods that are inherently compatible with MRI, which do not contain ferromagnetic or conductive materials and in which no AC or DC current is needed during the actuation in the MRI room. Depending on the design, non-ferromagnetic conductive materials can be used if they are not in contact with the patient/medical staff. Actuation mechanisms (hydrostatic, mechanical or pneumatic) which poses a master actuator located outside the MRI room can be listed as an example of this group.

2. Actuation methods in which electric energy is transported to the actuators which are located inside the MRI room with the help of shielded cables. These methods require using non-ferromagnetic materials and filtering to avoid signal and power interference. Electrostatic, ultrasonic and piezoelectric actuators can be listed in this group.

3. Actuation methods which use conventional electromagnetic actuators and ferromagnetic materials. In these methods these non-MRI compatible materials should be fixed at a certain distance from the MRI scanner and should be shielded to avoid interference.

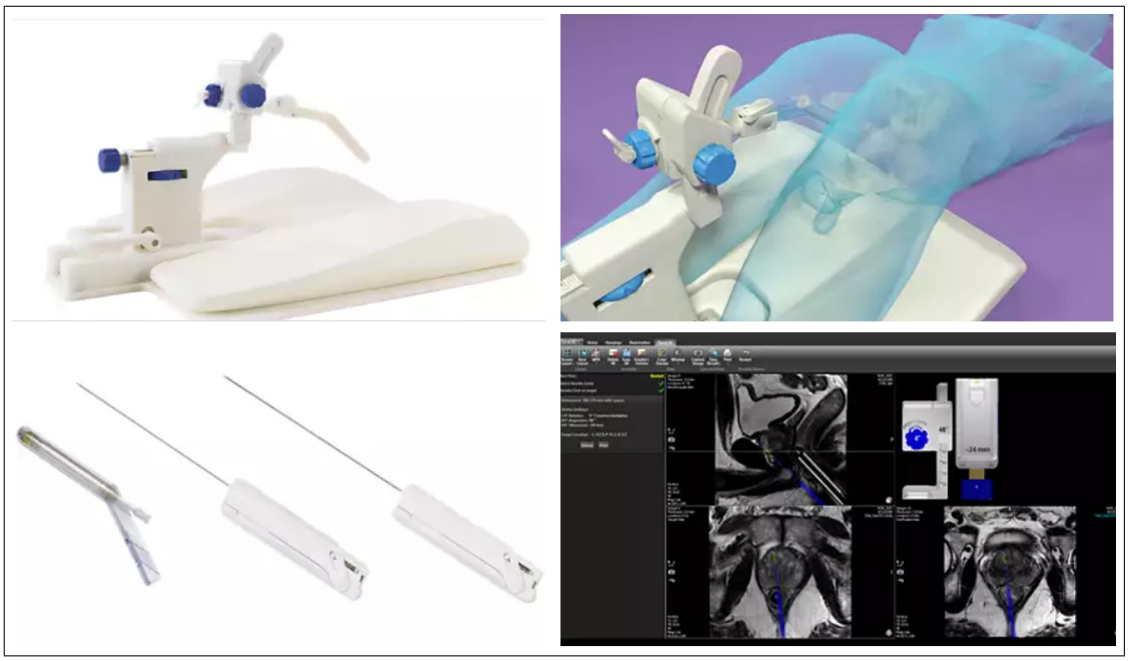

Figure 1.16 Philips Dynatrim Solution for Targeted Prostate Biopsy Procedure

The actuation methods that are used in MRI applications can be grouped and analyzed as:

1. mechanical actuation,
2. pneumatic actuation,
3. hydraulic actuation,
4. electric actuation,
5. electromagnetic actuation in terms of actuation principles

1.3.1 Mechanical Transmission Systems and Actuators

The simplest type of actuation from the MRI compatibility standpoint is mechanical actuation. In mechanical actuation relevant components are used to store

energy and convert the energy to mechanical power where the actuation is needed. Mechanical actuation also allows master-slave type of actuation in which master actuator is positioned at a sufficient span with the MRI scanner or completely exterior of the MRI room and power is transferred to the slave actuator.

1.3.1.1 Potential Energy Based Actuation. The use of mechanical actuation does not necessitate the use of a power source or electronic components. It has been shown that to control basic devices and to manage friction and mass, mechanical actuators that are based on gravitational or elastic potential energy can be utilized [14]. This approach is intriguing because the actuation if performed on the mechanical structure while eliminating the need for an external source of energy (electrical or mechanical). The potential energy base actuators usually utilize springs which must be reloaded before each trial. The material of the spring is important in terms of MRI compatibility and device characteristics. There are commercially available copper alloys which are shown to be MRI compatible and provide sufficient characteristics for steady operation such as Phosphorus Copper (CuP), Beryllium copped (CuBE) or brass [61]-[62]-[63].

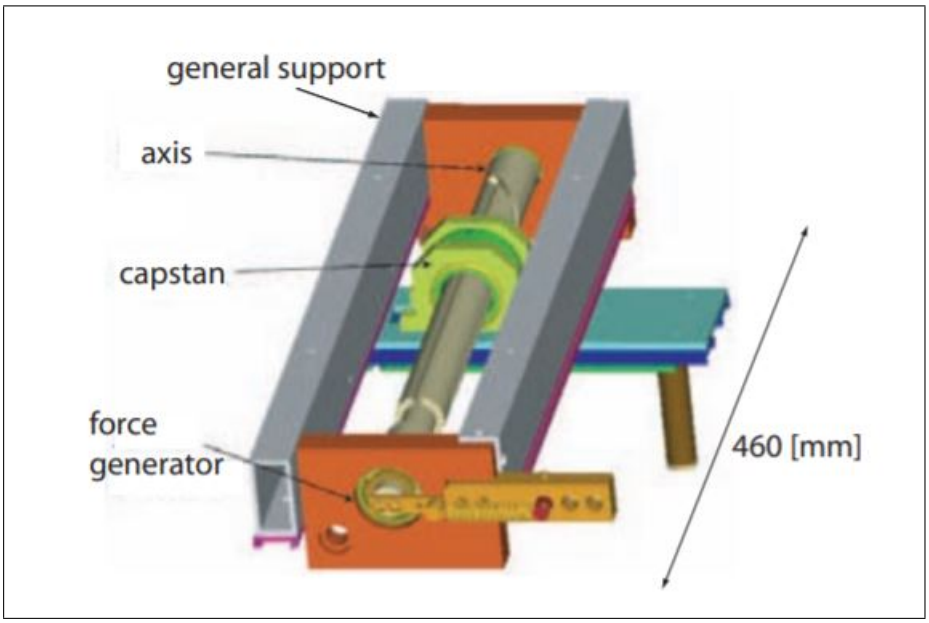

Figure 1.17 Design of the potential energy based actuator using a capstan mechanism. This 2 DOF mechanical interface was designed to transform the force induced by a groove carved on a shaft. [14]

The potential energy based actuators offer advantages like lower cost and simple implementation, high bandwidth without significant delay and unnecessity of external power supply which also simplifies the design. On the other hand, there are some disadvantages like short motion range and lack of precise control and no feedback mechanism with a computer system which limits the application areas of the potential energy based actuators.

1.3.1.2 Mechanical Transmission Systems. Mechanical transmission systems are frequently utilized to transmit power for a long distance into a confined location. Because access to the MRI scanner bore is limited in MRI applications, remote actuation has found various use cases. In MRI applications, a specially designed waveguide can be used to transmit force and motion inside the MRI room through the penetration wall. This enables for the use of traditional electromagnetic actuators outside the MRI room while also preventing the infiltration of electromagnetic interference sources.

Belt/Cable Transmission

Belt/Cable transmissions are mainly used when it is not practical to place actuators directly on the robotic system in order to enable remote actuation. There are various applications of belt/cable transmission in medical applications such as robotic assisted surgical systems like the da Vinci Robotic-Assistend Surgical System (Intuitive Inc.l, USA), force rendering platforms like Phantom (Sensable Tehnologies, USA) and haptic application devices like Freedom 6S (MPB Technologies, Canada). A 4-DOF robotic system was proposed by Oura et. al [15] for minimally invasive procedures which transmitted motion generated by ultrasonic motors using belts. When robots interact with human in an MRI environment, MRI compatibility and safety must also be taken into account. The demand for a sturdy and fixed guiding structure, which results in a non-flexible design, is the fundamental disadvantage of belt/cable transmissions. The master actuator could be positioned inside the MRI room to alleviate this issue. This also eliminates the need to pass through the waveguide which is placed on the penetration wall. A torque motor, when combined with a short cable transmis-

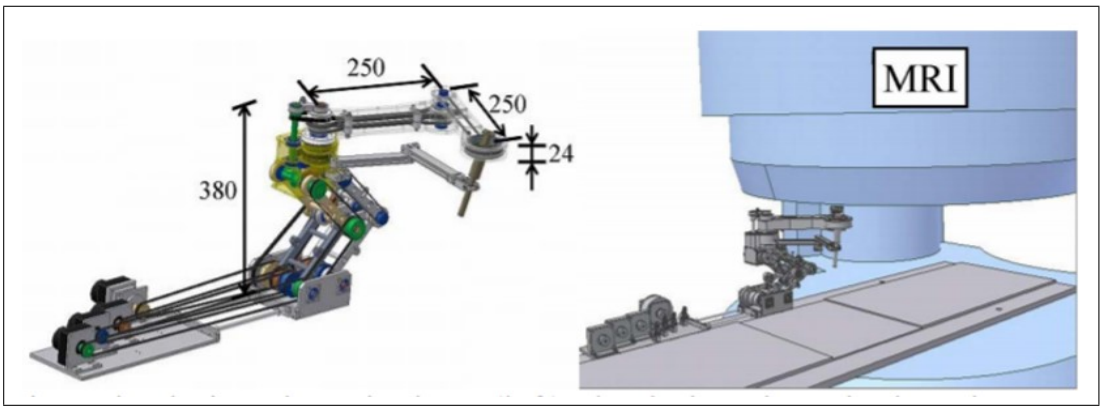

Figure 1.18 Belt/Cable transmission based actuator [15]

sion, produces an intriguing MRI-compatible actuation principle with high bandwidth, low inertia and friction, making it excellent for applications needing force rendering. Due to the possibility of slippage, position encoders that are MRI compatible may be installed in such devices in order to improve safety measures.

Shaft/Rod Transmissions

Mechanical transmission of rotational and translational motions from an actuator to a robotic system is possible with utilization of the shaft/rod transmissions. Shaft/Rod transmissions require fixed anchoring structure which results in non-flexible installation and placement. There are various applications of shaft/rod transmission in the literature. A leverage parallelogram mechanism (LPM) based transmission is proposed by Koseki el al. [64] for a 6-DOF robotic system for a length of 1.8 meter. To excite touch senses in the hand during an fMRI examination, a 2-meter-long carbon-fiber rod was proposed to transfer DC motor rotation which is located outside the MRI room [65]. Krieger et al. [16] demonstrated a robotic system to perform prostate biopsy procedure with MRI guidance such that the physician could operate manually from outside the MRI scanner.

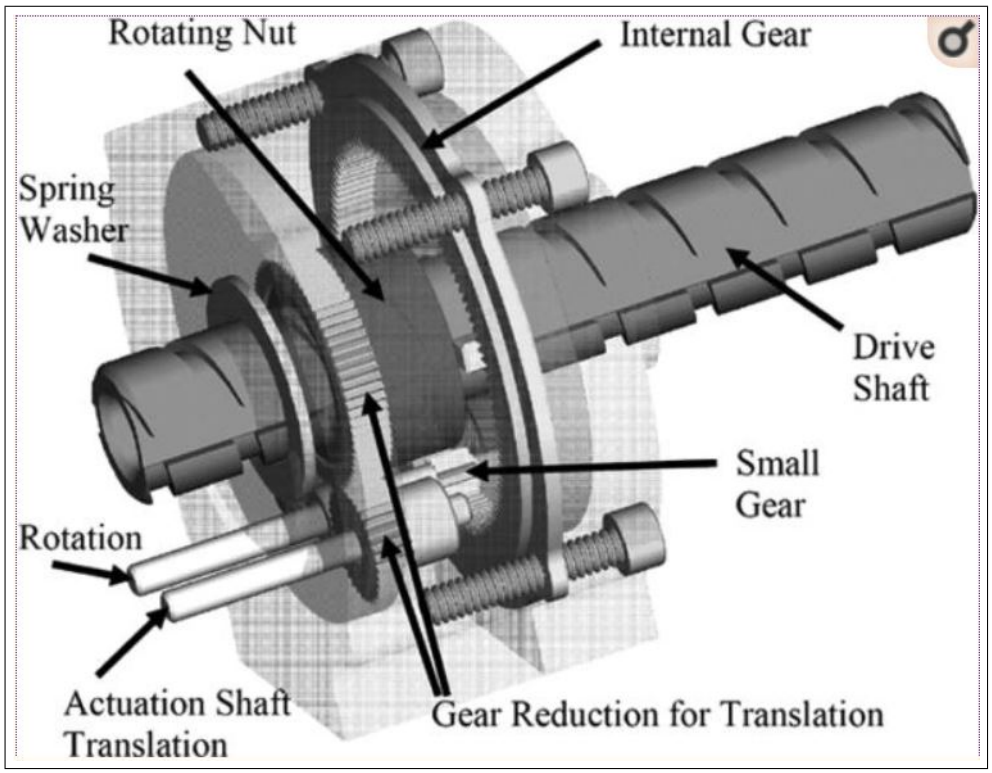

Figure 1.19 Shaft transmission based actuator [16]

1.3.2 Pneumatic Actuators and Transmissions

In an MRI setting, pneumatic actuators are one of most preferred transmission principle to generate basic force pulses and movements due to the simplicity of implementation and high efficiency. Pneumatic cylinders that are made of MRI-compatible materials are commercially available or custom-made MRI-compatible pneumatic cylinders can be designed and produced easily. In a hospital setting it is easy to access compressed air supplies and it is usually available in MRI settings which provides operational simplicity. Besides, flexible tubes can be shaped and positioned without requiring massive modification inside the MRI room. If an external air compressor is required, it can be positioned outside of the MRI room. Additionally, working with air does not pose leakage related safety threat in clinical settings and does not require a return pathway in case of an air leakage. The main disadvantages of pneumatic actuators are compressibility of the air which results in limited bandwidth and considerable delay.

Pneumatic actuators were proposed for various fMRI applications that are concentrating on sensorimotor cortex mapping [66]-[67]-[68] and studies that are investigating control of the human motor system [69]-[70]. Pneumatic transmissions are preferred in MRI-compatible emergency buttons and headphones which exist in many MRI systems for patient safety concerns.

Pneumatically actuated pistons and double-acting diaphragms are an ideal method of activating clamping systems that can be used to mechanically release or fix mechanical structures such as the fixation of a needle guide that is used during a brachytherapy procedure [71].

A rotary wave generating motor was proposed by Stoianovici [72] which is deformed by three pulse-like sequential pneumatic pistons, which resulted in rotation. These actuators allowed open-loop control for position. DiMaio et al. [17] utilized piezo-electric valves, in contrast to conventional electromagnetic valves, to increase the bandwidth and to reduce inherent delays. An MRI compatible assistance system was developed by Innomotion which leveraged plastic-made pneumatic actuators. These pneumatic actuators were used to obtain steady, slow motion with special algorithms.

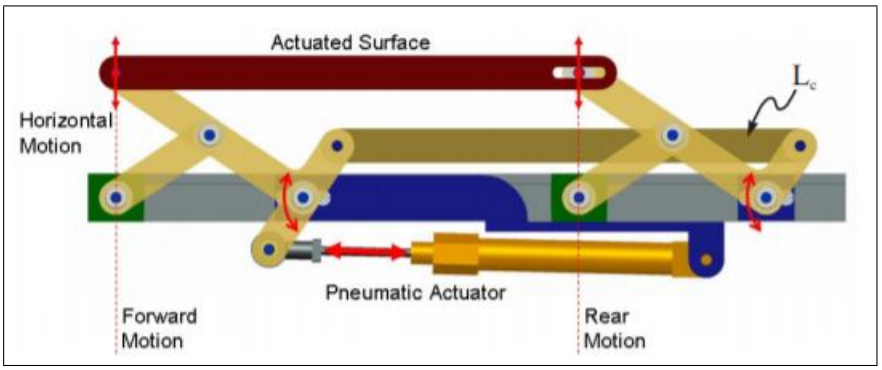

Figure 1.20 Pneumatic actuator mechanism for horizontal motion for both rotation and translation[17]

1.3.3 Hydraulic Actuators and Transmission Systems

Hydraulic transmission systems offer two different actuation principles. The first principle is to generate hydraulic pressure with a pump and to actuate remotely located hydraulic cylinder with the pressurized fluid. The second principle is to form a closed-loop master-slave type hydrostatic system in which master cylinderâs motion is replicated by the slave cylinder. In this way, the master cylinder does not require a hydraulic pump and can be controlled with conventional electromagnetic motors and with a linear stage that are located at a remote location. In hydraulic system flexible hoses are used which allows to place hoses in desired orientations and positions based on the system design. The choice of the materials for hydraulic cylinders determines the MRI compatibility of the system. Therefore, hydraulic cylinders that are made up of MRI-compatible materials ensures MRI compatibility of the system.

It has been shown that hydraulic transmissions can be used for both controlling the position for robotic applications and measuring the force feedback for haptic applications where there is an interaction of the patient and the robot. For 10-meter-long hydraulic transmission the bandwidth was measured as 20 Hz and the resonance frequency was measured as 9 Hz [73]. If required, the transmission length can be reduced to boost bandwidth.

Kim et al. [18] used ultrasonic motors to actuate a hydraulic transmission based manipulator to perform surgeries for liver diseases. An MRI-compatible robotic system that is powered by two electric motors which are located at a long distance (ideally not within the MRI room) to run a hydraulic actuation system was proposed by Hogan et al. [74]. The actuators' performance is limited by joint friction, fluid type and by the viscosity and compression of the oil. In medical applications, the leakage of oil, although small, is not desirable. By adjusting the tension of the joints, the friction can be reduced by the compensation of increased bleeding. Hydrostatic transmission needs extra mechanisms in which electromechanical power is converted into hydraulic power before being transformed at output into mechanical power.

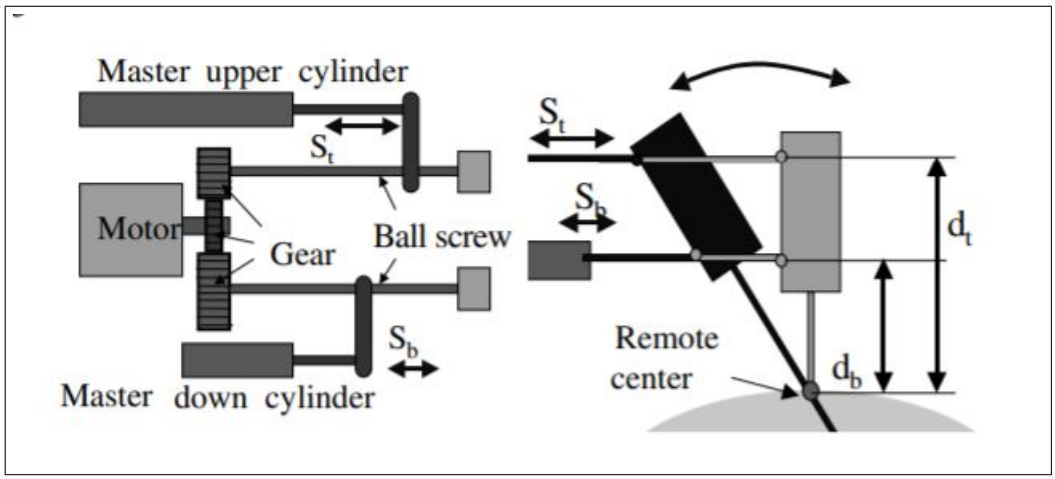

Figure 1.21 Master-Slave type hydraulic actuation[18]

1.3.4 Electrical Actuators

Electrical actuators benefit from the transmission of electric power over flexible and small cables and from the direct conversion of the electricity into mechanical energy. Actuation comes from low current and high voltage electric fields. Multiple conversion of energy can be avoided as opposed to mechanical transmissions. However, the use of such actuators is limited to the safety and MRI compatibility issues and requires a minimum distance from the magnet iso-center and ROI of imaging.

In addition, it may be necessary to filter signaland shielding depending on the systemâs working principle and the imaging sequences. The most widely used actuators for MRI compatible robotic systems are ultrasonic and piezoelectric motors, although several groups proposed other types of electric actuators.

1.3.4.1 Ultrasonic/Piezoelectric Actuators. The most commonly preferred MRI compatible actuator is the ultrasonic motors. The ultrasonic motors were firstly studied for positioning purposes for MRI guided interventional applications [75]-[49]-[76]. Compression and stabilization of body parts [19], as well as actuation of an arm to induce the strain of tissue plane for MR elastography, were among the other use cases [77]. An intrauterine fetal surgical micro-manipulator was developed by Harada

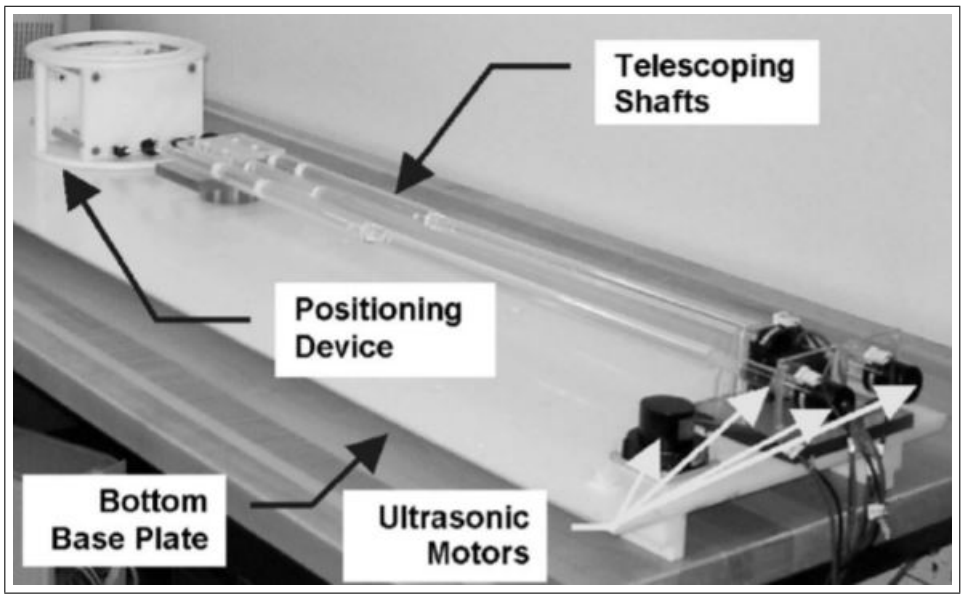

Figure 1.22 Ultrasonic Actuation[19]

et al. using ultrasonic motors and tested [78] in an open MRI scanner. Hata et. al proposed a robotic system to assist operators inside the MRI room to perform microwave thermotherapy for addressing liver tumors [79].

Piezoelectric actuators were also used by different groups for various applications such as the vibrotactile stimulation for somatotopic mapping of the brain cortex [80] or excitation of tissues during MRI elastography [77].

Although, in many applications the output of the ultrasonic motors was transmitted using linkages or levers in some applications ultrasonic motors were used to drive the manipulations directly depending on the position of the ultrasonic motors and shielding degree of the ultrasonic motors. It has been shown by Gassert et al. [81] and Hartwig et al. [62] with proper shielding and filtering ultrasonic motors can be used even for fMRI applications such as haptic applications and studies for human motor control.

1.3.4.2 Electrostatic Actuators. In an MRI environment electrostatic motors may also be used as they produce negligible electromagnetic field and do not contain ferromagnetic materials [82]. High-performance electrostatic actuators were developed by some research groups, which generate enough torque or thrust to power conventional mechatronic devices. The film actuator Dual Excitation Electrostatic Drive is one of the

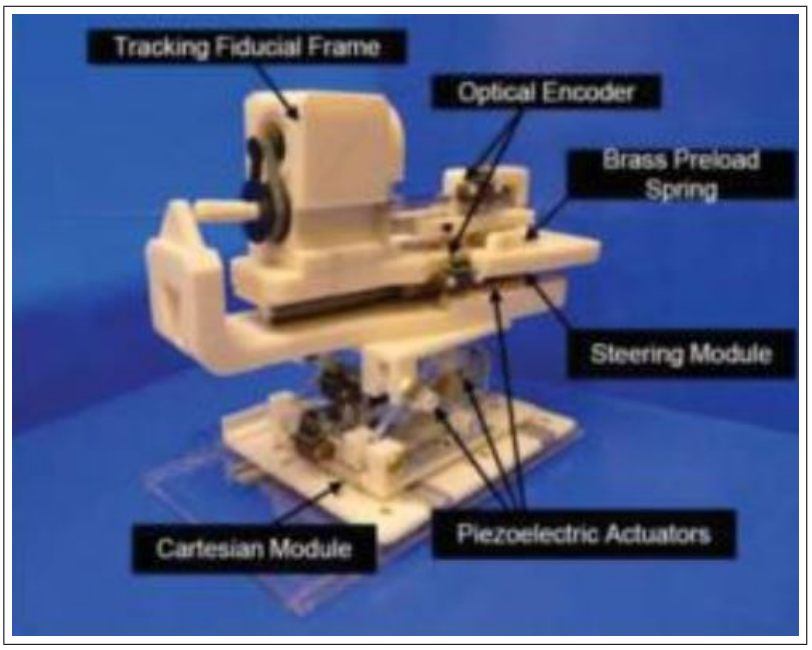

Figure 1.23 Piezoelectric Actuation[20]

strongest [83]. Electrostatic actuators, on the other hand, still require advancements in power electronics before becoming a viable option.

1.3.4.3 Electroactive Polymers. Electro-active polymers (EAPs) offer a relatively new form of actuation that go by a variety of names, including ionic polymer-metal composite (IPMC) actuators and electrostrictive polymer actuators (EPAMs). EAPs are the actuators that alternate the physical properties of the materials in response to changes in electric/chemical potential or temperature. The functioning principle and needed driving voltage are the fundamental differences between EPAMs and IPMCs [84]-[85]-[86]. When the voltage is applied to across EPAM its thickness decreases and surface area increases. On the other hand, IPMCs bend when voltage is applied in the direction of the cathode. Another major variance between EAPs and IPMCs is the required voltage; EAPs are driven with kilovolts whereas IPMCS require very low voltages. Furthermore, IPMC are continuous and EAPs are on-off type actuators. Nakano et al. [87] proposed usage of these actuators for fMRI applications in neuroscience field by creating haptic displays. Also, these actuators are promising for applications for tactile simulators. Vogan et al. [21] used EAPs to create an adjustable

MRI coil which can change its size according to the ROI in order to gain the best image resolution and quality. In this way the patient comfort is improved by reducing the imaging time. Also, it has been shown that these actuators offered sufficient MRI compatibility and did not distort the MR images. However, the safety issues related to these actuators should be investigated for applications which requires patient contact.

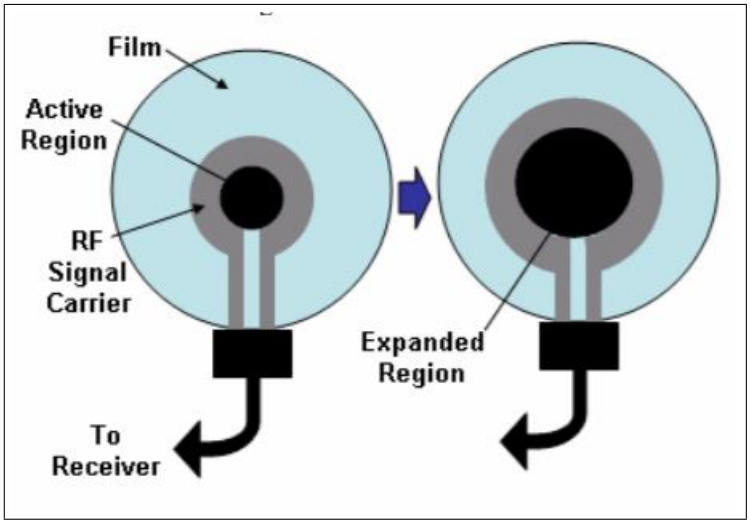

Figure 1.24 The Single Actuator Integrated Coil Design [21]

1.3.4.4 Electrorheological Fluid (ERF) Actuators. When an external electrical field is applied the flow properties changes for certain fluids called electrorheological fluids (ERF) which can be used to control torque. These fluids behave like a Newtonian fluid under normal circumstances. However, when the electrical field is present they behave like Bingham fluid which means that the yield stress varies by changing current. Therefore, it is possible to generate blocking or resistive torques by varying the electric field.

Khanicheh et al. [22] proposed a rehabilitation device which used an MRI-compatible ERF. Because ERF materials can be made MRI compatible and the force and torque can be regulated directly, it is an appealing actuation method for rehabilitation and haptic devices.

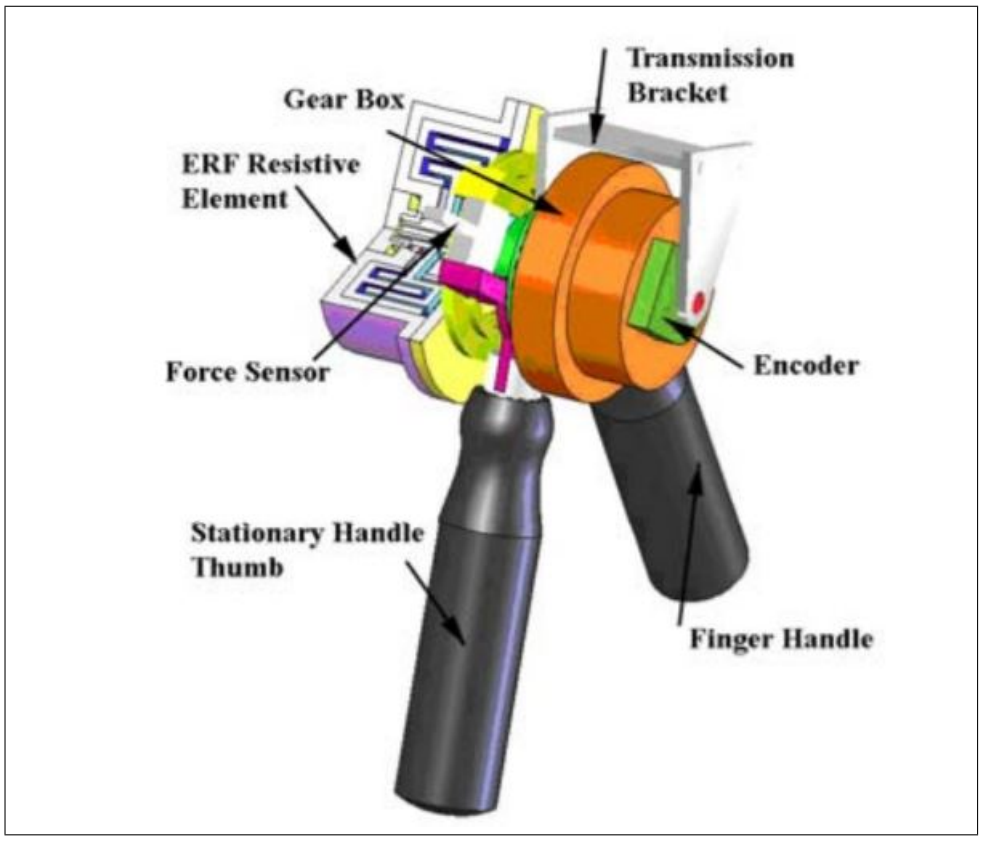

Figure 1.25 MR compatible ERF Driven Hand device [22]

1.3.5 Electromagnetic Actuators

Despite the fact that electromagnetic actuators are neither fundamentally MRI safe nor MRI compatible, they provide for simple velocity, position and torque control, as well as precise force feedback to detect human actions. Therefore, electromagnetic actuators are employed in many traditional haptic applications. Electromagnetic actuators usually contain a permanent magnet and a soft magnetic material which are used to condense the electromagnetic flux are the source of the safety concern. As a result, the static magnetic field will strongly attract such a motor, which should be tightly fixed at certain span from the MRI magnet. The necessity of relatively excessive current to run the motor and noise created by the power supply all contribute to electromagnetic compatibility difficulties. Nonetheless, similar actuators have been employed in MR contexts, where they take use of the scanner's static magnetic field or use electromagnetic filtering and shielding.

1.3.5.1 Magnetomechanical Vibrotactile Devices and Lorentz Actuators.

Lorentz actuators are topic of interest for several research groups which aim to minimize the safety and MRI compatibility issues of electromagnetic actuators. The main reason for this interest is that Lorentz actuators do not contain ferromagnetic materials and use the static magnetic field of the MRI scanner.

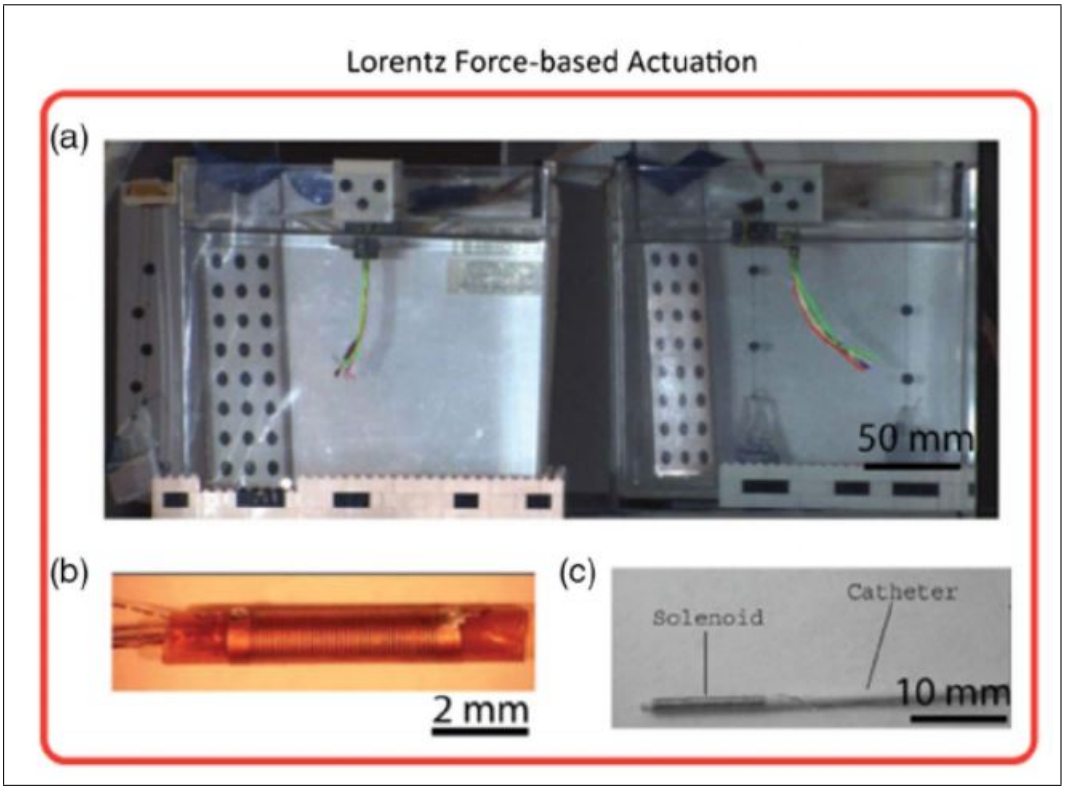

Figure 1.26 Examples of MRI-driven robots actuated by the Lorentz forces in the literature. aâ c) MRI-driven catheters with Lorentz coil embedded. [23]-[24]The torque induced on an active Lorentz coil deforms the tip, which enables precise tip control within MRI.

Magnetomechanical vibrotactile devices (MVD) are used by Graham et al. [88] in order to develop a somatotopic mapping during fMRI. It has been also used in MR elastography applications to create shear and compression waves [66] and to navigate the catheter tip in several MRI applications [89]. Riener et al. [90] used this technique to control a one-degree-of-freedom haptic sensing with a force sensor to detect the motion of wrist during an fMRI application. A hall-effect type sensor was included into the haptic sensing system, enabling measurement of density of the magnetic flux and thereby reducing the reliance on the device's position within the scanner's static magnetic field.

The proposals of Graham et al. [88] and Reiner et al. [90] showed sufficient MRI compatibility and sensitivity of positioning and orientation. However, this depends on the clinical setting and used MRI sequences. Therefore, in each application the performance of the proposed solutions should be assessed.

1.3.5.2 Shielded Direct Current (DC) Motor. Traditional Direct Current motors, while commonly preferred in various applications and great for positioning and haptic sensing applications, have major MR safety and compatibility issues. The ferromagnetic components that will be attracted by the scanning magnet are the source of the safety concerns. It should be noted that electromagnetic interference would possibly occur is the DC motor is not shielded or poorly shielded.

2. SOLUTION DESCRIPTION AND SPECIFIC AIMS

In this thesis, we introduce a hydraulic based biopsy needle drive system and passive prostate biopsy needle design to perform prostate biopsy procedure under real-time MRI guidance in order overcome the existing problems in clinical practice. The solution, i) will address the reliability concerns of TRUS biopsy by offering a targeted biopsy procedure, ii) will ease utilization of MRI images during the biopsy procedure by eliminating the necessity of image registration of different modalities, iii) will address all the technical limitations by offering the ultimate design features in terms of material selection, mechanical design and actuator selection and iv) will offer enhancement of needle visibility with passive tracking approach in order to improve the targeting accuracy. The proposed solution includes the design, driving the kinematic equations, production, characterization and experimental validation stages of a robotic prostate biopsy system.

The proposed robotic prostate biopsy system is composed of following components;i) needle delivery unit, ii) control unit, iii) hydraulic actuators, iv) biopsy gun and v) biopsy needle. Although, there are similar studies that are available in the literature the main specific aims and possible contributions of this thesis are;

1. Adoption of rolling diaphragm cylinders in the hydraulic actuator design and providing its characterization. The inclusion of rolling diaphragm cylinders brings significant benefits like reduction of internal friction, fast response, precise open-loop control, high output torque over long hydraulic lines and high sensitivity to support haptic applications. Therefore, rolling diaphragm cylinders play an important role for the system.

2. Designing a compact, low-cost and simple robotic system for real time prostate biopsy under MRI with required specifications in term of targeting accuracy, total procedure duration, robustness, patient safety measures and anatomical compliance.

3. Driving inverse kinematic equations specific to the robotic system in order to register the patient with the robotic system and to perform calculations required for the robot manipulation.

4. Preclinical evaluation of the robotic biopsy system with MRI experiments using a prostate phantom.

5. Demonstration of complete systemâs feasibility in terms of key performance metrics (e.g. targeting accuracy, procedure duraction etc)

6. Investigation of active tracking techniques that can be applied for the biopsy needle and conducting animal experiments.

3. MATERIALS AND METHODS

3.1 System Design

A hydraulically-actuated needle delivery system was designed to drive the prostate biopsy needle under real time MRI guidance. The system was composed of five main components: i) needle delivery unit with 6 DOF, ii) hydraulic actuator system, iii) motor controller user interface, iv) MRI compatible biopsy gun and v) biopsy needle. The needle delivery system was designed to be anatomically compliant based on similar medical device specifications in the market. The design was simulated using an anatomical model in order to ensure that every voxel inside the prostate can be traced with the needle tip. Additionally, patient comfort was also considered during design stages and it was aimed to obtain biopsy samples without causing any unnecessary discomfort for the patient. The hydraulic actuator was designed in a master-slave configuration such that the master unit was controlled by the operator in the control room and motions of the master were precisely replicated by the slave unit which is located in the MRI scanner room. The master-slave configuration enabled us to use low-cost conventional components (non-MRI compatible) for the master system which is located outside of the MRI scanner room. The hydrostatic transmission mechanism was preferred to transfer the required force and/or torque during the biopsy needle insertion. In principle, the required force or torque is first created on the master unit and transferred to the slave unit using the hydrostatic transmission mechanism. An MRI-compatible biopsy gun and biopsy needle were designed and produced in order to acquire biopsy samples.

3.1.1 Biopsy Needle, Biopsy Gun Design and Passive Tracking

SolidWorks design and drawing tool (Dassault Systems SOLIDWORKS Corp, MA, USA) was used to design the bevel cut distal tip and biopsy reservoir of the

coaxial biopsy needle. The design file was then converted to the required format for the laser cutting system using Alphacam Software (Vero Software, UK). Both inner and outer components of the The biopsy needle was formed through laser cutting process by using a Nd:YAG laser cutting device at Bogazici University Center for Life Sciences and Technologies. The maximum power of this device is 400 W and the beam diameter is 18-20 microns. Initially, the laser cutting device was brought to the tube cutting mode and this modification of the setup required additional parts to hold and fix the low profile nitinol tubes. These support parts were designed using a computer aided design (CAD) software (Dassault Systems SOLIDWORKS Corp, MA, USA) and fabricated using the 3D printing device(Zortrax M200, Zortrax S.A, Poland).
The nitinol tubes were processed after bringing the laser cutting device to the tube cutting mode. In tube cutting process, argon gas was used in order to prevent excessive oxidation on the cutting surfaces and because titanium is a flammable metal, and a water cooling system was used to reduce the heating. Laser cutting process requires fine tuned settings depending on the type of the material, physical parameters such as width, thickness of the nitinol tube and the cutting process. The key success factors for the laser cutting process are

- To obtain planar cutting profile which requires proper adjustment of the laser cutting device settings such as power, pulse width and frequency of the laser
- To prevent attachment of removed parts of the tube which requires proper adjustment of the pressure settings for argon gas, dry air
- To obtain desired design at the end of the laser cutting process with desired precision which requires proper positioning of the tube to enable 360 degrees cutting profile and proper adjustment of all device and pressure settings.
- Repeatability of the process with the same materials and settings to produce multiple needles with the same characteristics
- Proper focusing of the laser beam to avoid unintended cuts on the reverse side of the tube.

  In the proposed thesis, several settings were tested to optimize the laser cutting

process and to obtain desired needle design and characteristics. Finally, biopsy needle production process was performed with following settings:

- Laser Power: 100 W
- Pulse Width: 0.6 msec
- Frequency:250 H
- Speed: 0.4 inch/sec
- Argon Gas Pressure: 6 bar
- Dry Air Pressure: 8 bar
- Water Cooling Line Pressure: 3 bar

Figure 3.l depicts the laser cutting device in tube cutting mode.

Several biopsy needle designs were fabricated using the laser cutting device and

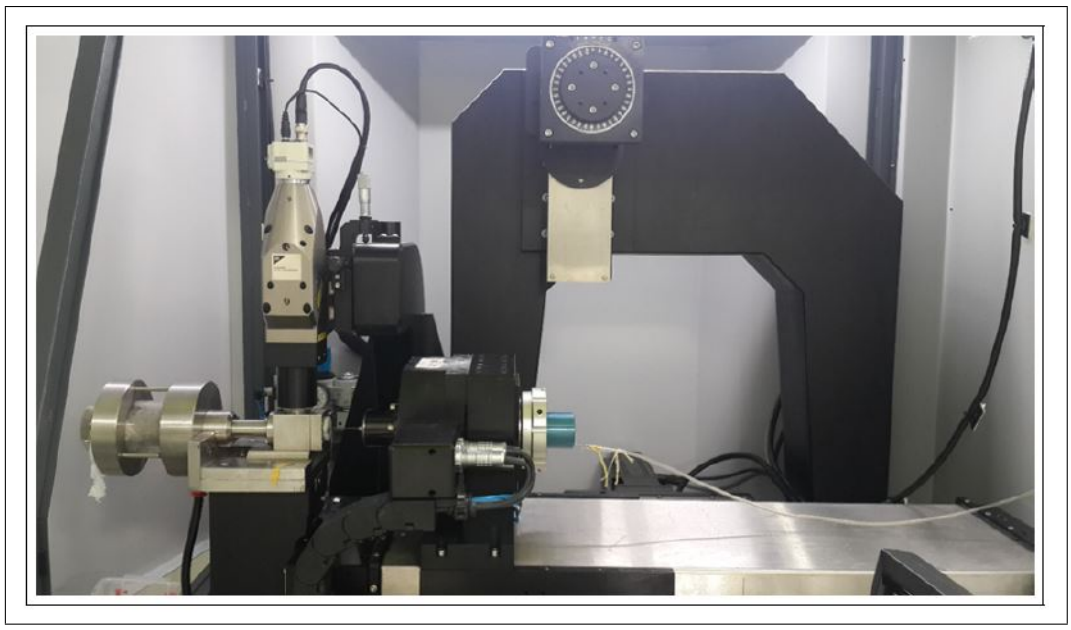

Figure 3.1 The Laser Cutting Device

these designs were tested to minimize the unintended deflection of the needles during tissue-needle interaction and to maximize the sample acquisition efficiency. After several experiments the most suitable design was chosen fabricated from tight fit coaxial nitinol tubes (Confluent Medical Technologies, CA, USA) which have 0.037" outer diameter for the inner needle and 0.058" outer diameter for

the outer needle. The final design of the biopsy needles were fabricated using a Nd:YAG laser cutting system with bevel tip angle of 26 deg as shown in figure 3.2.

Micro-blasting process was used to remove the oxide layer and burrs formed

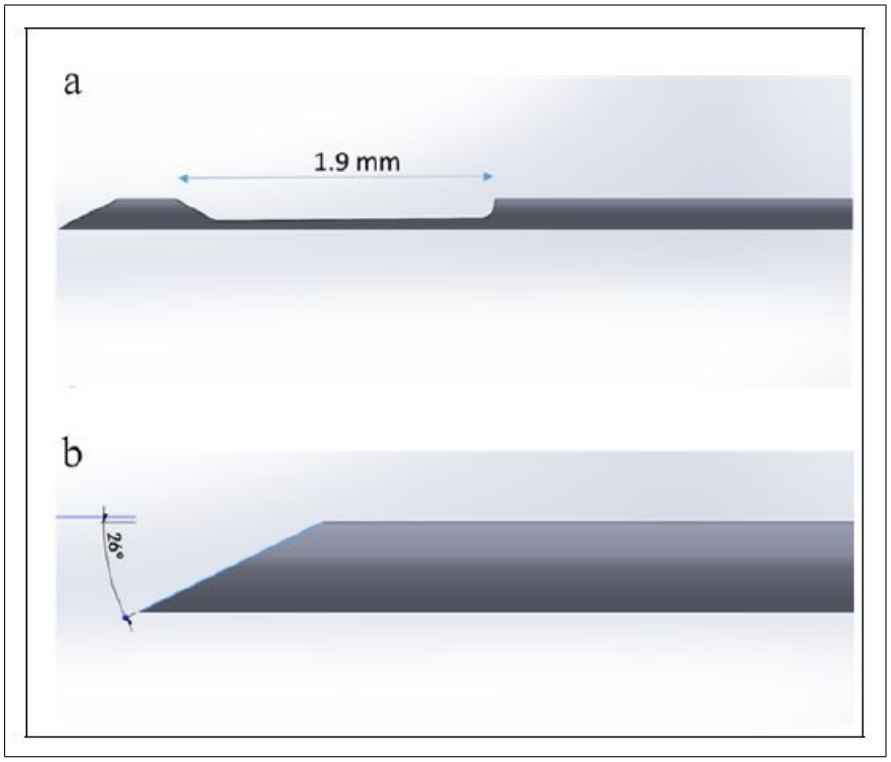

Figure 3.2 Biopsy Needle Design

during the laser cutting process. To remove the burrs, a micro-abrasive blaster system (COMCO INC. AccuFlo, USA) was used with 50 microns aluminum oxide precision micro abrasive powder at Bogazici University Center for Life Sciences and Technologies and Figure 3.5 depicts images taken after and before microblasting process. In order to assess and improve the tracking performance of the robotic system the biopsy needle should be tracked precisely real time during the procedure. The most convenient way to track the biopsy needles is enhancing their visibility by either incorporating a passive or an active tracking method because the nitinol-made needles cannot generate MRI signals to be tracked under MRI. In our study, we prefer to implement the passive visualization technique to the biopsy needle design to make it visible under MRI. The biopsy needles were deposited with equidistantly spaced thin film Fe_2O_3 strips using physical vapor

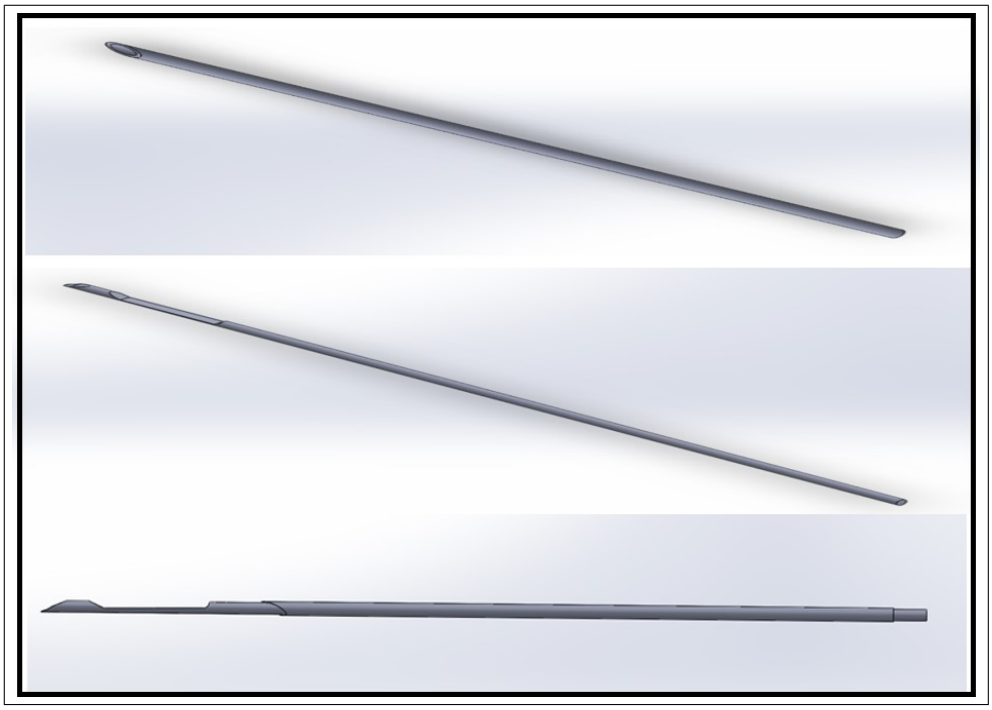

Figure 3.3 Assembly of Inner and Outer Biopsy Needle

deposition (PVD) coating. In PVD coating atoms are removed from a solid or a liquid by means of an energetic method and these atoms are deposited on a nearby surface. There are different types of atom removal methods for PVD such as thermal evaporation, physical sputtering, laser ablation, and arc-based emission [91]. In order to find the optimal recipe for the thin film Fe_2O_3 we played with the parameters such as PVD duration, strip spacing and strip width. As shown in figure 3.6 the plastic tape strips were used to create equidistant Fe_2O_3 thin film marker over the needle length. The PVD duration has a direct impact on the thickness of the strip. It has been seen that the signal intensity increased with the increasing thickness. However, increasing the strip thickness too much caused excessive distortion on the MRI images of the surrounding medium and signal interference between adjacent strips. Besides, increasing the strip thickness also increased the surface resistance of the needles during penetration and removal of the needles. In this study, the PVD system (Vaksis, Angora, Turkey) at Bogazici University Center for Life Sciences and Technologies was used with following settings:

Figure 3.4 The Microblasting Device

- Base presure: $2.3x10^{-7}$Torr
- Coating pressure : $0.5x10^{-3}$ Torr
- Argon flow rate : 22 Sccm
- Coating temp : RT
- Sample longitude axis rotation : 20 rpm
- Coating power source : DC
- Coating Power : 100 Watt
- Film growth rate : 20 nm / min
- Coating time :30 min
- PVD duration was chosen as 30 minutes in order to maintain the optimal efficiency from the Fe_2O_3 strips for tracking the needles. The strip spacing was chosen as 5 mm to prevent signal interference between adjacent strips

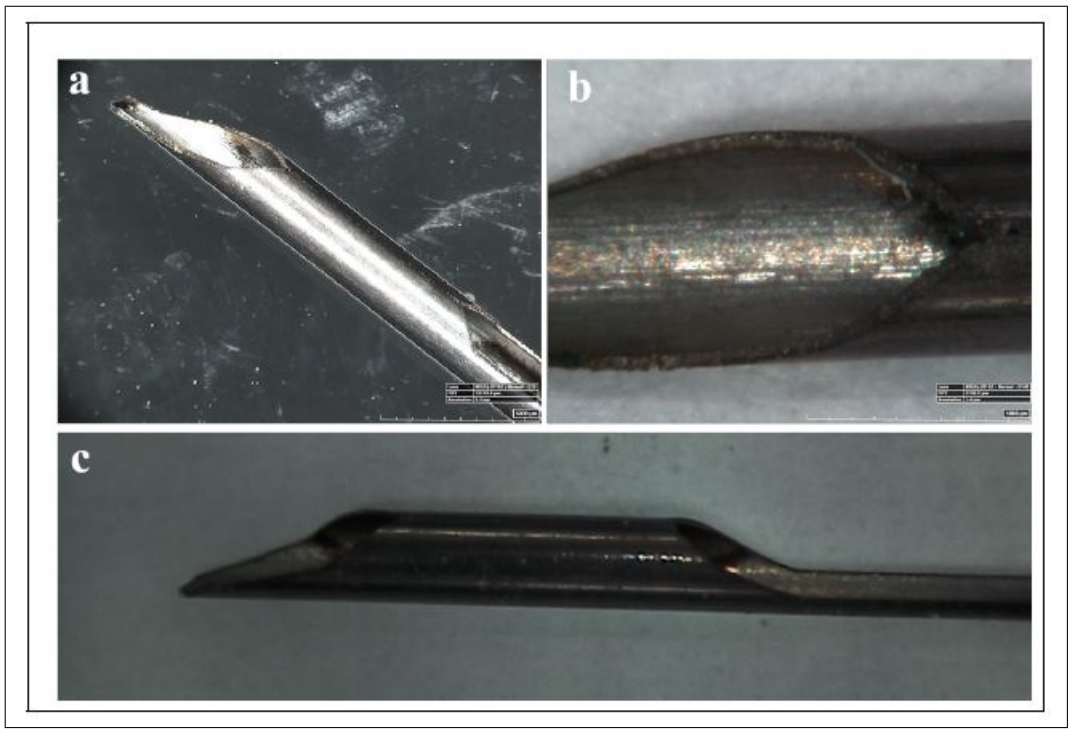

Figure 3.5 Biopsy needles a-b) without microblasting and c) with microblasting.

but not to compromise tracking precision. Lastly, the strip width was chosen as 1 mm.

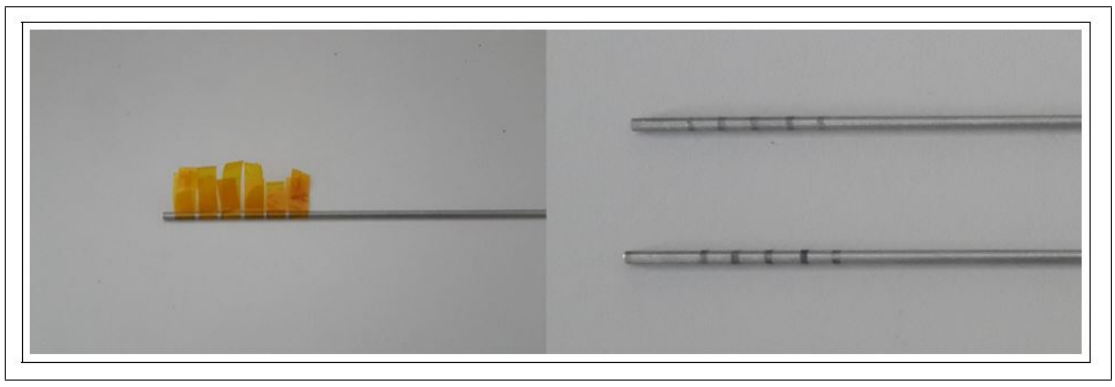

Figure 3.6 Iron oxide nanoparticle coating

The biopsy gun was designed to fit onto the needle delivery unit with a fixed position. The inner and outer biopsy needles were mounted to the biopsy needle holder and biopsy gun was assembled as shown in figure 3.7. An MRI compatible spring which was made of brass was used to load the biopsy gun. The biopsy gun is loaded manually by the operator before the procedure. During the procedure

the biopsy gun is fired again manually by the operator. The firing mechanism is designed to avoid unintentional motions of the biopsy needles which can result in a decrease in targeting accuracy. The MRI visibility of the endorectal guide

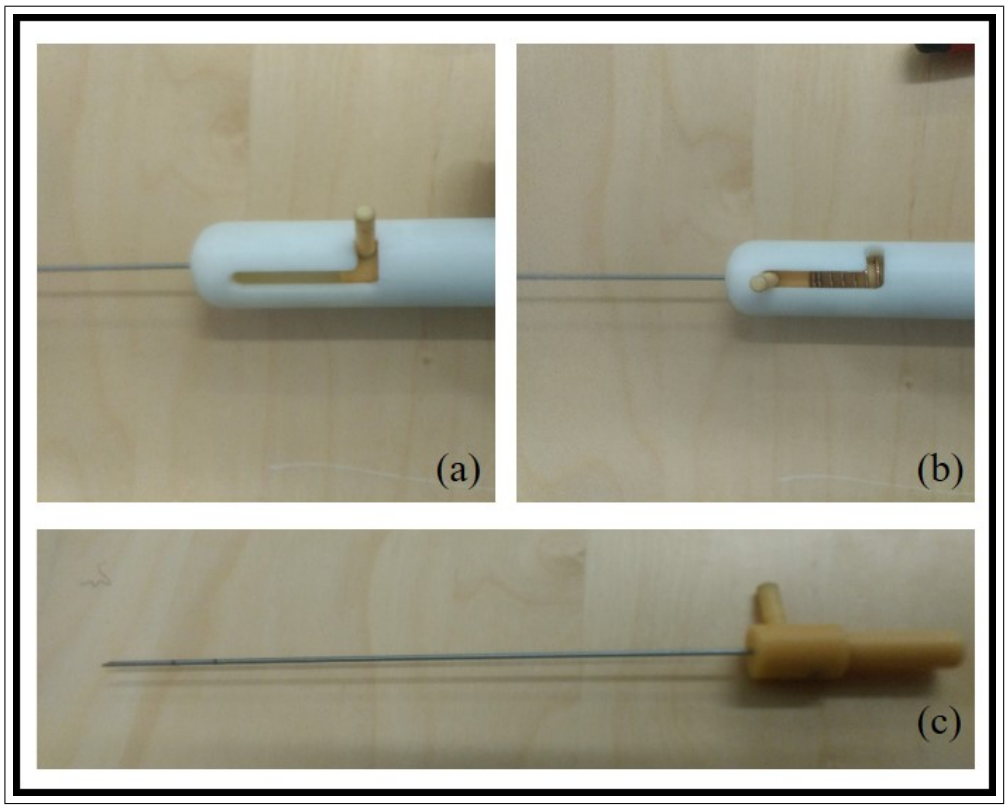

Figure 3.7 Biopsy gun a) before the gun is fired b) after the gun is fired c) needle holder is used to separate the multiple sentences.

also was improved with fiducial markers in order to enable registration of the phantom with the needle delivery unit.

3.1.2 MRI Compatibility and Material Selection

In MRI applications, material selection is an important stage in the design process. Inconvenient selection of materials might bring adverse effects which may cause significant problems from patient safety and image quality standpoint. As discussed, ferromagnetic materials can be pulled strongly by the static magnetic field in the vicinity of MRI bore which may cause serious safety issues. Similarly, conductive materials with long electrical lengths (i.e. longer than the quarter wavelength of transmit RF signal) may experience excessive temperature rise

due to induced current. Also, the eddy currents that are induced over the conductive system components may degrade MR image qualities.

From the safety standpoint, the American Society of Testing and Materials (ASTM) standard F2503-13 classifies devices in the MRI environment into three distinct classes:

(1) MR Safe: the materials and devices that cause no negative impact or harm to the patients and medical staff in any MRI environment,

(2) MR Conditional: the materials and devices that cause no negative impact or harm to the patients or medical staff when used in certain conditions, and

(3) MR-Unsafe: the materials and devices that can cause negative impact or harm to the patients or medical staff or other people within the MR environment. Figure 3.8 shows the labeling for ASTM standards. In the proposed thesis, the body

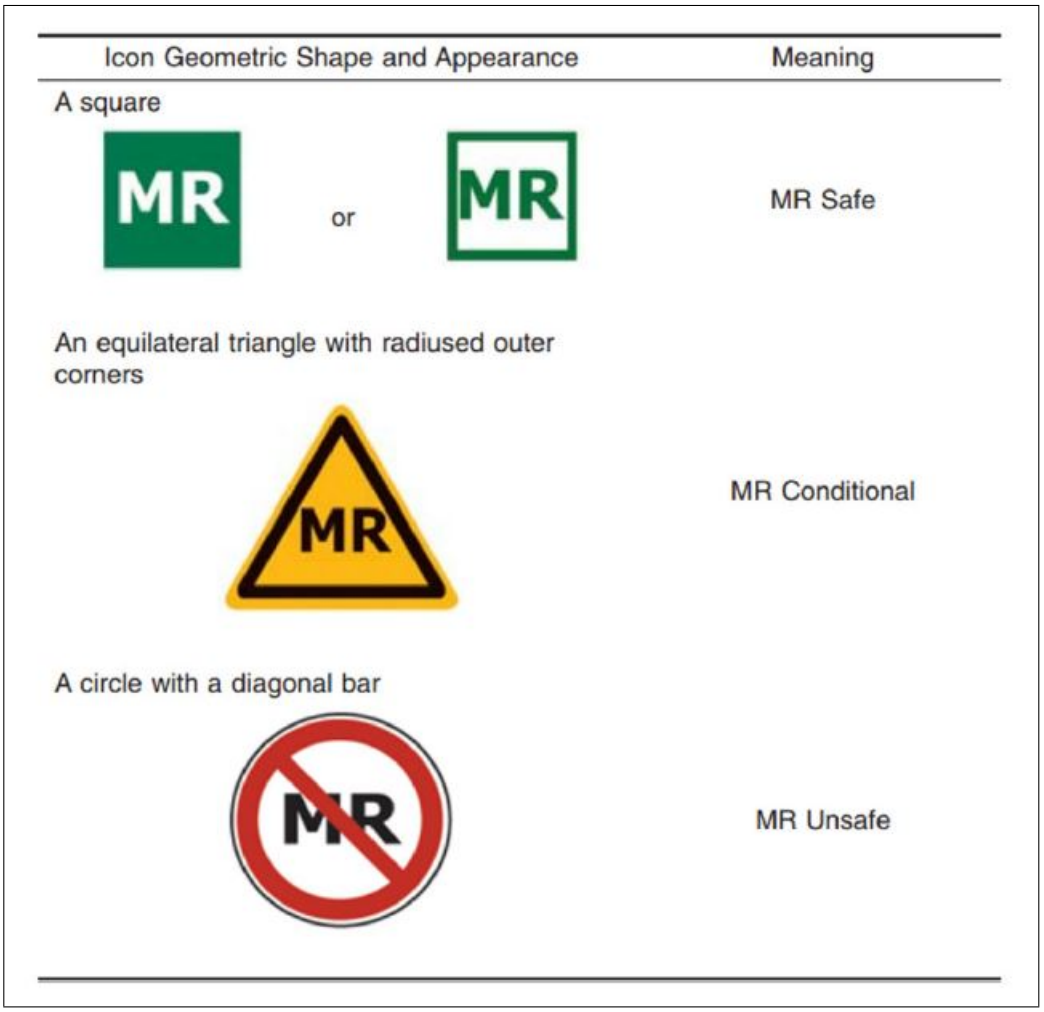

Figure 3.8 ASTM MRI Compatibility Icons

of needle delivery or robotic system was produced using an engineering plastic material called castermid, utilizing a 3-axis Computer Numerical Control (CNC) system. Castermid does not have any magnetic property such that is it not pulled by the strong magnetic field of the MR bore. Furthermore, castermid does not show any electrical conductivity property which means that it does not carry any safety risks due to the RF signal induced heating. Therefore, castermid is listed as an MRI-compatible material according to the ASTM standards. Furthermore, in this thesis castermid was chosen because it shows excellent physical and mechanical properties for robotic applications. For instance, it is a very light, rigid and durable material which offers excellent mechanical advantages against other commonly used materials such as copper, steel, bronze, aluminum, brass, fiber, brass and other metals. Thanks to its low surface friction castermid does not require lubrication which is also very desirable in robotic applications. Additionally, the cost of ownership for castermid is very low compared to other materials which makes it appealing for profitable mass production. Lastly, castermid can be processed with standard manufacturing methods such as CNC systems which enables precise manufacturing of the desired designs with computerized systems. Once the robotic components were manufactured the body of the robotic system was assembled. Custom made joint pins were used at the articulation points. Conventional, metallic joint pins were not preferred not to degrade the MRI compatibility of the robotic system. Therefore, the joint pins were specially designed using Solidworks CAD program (Dassault Systems SOLIDWORKS Corp, MA, USA) and manufactured from castermid with the utilization of a CNC system.

Some of the physical and mechanical properties of castermid is listed as follows:

- Density: 1.15 g/cc
- Tensile Strength: 83.4 MPa
- Tensile Modulus of Elasticity: 4 GPa
- Compression Stress: 93.2 MPa
- Compression Modulus: 2.7 GPa
- Coefficient of Friction: 0.39

- Wear Factor 0.44 mg/km
- Volume Electrical Resistivity: 1.0e14 ohm.cm
- Surface Electrical Resistivity: 1.0e13 ohm

In the proposed robotic system, the kinematics design required two rotational motions mainly to rotate the endorectal guide around its axis. In order to enable rotational motions two bearings were included in the robotic system's design. However, conventional bearings were not preferred in this design because the conventional bearings usually include materials that are MR-unsafe. Therefore, the special bearings which are composed of ceramic beads and a polymer enclosure(NSK Europe, Berkshire, England) were utilized to enable rotational motions for the robotic system.

As discussed in section 3.1.1, the biopsy gun was fabricated from acrylonitrile butadiene styrene (ABS) which is an MRI compatible material and the biopsy needles were fabricated using a Nd:YAG laser cutting system from MRI-compatible nitinol tubes.

In the proposed robotic system design, the master actuator, control system and the other electromechanical components were kept outside of the MRI room. Therefore, MRI compatibility was not required and material selection was arbitrary for these components. As a part of master-slave type hydraulic actuator design only the slave hydraulic cylinders were fixed on the robotic needle delivery system. The slave cylinders were chosen from commercially available rolling diaphragm hydraulic cylinders (ControlAir Inc, NH, USA). The physical specifications of these cylinders were length: 7.13 cm, diameter 2.38 cm, bore diameter: 1.78 cm, maximum operating pressure: 8.62 bar. The rolling diaphragm cylinders had single input port which also allowed easy sealing of hydraulic pipes in range of operating pressure. The shell, head and piston of the rolling diaphragm cylinder were made of aluminum, and the diaphragm was made of neoprene rubber with dacron fabric. Only the steel rods of the cylinders were replaced with same size aluminum rods in order to ensure MRI compatibility.

3.1.3 Mechanical Design

The main design criteria of the robotic system was to keep the overall system design compliant with the human anatomy. In this regard following criteria were considered in the design process:

- the components of the robotic system that are in contact with the patients should have proper dimensions with respect to the human anatomy e.g. diameter of the endorectal guide, size of the biopsy needle etc.
- the initial pose of the needle delivery system should be adjustable to be able to target the prostate.
- the kinematics of the needle delivery system should allow scanning of the biopsy needle tip throughout the whole volume of an average size prostate.
- the needle delivery system should have a compact design to be able to fix the system to the MRI table without disturbing the patient.
- the needle delivery system should be able to withstand external forces (e.g. patient movements) when fixed to a certain position in order to preserve the desired targeting accuracy.
- the operation of the robotic system should not create any disturbance for the patient.
- the operation and the initial pose of the robotics system should not alter the location and shape of the prostate
- the initial insertion of the biopsy needle should be manual to ensure patient safety and should be fixed to the robotic system after initial insertion.
- the kinematics of the robotic system should be as simple and as efficient as possible to avoid complexity inside the MRI room.

In the proposed needle delivery system design, in total there 6 DOF. The first 3 DOF were controlled manually and the remaining 3 DOF were controlled remotely as shown in figure 3.8. The manual controls were used to bring the needle delivery system to its reference position or so called âzero positionâ. In the zero

position, the initial pose of the needle delivery system is given to adjust the system with respect to the patient and insert the endorectal guide through the rectum. The manual controls 12 were used to adjust the height and lateral position of the needle delivery system. The manual control 3 was used to adjust the angular position of the endorectal guide. Once the needle delivery system was brought to its zero position, all the manual controls were fixed by using the clamps to prevent unintended motions of the manual arms and to fix the needle delivery system's base with respect to MRI scanner. The joints of the needle delivery system designed such that they can withstand 20 N force in its zero position.

The body of the needle delivery system was composed of three main parts; base, inner and outer part as depicted in figure 3.8. The outer part was connected to the base of the system from the 3rd manual control joint. The outer and inner parts were connected by using two bearings. The first remote control axis R_1 and the bearings enabled rotation of the inner part with respect to the outer part. The first hydraulic cylinder which is coupled to the inner part was used to rotate the endorectal guide around its own axis. The angular position of the biopsy gun or the needleâs axis was controlled with a second hydraulic cylinder R_2. The third remote controlled hydraulic cylinder which was coupled to the biopsy gun housing was used to adjust the insertion depth of the biopsy needle (L).

3.1.4 Kinematics

In the proposed design, the needle delivery system is fixed to its zero position after inserting the endorectal guide through the rectum. Once the needle delivery system is in its zero position only the endorectal guide is in contact with the patient. It has been shown that the angular movement of the endorectal guide does not alter the place and shape of the prostate [11], which thus enables precise targeting of the biopsy needle with inverse kinematic calculations. In addition, it

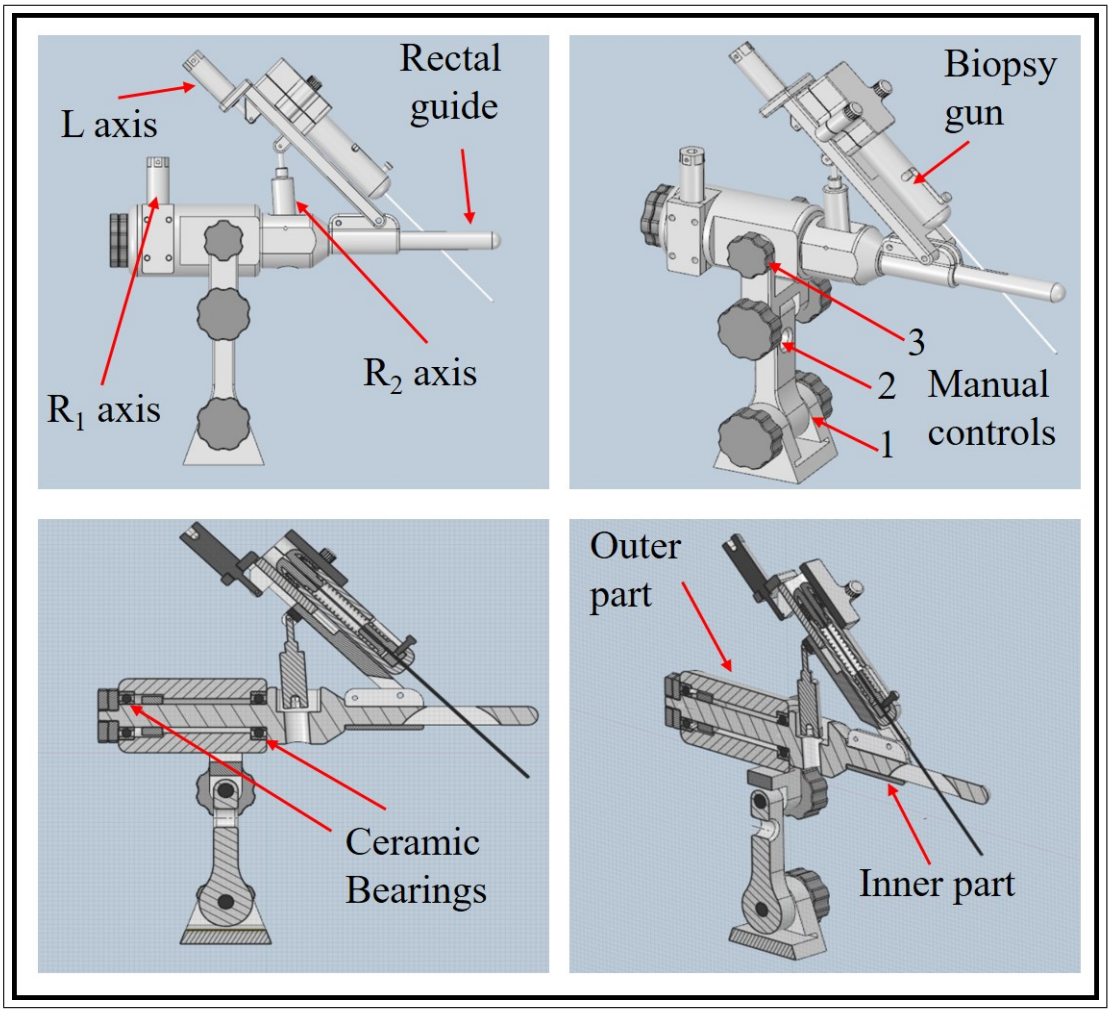

Figure 3.9 Design of the needle delivery unit and the biopsy gun

is possible to target the prostate with minimum manipulation of the system and potential infection risk is lower than other methods because the biopsy needle has minimum contact with the anal sphincter [11].

The kinematic diagram is shown in figure 3.10-a and the kinematics of the tele-operated 3 DOF can be derived as follows:

The rotation of the endorectal guide R_1 is established with the linear motion of the hydraulic cylinder. The angular rotation of the endorectal guide can be calculated from $R_1 = L_1/r_1$ where L_1 is the linear motion of the cylinder and r_1 is the radius of the gear. If we define xyz needle delivery unit coordinate system,

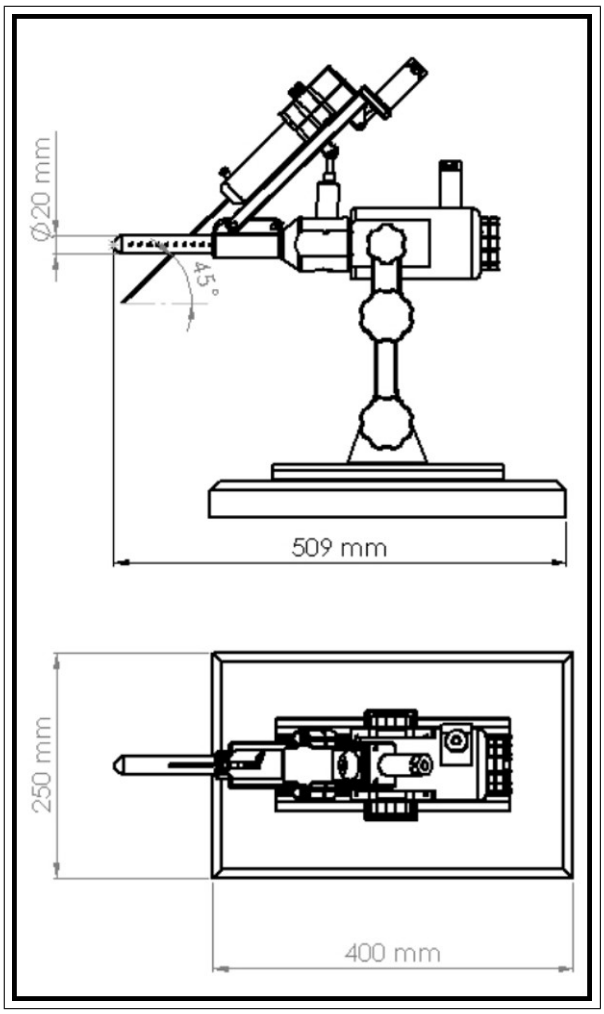

Figure 3.10 Dimensions of the needle delivery unit

the rotation R_1 causes rotation of the joint point M as shown in figure 3.10-b:

$$\begin{bmatrix} M'_x \\ M'_y \end{bmatrix} = \begin{bmatrix} cosR_1 & sinR_1 \\ -sinR_1 & cosR_1 \end{bmatrix} \begin{bmatrix} M_x \\ M_y \end{bmatrix} \tag{3.1}$$

$$Y' = \begin{bmatrix} sinR_1 \\ cosR_1 \\ 0 \end{bmatrix} \tag{3.2}$$

In y'z plane the biopsy needle is rotated by β in order to align with the target point. The direction of the needles becomes as shown in figure 3.10-c;

$$\vartheta = -\sin R_2 \cdot y' + \cos R_2 \cdot z \tag{3.3}$$

where $R_2 = \alpha + \beta$ and $\alpha = \arctan(h/d)$. L_3 is the insertion depth and L is the length of the biopsy needle. The position of the needle tip can be calculated from direct kinematics as follows:

$$\tau = M + (L + L_3) \cdot \vartheta \tag{3.4}$$

The inverse kinematics can be calculated as follows:

$$R_1 = \arctan(T_x/T_y) \tag{3.5}$$

The rotation of endorectal guide R_1 is obtained with the linear motion of the hydraulic cylinder. The linear motion of the 1st hydraulic cylinder can be calculated from $L_1 = R_1 \cdot r_1$ where L_1 is the linear motion of the cylinder and r_1 is the radius of the gear.

$$R_2 = \arctan(T_y - M'_y)/(T_z - M'_z) \tag{3.6}$$

$$L_2 = (\tan(R_2) \cdot d) - h \tag{3.7}$$

Where L_2 is the linear motion of the second hydraulic cylinder. Finally, the insertion depth of the needle can be calculated as:

$$L_3 = \sqrt{(T_y - M'_y)^2 + (T_z - M'_z)^2} - L \tag{3.8}$$

3.1.5 Actuator Design

One of the main challenge during a robotic system design for MRI applications is the choice of the actuator and the transmission system. The proper choice mainly depends on the purpose of the application, required power, required force, required output torque, MRI compatibility and speed. As discussed in section 1.3 there are 5 main types of actuators that are used in MRI applications; 1)Pneumatic Actuators 2)Hydraulic Actuators 3)Mechanical Actuators, 4)Electrical Actuators and 5)Electromagnetic Actuators. However, in recent literature

pneumatic and electrical actuators appear as the most preferred actuators in MRI applications.

In the proposed robotic system, a master-slave type actuator was preferred to be able to use MRI-Unsafe commercial components. Using such commercially available products reduced the complexity of the robotic system and also reduced the cost of materials. To ensure MRI compatibility MR-Unsafe materials were kept outside the MRI room and output torque of these actuators was transferred to the MRI room via a transmission line. Furthermore, the prostate biopsy procedure and the proposed kinematic design required fast response time and precise open-loop control to be able to work under real-time MRI guidance. Considering these design criteria master-slave type hydraulic actuation was preferred in this robotic system.

The hydraulic actuation was established by end to end connection of two hydraulic cylinders. The master units were actuated by conventional step motors (M542 CNC, Changzhou Fengyuan Micro Special Motor Co. Ltd, Changzhou, China) which were located outside of the MRI room. The rotational motion of the step motors were converted to linear motion with a custom made linear stage. The linear stage was connected to the slave hydraulic cylinder to transmit the torque of the master cylinder.

The hydraulic actuation using incompressible fluid enables transmission of power over long distances (in our design, it is up to 10m). Furthermore, hydraulic transmission offers a fast response and steady transmission [73]-[92] which makes it preferable to pneumatic transmission especially for MRI applications. Hydraulic transmission with standard cylinders brings the disadvantage of high friction and energy loss due to the tight O-ring sealing. For this reason, rolling diaphragm cylinders were preferred in this design as shown in figure 3.11. In a rolling diaphragm cylinder, a U-shaped rubber diaphragm is used for sealing which brings negligible internal friction at the expense of working with low pressure. However, the pressure range was shown to be sufficient for medical applications which also require haptic feedback [93].

In this design, the transmission lines were filled with oil and the line pressure

was monitored continuously with a mainstream pressure gauge. The initial pressure was set to 2 bar in order to prevent any mismatch due to the elasticity of the transmission lines [94]. It has been shown that with hydraulic transmission using rolling diaphragm cylinder mechanical power can be transferred through the passive hydrostatic transmission along the long hydraulic tubes. Besides, rolling diaphragm cylinders also offer fast response (rise time $<$ 40 ms), precise open-loop control of position (average error of 0.64Â°) and high output torque (0.49 NÂ·m) through 10-meter long hydraulic pipelines [95]. When compared to pneumatic actuators hydraulic actuation offered following advantages:

1. Using hydraulic actuators brings the advantage of master-slave actuation which has great potential for large torque actuation under MRI and offers quick response time [96] and simplifies the actuation and motion control.
2. Hydraulic actuation offers simple and low cost design compared to pneumatic actuators. Whereas, pneumatic actuators require more complex setup e.g. pressure controllers, compressors, brakes, position sensing setup etc. [8]-[60].
3. Hydraulic actuation offers sufficient motion and force tracking accuracy between master and the slave which eliminates the need for additional components and simplifies the design significantly [97].
4. Pneumatic actuation does not provide flexibility to position control setup at a large distance. However, hydrostatic control unit can be kept at a large distance [8]-[95].
5. Rolling diaphragm based hydraulic actuation offer accurate feedback of forces and motions between master and slave which enables possibility of haptic sensing for future studies [97].
6. The rolling diaphragm cylinders also helped to assemble a closed loop system without a need for expensive equipment to control and monitor the line pressure which is usually required for pneumatic systems.

3.1.6 Controller and User Interface

The control unit was kept outside the MRI room in order to use commercially available materials such as stepper motors. The rotation of the stepper motors was translated into linear motion by using custom-made linear stages. The Raspberry-Pi platform was used to create the user interface and run the motion control cards as shown in figure 3.12. The user interface allowed to adjust the hydraulic cylinder linear motions gradually or to a pre-set value which is translated from motor motion to linear stage. MRI images were processed in a manual navigation tool, phantom-robot registration was done with this tool and the needle-to-target trajectory was calculated.

3.2 Validation Through Phantom Experiments

The open-loop experimental workflow of the prostate biopsy procedure with the proposed prostate biopsy system is designed as follows:

1. The prostate phantom is placed on the MRI patient table
2. The needle delivery system is mounted on the MRI table
3. The endorectal guide is inserted into the prostate phantom by controlling the manual DOFs and then the endorectal guide position is locked. This is called the zero position which is case or patient specific.
4. The prostate phantom is scanned to acquire a 3D volumetric MRI image of the phantom.
5. MRI Images are imported to the navigation tool. A target point is defined within the prostate phantom using the MRI images. Robot-phantom registration is done using markers on the endorectal guide and defined target point. The position of the target point in the phantom is calculated using the needle delivery systemâs coordinate system. The trajectory from needle tip at home position to the target point is calculated using the design parameters and position of the target point.

6. L_1, L_2 and L_3 parameters are calculated by solving the inverse kinematic problem of the needle delivery system.
7. Operator triggers the R_1 and R_2 motion by manipulating the master unit using the Raspberry-Pi user interface.
8. The biopsy gun is placed inside its housing on the needle delivery unit by the operator. The needle is inserted manually by the operator in order to minimize the bending risks during insertion. While inserting the needle the biopsy gun was advanced through its housing. When the biopsy gun reaches its final position inside the housing it is locked to the needle delivery unit.
9. A 3D MRI image is acquired again for confirmation of trajectory
10. Operator triggers the L_3 motion (target insertion depth) by manipulating the master unit using the Raspberry-Pi user interface.
11. A 3D MRI image is acquired at the final position of the biopsy needle
12. The needle tip position is compared with the target position and targeting error is calculated.
13. If the error is acceptable ($<$ 3 mm) then the biopsy gun is fired manually to take the sample.
14. If the error is not acceptable ($>$ 3 mm) then the needle is removed and procedure repeated.

R_1 and R_2 motions are performed while the needle is not mounted to the needle delivery unit. It is important is not preferred in our design because of the patient safety concerns and to minimize the risk of deviation from planned trajectory during initial needle-tissue interaction. Therefore, initial insertion of the needle is performed manually. The final insertion depth is adjusted by tele-operation after solving the reverse kinematic problem. Therefore, the biopsy needle travels only in a linear trajectory after finalizing the endorectal guide orientation and then it is inserted into the phantom which minimizes the risk of deviation from the planned trajectory. The endorectal guide is used to register the phantom with the needle delivery unitâs coordinate system maximizing the registration accuracy. Step 11 in our experiment procedure allows us to calibrate any registration error.

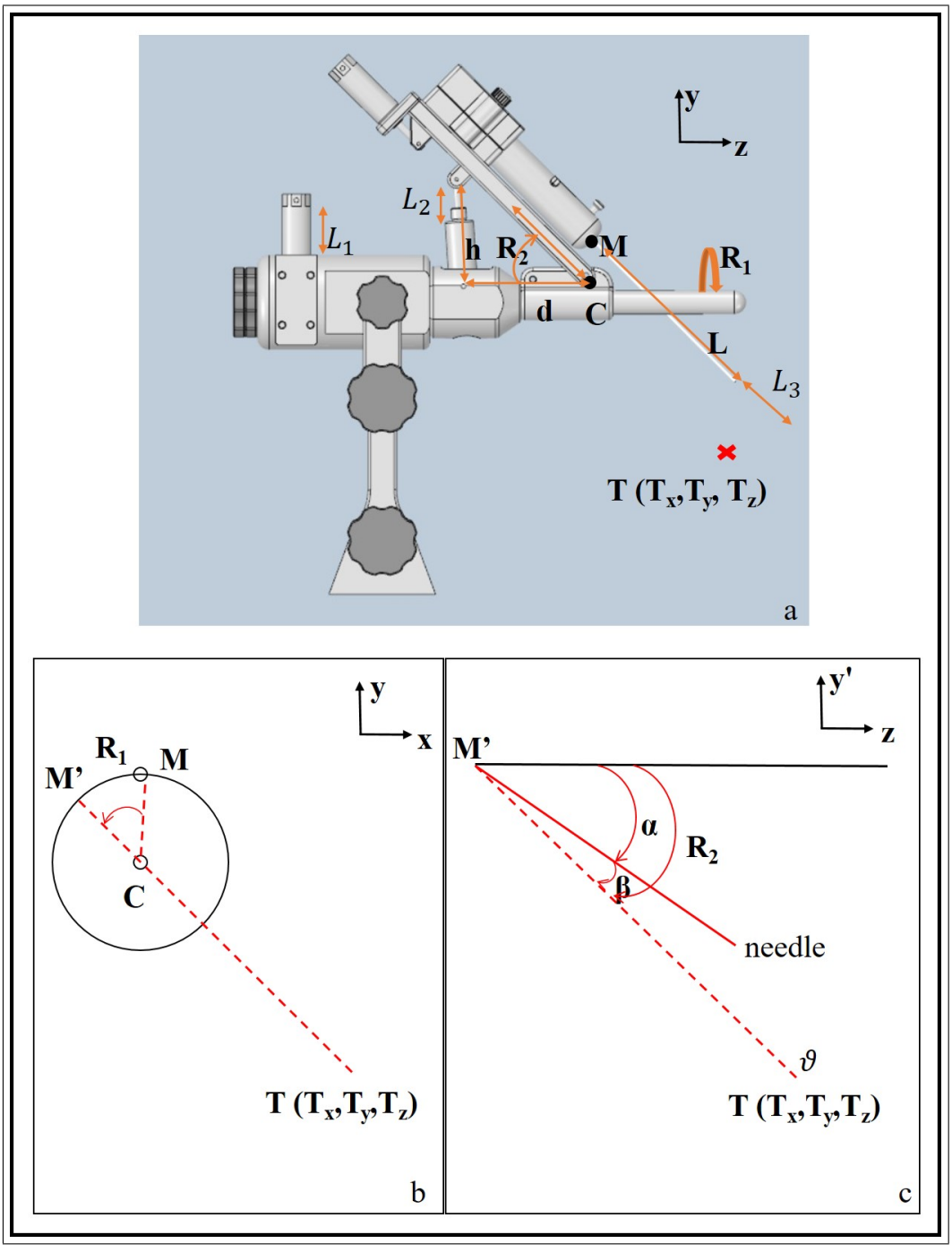

Figure 3.11 a) Kinematic parameters for the needle delivery unit b) Kinematic diagram for R1 rotation c) Kinematic diagram for R2 rotation

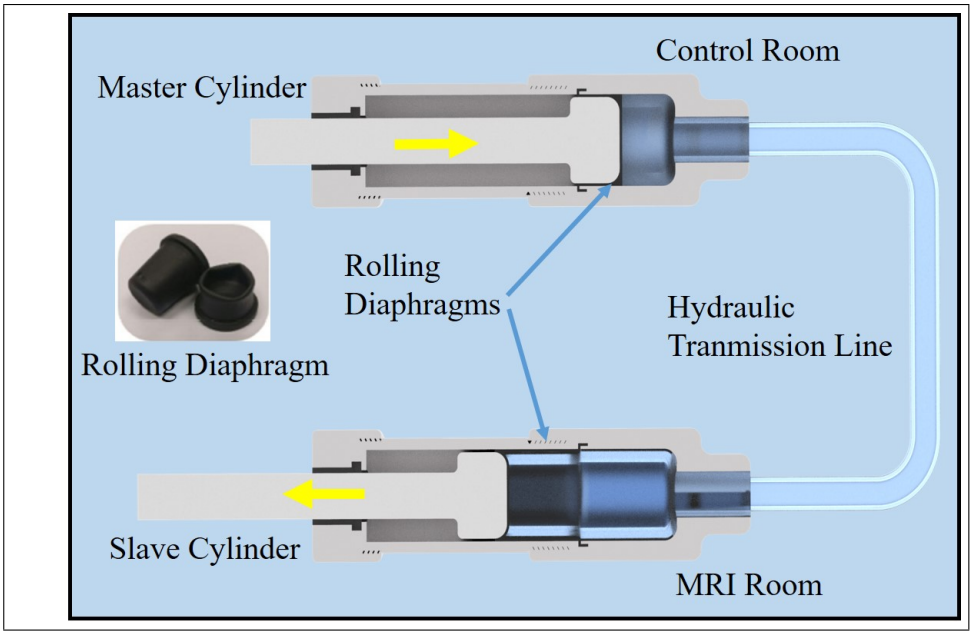

Figure 3.12 Hydraulic transmission with the rolling diaphragm cylinders

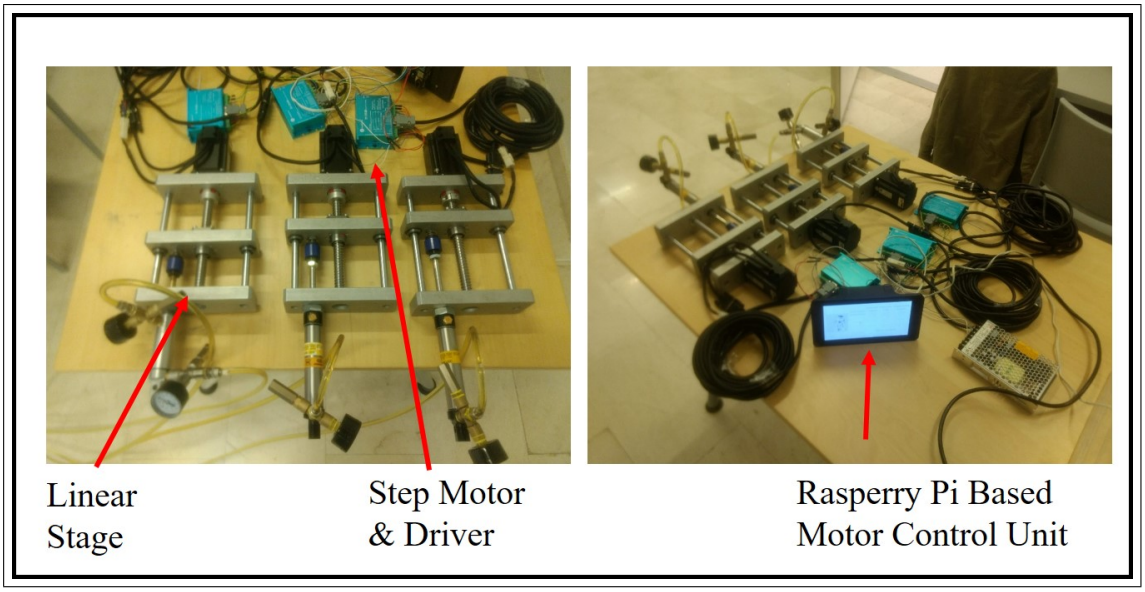

Figure 3.13 Linear stage, step motor and control unit

4. RESULTS

4.1 Improving Visibility of the Biopsy Needles

Biopsy needles were imaged under MRI (T2 weighted Turbo Echo sequence, TR: 4000 ms, TE: 102 ms) in order to assess the accuracy of distance measurement using Fe_2O_3 strips as shown in figure 4.1. It has been showed that passive tracking of the biopsy needles with Fe_2O_3 strips offered sufficient accuracy for the prostate biopsy procedure and the signal generated by the Fe_2O_3 strips does not distort the images of the surrounding medium.

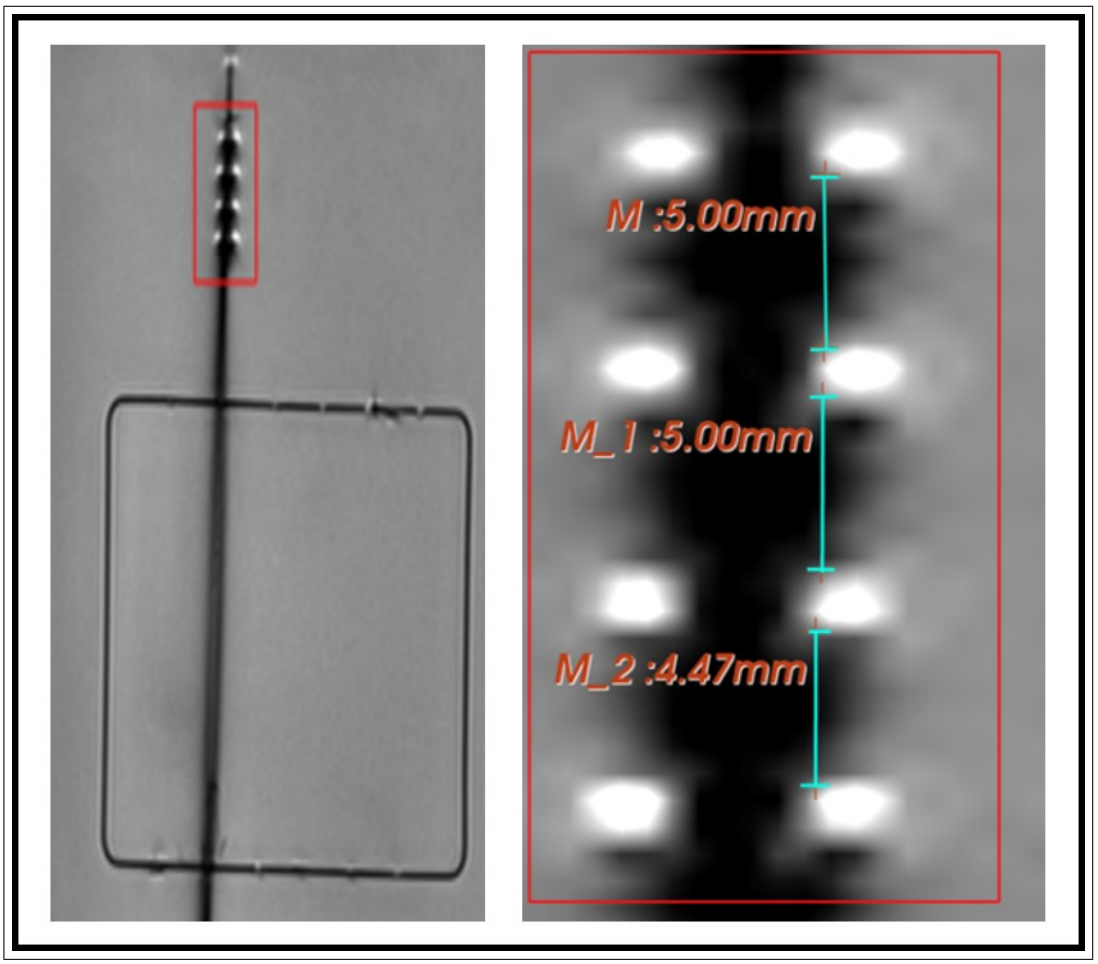

Figure 4.1 MRI image of the biopsy needle with Fe2O3 strips

4.2 Inverse Kinematics

In this section several target points were defined based on the design parameters, average size and location of the prostate. By using the inverse kinematics equations which were derived in section 3.1.4 the required manipulations R_1, R_2, L_1,L_2 and L_3 were calculated for each scenario as given in table 4.1. It has been shown that in each scenario the hydraulic cylinders remain within the dynamic motion range which are $\pm$ 1.75 cm for L_1,L_2 and L_3 and the system is able to trace the whole prostate volume.

4.3 In Vitro Experiments

In vitro MRI experiments were performed on a commercially available prostate phantom (070L, Computerized Imaging Reference Systems Inc., USA) to evaluate the performance of the proposed biopsy needle delivery design under 3T MRI System (Magnetom Trio, Siemens Medical Systems, Erlangen, Germany) as shown in figure 4.2. The prostate phantom includes a lesion inside the prostate in order to mimic the cancerous tissues (figure 4.2).

4.4 MRI Compatibility

Initially, MRI compatibility of the overall system was tested under 3T MRI. The prostate phantom was placed inside the 12 channels head coil (Siemens Medical Systems, Germany) and the needle delivery unit was placed on the MRI patient table. In phantom experiments 12 channels head coil was preferred instead of body or surface coils because the phantom was not able create strong MRI signal (figure 4.4). Moreover, lesions inside the prostate phantom were imaged with and without placing the needle delivery unit in position using T2 weighted Turbo Echo sequence (TR: 4000 ms, TE: 102 ms) and SNRs were compared.

In figure 4.3-a and figure 4.3-c the axial images of the prostate phantom were shown without the needle delivery system and with presence of the needle de-

Table 4.1
Inverse Kinematic Calculations for Different Target Points

Physical Constants (cm)	Coordinate X (cm)	Coordinate Y (cm)	Coordinate Z (cm)	Rotation (rad)	Linear Motion (cm)
d	T_x	T_y	T_z	R_1	L_1
5.65	-2	-3	6	0.588	1.176
h	M_x	M_y	M_z	R_2	L_2
4.85	0	2.2	0.35	0.707	-0.019
L	M'_x	M'_y	M'_z		L_3
7.55	1.22	1.83	0.35		-0.117
d	T_x	T_y	T_z	R_1	L_1
5.65	-2	-3	5	0.588	1.176
h	M_x	M_y	M_z	R_2	L_2
4.85	0	2.2	0.35	0.804	1.019
L	M'_x	M'_y	M'_z		L_3
7.55	1.22	1.83	0.35		-0.845
d	T_x	T_y	T_z	R_1	L_1
5.65	-2	-3	7	0.588	1.176
h	M_x	M_y	M_z	R_2	L_2
4.85	0	2.2	0.35	0.628	-0.746
L	M'_x	M'_y	M'_z		L_3
7.55	1.22	1.83	0.35		0.669
d	T_x	T_y	T_z	R_1	L_1
5.65	-2	-4	6	0.464	0.927
h	M_x	M_y	M_z	R_2	L_2
4.85	0	2.2	0.35	0.813	1.118
L	M'_x	M'_y	M'_z		L_3
7.55	0.98	1.97	0.35		0.668

Table 4.2
Inverse Kinematic Calculations for Different Target Points cont.

Physical Constants (cm)	Coordinate X (cm)	Coordinate Y (cm)	Coordinate Z (cm)	Rotation (rad)	Linear (cm)	Motion
d	T_x	T_y	T_z	R_1	L_1	
5.65	-2	-2	6	0.785	1.571	
h	M_x	M_y	M_z	R_2	L_2	
4.85	0	2.2	0.35	0.562	-1.294	
L	M'_x	M'_y	M'_z		L_3	
7.55	1.56	1.56	0.35		-0.874	
d	T_x	T_y	T_z	R_1	L_1	
5.65	-1	-3	6	0.322	0.644	
h	M_x	M_y	M_z	R_2	L_2	
4.85	0	2.2	0.35	0.733	0.237	
L	M'_x	M'_y	M'_z		L_3	
7.55	0.70	2.09	0.35		0.053	
d	T_x	T_y	T_z	R_1	L_1	
5.65	-3	-3	6	0.785	1.571	
h	M_x	M_y	M_z	R_2	L_2	
4.85	0	2.2	0.35	0.679	-0.294	
L	M'_x	M'_y	M'_z		L_3	
7.55	1.56	1.56	0.35		-0.292	
d	T_x	T_y	T_z	R_1	L_1	
5.65	3	-3	6	-0.785	-1.571	
h	M_x	M_y	M_z	R_2	L_2	
4.85	0	2.2	0.35	0.679	-0.294	
L	M'_x	M'_y	M'_z		L_3	
7.55	-1.56	1.56	0.35		-0.292	

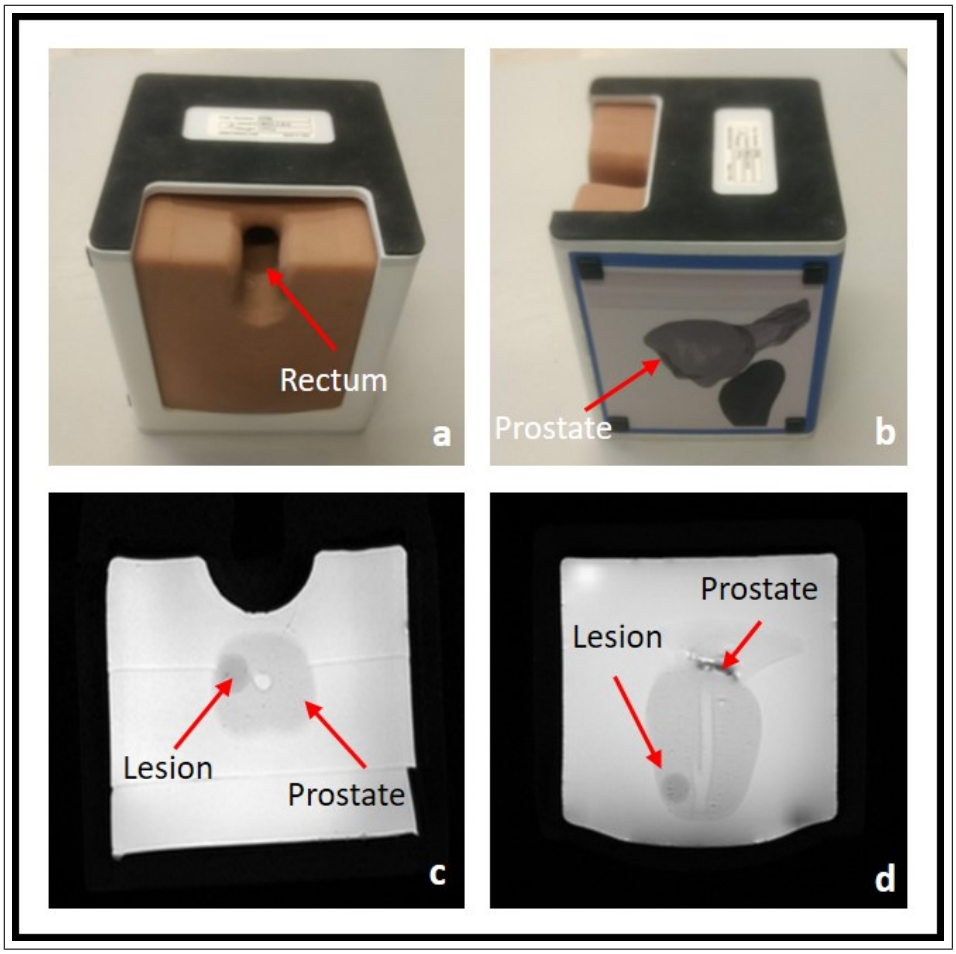

Figure 4.2 a,b) Prostate phantom c) T2 weighted MR image in axial plane d) T2 weighted MR image in coronal plane

livery system respectively. In figure 4.3-b and 4.3-d the coronal images of the prostate phantom were shown without the needle delivery system and with presence of the needle delivery system respectively. The SNR comparison between MRI images was performed using NEMA standard [98]. A region of interest including the prostate tissue was identified and signal was calculated as the average pixel values, noise was calculated as standard deviation of the difference between two images divided by â2. It has been shown that the SNR loss was negligible ($<3\%$) in the presence of the hydraulic needle delivery system compared to single phantom imaging. The only source of image degradation was the Fe_2O_3 strips that were intentionally placed on the needle to enhance the needle visibility under MRI.

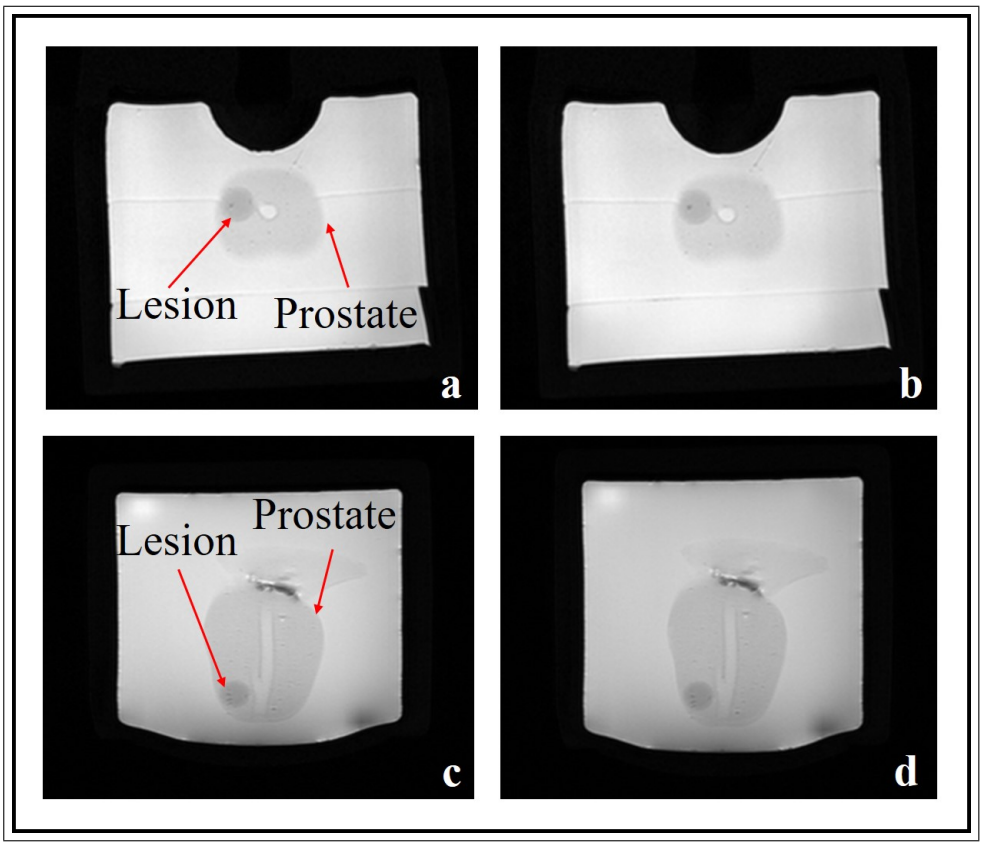

Figure 4.3 SNR comparison a) axial plane image without the needle delivery system b) axial plane image with the needle delivery system c) coronal plane image without the needle delivery system d) coronal plan image with the needle delivery system

4.5 Performing Prostate Biopsy Procedure Under MRI

The functionality of the needle delivery system was also tested under MRI. In order to obtain 3D images, a T2-weighted SPACE sequence (TR: 3000 ms, TE: 424 ms) was used to identify the lesions within the prostate phantom. Initially, using the 3D SPACE images, the target point on the lesion was identified and registered with the endorectal guide and with the needle delivery system's co-ordinate system. Using the design parameters and reverse kinematic equations required manipulations for hydraulic cylinders (L_1, L_2 and L_3) were calculated and translated into required step motor motions. The hydraulic cylinders (L_1, L_2) were actuated one-by-one and after this step the biopsy gun was placed into its housing. In this stage the biopsy needle was inserted to the phantom manually. After placing the biopsy gun in its final position inside the housing the position of

the biopsy gun was fixed. The housing of the biopsy gun was designed precisely such that positioning error for the biopsy gun was negligible. After insertion of the biopsy needle, a 3D MRI image of the phantom and the biopsy needle was acquired using the T2-weighted SPACE sequence (TR: 3000 ms, TE: 424 ms) and the planned trajectory was verified in the image planes. Finally, the biopsy needle was inserted by L_3 length to its final position with a constant speed of 2 mm/sec and the biopsy sample was acquired after the biopsy needle reached its target position by manually firing the biopsy gun. The total biopsy procedure time was measured as 40 ± 5 minutes in average after 7 experiments as shown in table 4.3. In total 7 experiments were performed because some distortions were observed inside the phantom due to the consecutive needle insertions and taking samples from the phantom.

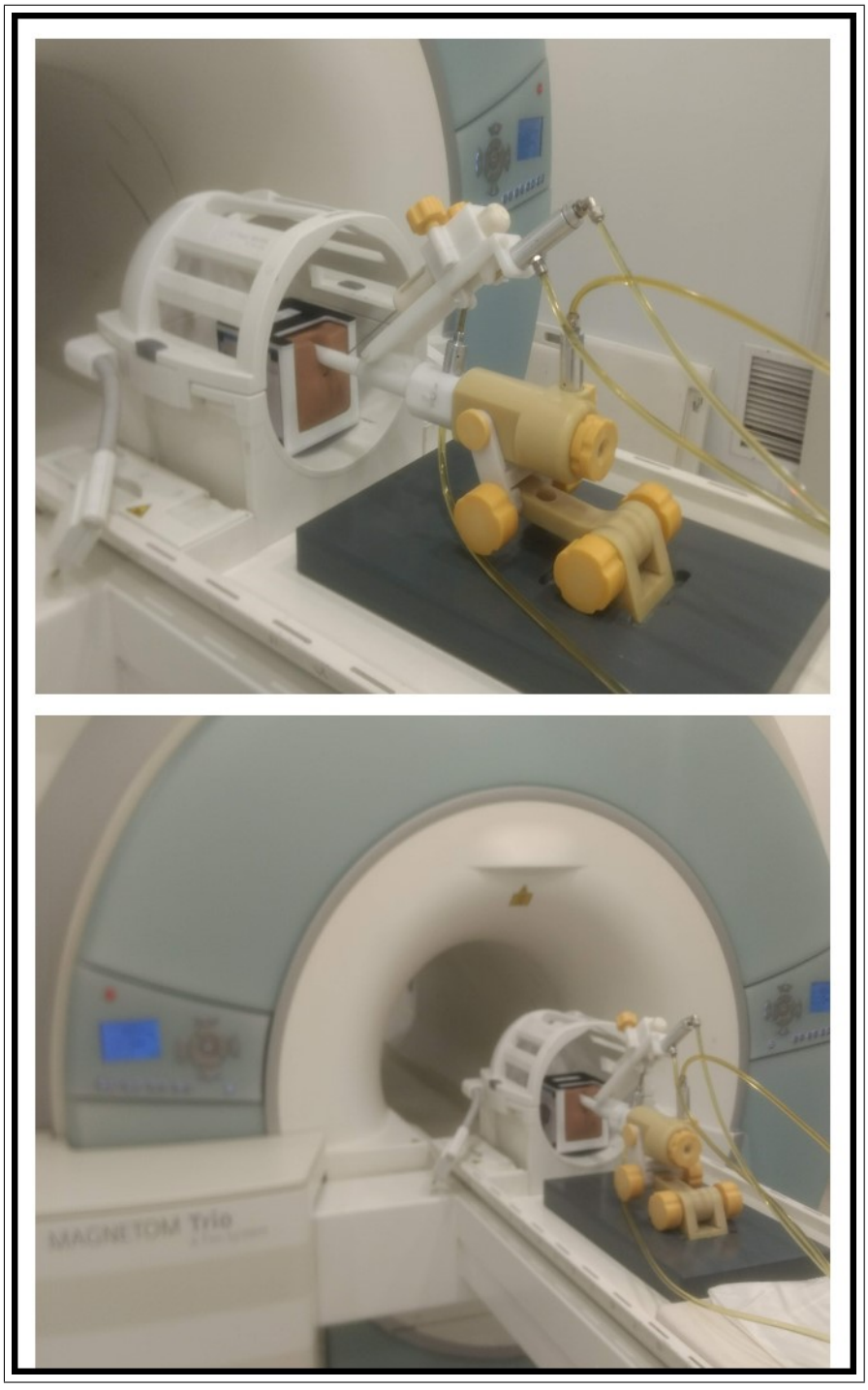

Figure 4.4 Experimental setup under 3T MRI

In figure 4.5.a, the MRI image of the phantom and the biopsy needle was shown after the needle delivery system was moved on the R_1 and R_2 axes, and the biopsy needle was inserted manually. In figure 4.5.b, the MRI image of the phantom and the biopsy needle was shown after the biopsy needle was inserted to its final po-

Table 4.3
Duration of MRI experiments.

Experiment Step	Time (min)
Preparation of Needle Delivery Unit and Phantom	10
MRI Scan for Localization and Registration	7
Exporting MRI Images for Calculations	3
Calculation of Inverse Kinematics	2
Adjustment of manual controls	2
Manuel insertion of the biopsy needle	2
MRI Scan to confirm the targeted trajectory	5
Firing the biopsy gun and obtain the biopsy sample	4
MRI Scan to calculate targeting error	5
Total	40

sition. In figure 4.5.c the MRI image of the phantom which is indicating the void inside the lesion was shown to verify the success of the biopsy operation.

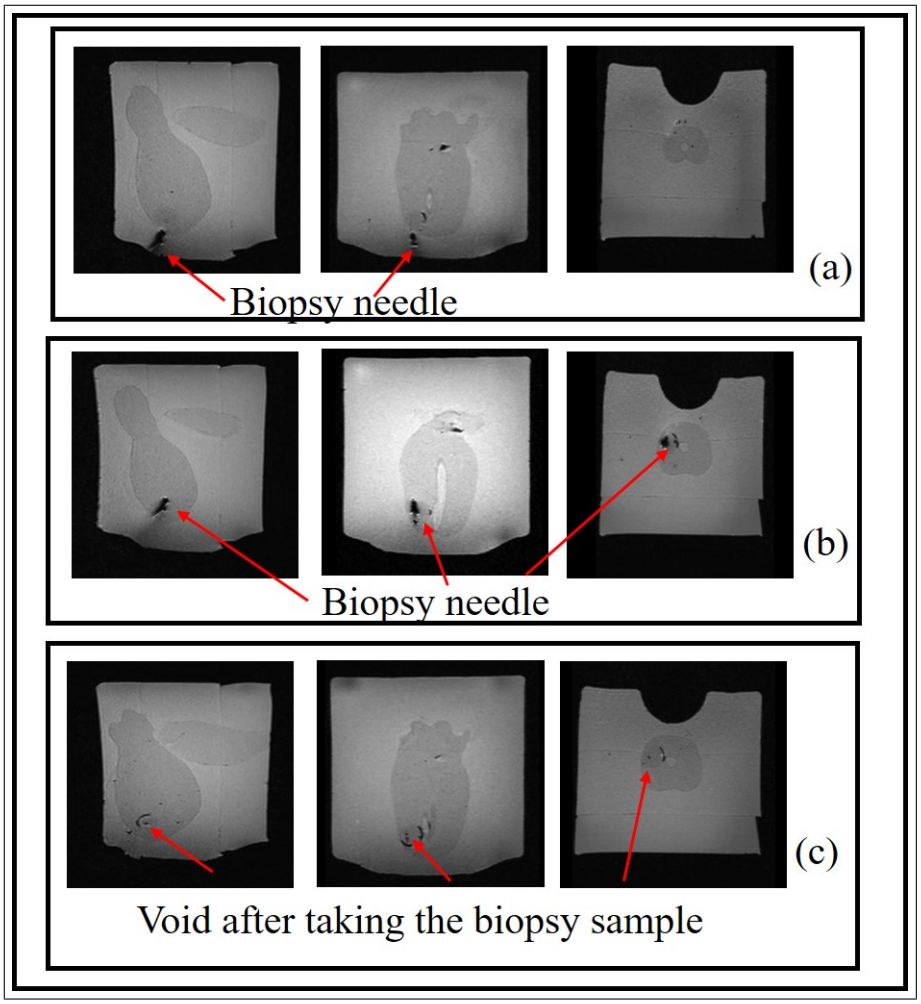

Figure 4.5 In vitro phantom MRI experiment - target localization a) Manual insertion of the biopsy needle after manipulations in R1 and R2 axes b) Tele-operated insertion of the biopsy needle by L3 length c) Image of the prostate phantom after removal of the biopsy needle and sample

Experiments showed that it was possible to reach the lesions and acquire biopsy samples with the needle delivery system. The accuracy of the needle delivery system was calculated as 2.05 $\pm$ 0.46 mm after seven phantom experiments as shown in table 4.4

Table 4.4
Targeting performance under MRI

Experiment	Error (mm)
1	2.32
2	1.84
3	2.21
4	1.53
5	2.45
6	2.67
7	1.34
Max	2.67
Average	2.05
StDev	0.46

5. DISCUSSION

In this thesis, a novel robotic system was proposed to perform prostate biopsy procedure under MRI guidance to cope with the challenges that exist in the current clinical practice. The robotic system was designed such that it is compliant with the human anatomy to ensure proper functionality and to ensure patient comfort and safety. In the design process, the number of required manual and remote controls and dimensions of the robot were selected carefully to be able to scan the whole prostate volume with minimal manipulation of the robot and also to avoid complexity. It was aimed to minimize complexity because working under MRI bring significant technical challenges and keeping the design as simple as possible would help to cope with these technical challenges. For instance, we achieved to obtain reasonable mix of manual and remote controls. With the manual controls the robot is brought to its zero-position and fixed to the patient. The needle is inserted manually by the operator which increased the safety of the procedure. The remote controls were used to manipulate the needle's position in order to reach the target point based on the acquired MRI images and calculations. Additionally, the overall system was fixed to the MRI table in order to prevent unintentional motions with respect to the patient. On the other hand, MRI room bring physical limitations such as working inside the narrow MRI bore and isolation requirements of the MRI room. Therefore, utilization of master-slave type of actuation and transmission of power through hydraulic lines eased to manage such limitations. One of the important metric of the design success was to minimize the distortion of the anatomical images during the biopsy procedure. In order to achieve this the materials that used for manufacturing the robot, actuators, biopsy gun and biopsy needle were selected very carefully. The hydraulic actuation allowed real time monitoring of the patient and manipulations of the remote controlled arms at the same time thanks to excellent MRI compatibility. The robotic system's mechanical components were manufactured with high quality standards and all the materials were processed with high finishing quality which maximized the targeting performance of the

system. After completion of the manufacturing process of the robotic components the robotic system was assembled and electronic components attached to the robotic system. The biopsy gun and biopsy needles were not chosen from commercially available products which brought flexibility during the design process. Initially, the biopsy needles were designed to obtain maximum efficiency in a single biopsy shot. Other important design criteria were to minimize unintended deflection of the biopsy needle and to enhance MRI visibility of the biopsy needle which were met in the final design. The customized biopsy gun was also eased the mounting of the biopsy needles inside the biopsy gun and mounting of the gun on the robotic system as well. Additionally, biopsy gun's shooting mechanism was produced from MRI-compatible materials which also improved the performance of the overall system. The robotic system's control was based on the hydraulic actuation which utilized rolling diaphragm cylinders [99]. The validation of the clinical work-flow and feasibility of the system was shown with in-vitro MRI experiments using a commercial prostate phantom which contained MRI visible lesions inside.

The system showed excellent MRI compatibility by offering a maximum 3% SNR degradation thanks to the selected MRI-compatible materials for the needle delivery unit, biopsy gun, biopsy needle and preferred hydraulic actuators. The main source of SNR degradation was observed as the Fe_2O_3 strips which were placed on the biopsy needles in order to enhance tracking the biopsy needles under MRI.

Hydraulic actuators, significantly improved the performance of the system when compared to other actuators. Using hydraulic actuators enabled to have a master-slave type actuation which simplified the design and operation significantly. Furthermore, utilization of the rolling diaphragm cylinders provided significant enhancement over the performance of the robotic system. Rolling diaphragm cylinders ensured torque tranmission over a long distance and supported the proposed clinical workflow which requires fast response time and precice open-loop control. In first set of experiments the hydrostatic lines were filled with oil. One of the important concern in hydraulic systems is the possible leakage in hydraulic cylinders or joint points. In our experiments, we did not encounter any leakage problem

thanks to the better sealing of rolling diaphragms compared to conventional O-ring sealings and single acting mechanism of the rolling diaphragm cylinders. However, in order to eliminate patient safety concerns distilled water can be used in clinical experiments instead of oil. Burkard et al. reported the feasibility of using water as a working fluid for rolling diaphragm based applications [97].

In our design, the equidistantly deposited Fe_2O_3 markers on the biopsy needle helped to correct the deviations from the planned trajectory after the needle is inserted to the phantom/patient and therefore provided better performance in terms of targeting accuracy compared to other studies in the literature. Besides, the markers on the tip of the endorectal guide helped to simplify the registration of the robot and the phantom with respect to the MRI scanner.

Although, there is no defined standard on the required targeting accuracy for a prostate biopsy, it was reported that maximum 3 mm targeting accuracy should be achieved [100]. Therefore, we believe our design showed sufficient accuracy by providing 2.05 $\pm$ 0.46 mm targeting accuracy. The main sources of error were identified as robot-phantom registration error and systematic errors (e.g. gear size, master-slave actuation etc.). In clinical trials there might be additional sources of errors like tissue deformation, patient movement etc. In order to minimize such errors encoders might be added to the needle delivery unit to monitor and adjust motions of remote-controlled arms. Moreover, robot-patient registration may be improved with replacing the markers on the endorectal guide and biopsy needle with active RF receive antennas as proposed by Yildirim et al. [5] in order to improve the visibility of the endorectal guide and minimize robot-patient registration errors.

The proposed system is promising in terms of overall procedure time (40$\pm$5 minutes) in phantom trials compared to the TRUS biopsy procedure time in clinics and other MRI-guided biopsy systems in the literature [26].

5.1 Future Work

The proposed study needs further improvement in order to ensure the adoption of the proposed prostate biopsy system for the clinical practice. Firstly, the visibility of the biopsy needles and the endorectal guide can be improved with an active tracking approach which has been showed as a promising method for real-time MRI applications by Yildirim et. al [5]. With this method, 3 dimensional RF antennas and electronic circuits can be printed on non-planar surfaces with a Computer Numerical Control (CNC) based conductive ink printing system. In this study, the conductive ink based surface printing technique was shown to be superior compared to the lithography based printing in terms of reproducibility, process time and simplicity of the process. Therefore, in our application active tracking elements can be printed onto the biopsy needles and endorectal guide to obtain better MRI visibility and better tracking accuracy under MRI. A possible improvement area for the proposed robotic prostate system is to develop a more comprehensive patient to robot registration tool which can calculate the required robot manipulations by looking at the MRI images of the patient, robot and biopsy needle. In this way, the calculation errors can be minimized and the procedure time can be shortened significantly. Also, such a tool may help to perform the procedure under real-time MRI by using fast MRI sequences and provide real-time feedback during the procedure.In order to enhance the accuracy of the proposed robotic prostate biopsy system and to ensure patient safety position encoders might be embedded to the robotic arms to provide real-time feedback during the procedure. In this way, the system can be automatized with a closed loop feedback and can be integrated with the patient to robot registration tool. The next step of this study will be to perform clinical trials with the proposed prostate biopsy system. Initially, the feasibility of the system can be validated with animal experiments. After completion of the suggested improvements the system can be tested with clinical trials and the feasibility of the system can be validated by human trials.

Similar hydraulic robotics systems were reported for different clinical applications with success. Kokes et al. showed the feasibility of an MRI-guided hydraulic nee-

dle driver system for the breast RF ablation procedure [101]. He et al. showed promising results with a MRI-guided hydraulic robot for percutaneous needle applications [102]. Guo et al. proposed a hydraulic driving robot for intra-operative MRI-guided bilateral stereotactic neurosurgery which showed sufficient stiffness during insertion and targeting accuracy [94]. Such clinical applications also show that there is a need for robust and reliable robotic tools for various MRI applications. Therefore, the proposed robotic prostate biopsy system can be modified and adapted for other interventional applications which require MRI guidance.

REFERENCES

1. Timms, B. G., "Prostate development: a historical perspective," *Differentiation*, Vol. 76, pp. 565–577, 2008.
2. Chinzei, K., N. Hata, F. Jolesz, and R. Kikinis, "Surgical assist robot for the active navigation in the intraoperative mri: Hardware design issues," *In Proc IEEE/ RSJ International Conference on Intelligent Robots and Systems (IROS)*, pp. 727–732, 2000.
3. Susil, R. C., K. Camphausen, P. Choyke, E. R. McVeigh, G. S. Gustafson, H. Ning, R. W. Miller, E. Atalar, C. N. Coleman, and C. M. . S. . 52(3):683â687, "System for prostate brachytherapy and biopsy in a standard 1.5 t mri scanner," *Magn Reson Med.*, Vol. 52, no. 3, pp. 683–687, 2004.
4. DiMaio, S. P., S. Pieper, K. Chinzei, N. Hata, S. J. Haker, D. F. Kacher, G. F. C. M. Tempany, and R. Kikinis, "Robot-assisted needle placement in open mri: System architecture, integration and validation," *Comput Aided Surg.*, Vol. 12, no. 1, pp. 15–24, 2007.
5. Yildirim, D. K., M. Sonmez, R. J. Lederman, and O. Kocaturk, "A novel active device fabrication method for interventional mri procedures," *CMBEBIH IFMBE Proceedings*, Vol. 62, pp. 978–981, 2017.
6. Yaras, Y. S., D. K. Yildirim, D. A. Herzka, T. Rogers, A. E. Campbell-Washburn, R. J. Lederman, F. L. Degertekin, and O. Kocaturk, "Real-time device tracking under mri using an acousto-optic active marker," *Magn Reson Med.*, Vol. 85, no. 5, pp. 2904–2914, 2021.
7. Krieger, A., I. I. Iordachita, P. Guion, A. K. Singh, A. Kaushal, C. Menard, P. A. Pinto, K. Camphausen, G. Fichtinger, and L. L. Whitcomb, "An mri-compatible robotic system with hybrid tracking for mri-guided prostate intervention. ieee transactions on bio-medical engineering," *IEEE transactions on bio-medical engineering*, Vol. 58, no. 11, pp. 3049–3060, 2011.
8. Fischer, G. S., I. Iordachita, C. Csoma, J. Tokuda, S. P. Dimaio, C. M. Tempany, N. Hata, and G. Fichtinger, "Mri-compatible pneumatic robot for transperineal prostate needle placement," *IEEE ASME Trans. Mechatron.*, Vol. 13, no. 3, pp. 295–305, 2008.
9. Seifabadi, R., S. E. Song, A. Krieger, N. B. Cho, J. Tokuda, G. Fichtinger, and I. Iordachita, "Robotic system for mri-guided prostate biopsy: feasibility of teleoperated needle insertion and ex vivo phantom study," *Int. J. Comput. Assist. Radiol. Surg.*, Vol. 7, no. 2, pp. 181–190, 2012.
10. Eslami, S., W. Shang, G. Li, N. Patel, G. S. Fischer, J. Tokuda, N. Hata, C. M. Tempany, and I. Iordachita, "In-bore prostate transperineal interventions with an mri-guided parallel manipulator: system development and preliminary evaluation," *Int. J. Med. Robot.*, Vol. 12, no. 2, pp. 199–213, 2016.
11. Stoianovici, D., C. Kim, G. Srimathveeravalli, P. Sebrecht, D. Petrisor, J. Coleman, S. B. Solomon, and H. Hricak, "Mri-safe robot for endorectal prostate biopsy," *IEEE ASME Trans Mechatron*, Vol. 19, no. 4, pp. 1289–1299, 2013.
12. Krieger, A., S. E. Song, N. B. Cho, I. Iordachita, P. Guion, G. Fichtinger, and L. L. Whitcomb, "Development and evaluation of an actuated mri-compatible robotic system for mri-guided prostate intervention," *IEEE ASME Trans. Mechatron.*, Vol. 18, no. 1, pp. 273–284, 2012.

13. Patel, N. A., G. Li, W. Shang, M. Wartenberg, T. Heffter, E. C. Burdette, I. Iordachita, J. Tokuda, N. Hata, C. M. Tempany, and G. S. Fischer, "System integration and preliminary clinical evaluation of a robotic system for mri-guided transperineal prostate biopsy," *Journal of medical robotics research*, Vol. 4, no. 2, 2019.

14. Dovat, L., R. Gassert, D. C. adn G Ganesh, E. Burdet, and H. Bleuler, "A haptic interface based on potential mechanical energy to investigate human motor control using fmri.," *IEEE Engineering in Medicine and Biology Society (EMBC)*, pp. 5021–5024, 2005.

15. Oura, M., Y. Kobayashi, J. Okamoto, and M. Fujie, "Development of mri compatible versatile manipulator for minimally invasive surgery," *In Proc First IEEE/ RAS-EMBS International Conference on Biomedical Robotics and Biomechatronics (BioRob)*, 2006.

16. Krieger, A., R. Susil, G. Fichtinger, E. Atalar, and L. Whitcomb, "Design of a novel mri compatible manipulator for image guided prostate intervention," *In Proc IEEE International Conference on Robotics and Automation (ICRA)*, pp. 377–382, 2004.

17. DiMaio, S., G. Fischer, S. Haker, N. Hata, I. Iordachita, and C. Tempany, "A system for mri-guided prostate interventions," *In Proc First IEEE/RAS-EMBS International Conference on Biomedical Robotics and Biomechatronics (BioRob)*, 2006.

18. Kim, D., E. Kobayashi, T. Dohi, and I. Sakuma, "A new, compact mr-compatible surgical manipulator for minimally invasive liver surgery.," *n Proc 5th International Conference on Medical Image Computing and Computer- Assisted Intervention (MICCAI)*, pp. 164–169, 2002.

19. Larson, B., A. Erdman, N. Tsekos, E. Yacoug, P. Tsekos, and I. Koutlas, "Design of an mri-compatible robotic stereotactic device for minimally invasive interventions in the breast.," *J Biomech Eng*, Vol. 126, no. 4, pp. 458–465, 2004.

20. Su, H., A. Camilo, G. A. Cole, N. Hata, C. M. Tempany, and G. S. Fischer, "High-field mri-compatible needle placement robot for prostate interventions," *Stud. Health Technol. Inform.*, Vol. 163, pp. 163–169, 2011.

21. Vogan, J., A. Wingert, J. Plante, S. Dubowsky, and M. Hafez, "Manipulation in mri devices using electrostrictive polymer actuators: With an application to reconfigurable imaging coils," *Proc IEEE International Conference on Robotics and Automation (ICRA)*, pp. 2498–2504, 2004.

22. Khanicheh, A., A. Muto, C. Triantafyllou, B. Weinberg, L. Astrakas, and A. Tzika, "Mr compatible erf driven hand rehabilitation device.," *Proc IEEE 9th International Conference on Rehabilitation Robotics (ICORR)*, pp. 7–12, 2005.

23. Wilson, M. W., A. B. Martin, P. Lillaney, A. D. Losey, E. J. Yee, A. Bernhardt, V. Malba, L. Evans, R. Sincic, and M. Saeed, "Magnetic catheter manipulation in the interventional mr imaging environment," *J. Vasc.Interv. Radiol.*, Vol. 24, pp. 885–891, 2013.

24. Settecase, F., M. S. Sussman, M. W. Wilson, S. Hetts, R. L. Arenson, V. Malba, A. F. Bernhardt, W. Kucharczyk, and . T P Roberts 2007, 34, "Magnetically-assisted remote control (marc) steering of endovascular catheters for interventional mri: a model for deflection and design implications," *Med. Phys.*, Vol. 34, pp. 3135–3142, 2007.

25. Sung, H., J. Ferlay, R. L. Siegel, M. Laversanne, I. Soerjomataram, A. Jemal, and F. Bray, "Global cancer statistics 2020: Globocan estimates of incidence and

mortality worldwide for 36 cancers in 185 countries," *CA. Cancer J. Clin*, Vol. 0, pp. 1–41, 2021.

26. Hoeks, C. M., M. G. Schoute, J. G. Bomers, S. P. Hoogendoorn, C. A. H. van de Kaa, T. Hambrock, H. Vergunst, J. P. Sedelaar, J. J. FÃ¼tterer, and J. O. Barentsz, "Three-tesla magnetic resonance-guided prostate biopsy in men with increased prostate-specific antigen and repeated, negative, random, systematic, transrectal ultrasound biopsies: detection of clinically significant prostate cancers," *Eur. Urol*, Vol. 62, no. 5, pp. 902–909, 2012.

27. Schroder, F. H., H. B. Carter, T. Wolters, R. C. van den Bergh, C. Gosselaar, C. H. Bangma, and M. J. Roobol, "Early detection of prostate cancer in 2007. part 1: Psa and psa kinetics," *Eur. Urol.*, Vol. 53, no. 2, pp. 468–477, 2008.

28. Schroder, F. H., P. van der Maas, P. Beemsterboer, A. B. Kruger, R. Hoedemaeker, J. Rietbergen, and R. Kranse, "Evaluation of the digital rectal examination as a screening test for prostate cancer. rotterdam section of the european randomized study of screening for prostate cancer," *J. Natl. Cancer. Inst.*, Vol. 90, no. 23, pp. 1817–1823, 98.

29. Takashi, H., and T. Ouchi, "The ultrasonic diagnosis in the field of urology," *Proc. Jpn. Soc. Ultrasonic Med.*, Vol. 3, no. 7, 1963.

30. Yeo, L., A. Papatsoris, C. Bach, D. Patel, I. Junaid, J. Masood, and N. Buchholz, "The development of the modern prostate biopsy," *INTECH Open Access Publisher*, 2011.

31. Trabulsi, E. J., D. Sackett, L. G. Gomella, and E. J. Halpern, "Enhanced transrectal ultrasound modalities in the diagnosis of prostate cancer," *Urology*, Vol. 76, no. 5, pp. 1023–1033, 2010.

32. Torre, L. A., F. Bray, R. L. Siegel, J. Ferlay, J. Lortet-Tieulent, and A. Jemal, "Global cancer statistics, 2012," *CA Cancer J. Clin.*, Vol. 65, no. 2, pp. 87–108, 2012.

33. Rabbani, F., N. Stroumbakis, B. R. Kava, M. S. Cookson, and W. R. Fair, "Incidence and clinical significance of false-negative sextant prostate biopsies," *J. Urol.*, Vol. 159, no. 4, pp. 1247–1250, 1998.

34. Terris, M. K., "Sensitivity and specificity of sextant biopsies in the detection of prostate cancer: preliminary report," *Urology.*, Vol. 54, pp. 486–489, 1999.

35. Siddiqui, M. M., S. Rais-Bahrami, H. Truong, L. Stamatakis, S. Vourganti, J. Nix, A. N. Hoang, A. Walton-Diaz, B. Shuch, M. Weintraub, J. Kruecker, H. Amalou, B. Turkbey, M. J. Merino, P. L. Choyke, B. J. Wood, and P. A. Pinto, "Magnetic resonance imaging / ultrasound-fusion biopsy significantly upgrades prostate cancer versus systematic 12-core transrectal ultrasound biopsy," *Eur. Urol.*, Vol. 64, no. 5, pp. 713–719, 2013.

36. Barentsz, J. O., J. Richenberg, R. Clements, P. Choyke, S. Verma, G. Villeirs, O. Rouviere, V. Logager, and J. J. FÃ¼tterer, "Esur prostate mr guidelines 2012," *Eur. Radiol.*, Vol. 22, no. 4, pp. 746–757, 2012.

37. Haas, G. P., and W. A. Sakr, "Epidemiology of prostate cancer," *CA: a cancer journal for clinicians*, Vol. 47, no. 5, pp. 273–287, 1997.

38. Turkbey, B., M. J. Merino, E. C. Gallardo, V. Shah, O. Aras, M. Bernardo, E. Mena, D. Daar, A. R. Rastinehad, and W. M. Linehan, "Comparison of endorectal coil and nonendorectal coil t2w and diffusion-weighted mri at 3 tesla for

localizing prostate cancer: Correlation with whole-mount histopathology," *Journal of Magnetic Resonance Imaging*, Vol. 39, no. 6, pp. 1443–1448, 2014.

39. Miao, H., H. Fukatsu, and T. Ishigaki, "Prostate cancer detection with 3-t mri: comparison of diffusion-weighted and t2-weighted imaging," *European journal of radiology*, Vol. 61, no. 2, pp. 297–302, 2007.

40. Basser, P. J., J. Mattiello, and D. LeBihan, "Estimation of the effective self-diffusion tensor from the nmr spin echo," *ournal of Magnetic Resonance*, Vol. 103, no. 3, pp. 247–254, 1994.

41. Pierpaoli, C., and P. J. Basser, "Toward a quantitative assessment of diffusion anisotropy," *Magnetic resonance in Medicine*, Vol. 36, 893–906 1996.

42. Hosseinzadeh, K., and S. D. Schwarz, "Endorectal diffusion-weighted imaging in prostate cancer to differentiate malignant and benign peripheral zone tissue," *Journal of Magnetic Resonance Imaging*, Vol. 20, no. 4, pp. 654–661, 2004.

43. Hansford, B. G., Y. Peng, Y. Jiang, M. W. Vannier, T. Antic, S. Thomas, S. McCann, and A. Oto, "Dynamic contrast-enhanced mr imaging curve-type analysis: is it helpful in the differentiation of prostate cancer from healthy peripheral zone?," *Radiology*, Vol. 275, no. 2, pp. 448–457, 2015.

44. Ratnayaka, K., A. Z. Faranesh, M. S. Hansen, A. M. Stine, M. Halabi, I. M. Barbash, V. H. Schenke, V. J. Wright, L. P. Grant, P. Kellman, O. Kocaturk, and R. J. Lederman, "Real-time mri-guided right heart catheterization in adults using passive catheters," *Eur. Heart. J.*, Vol. 34, no. 5, pp. 380–389, 2013.

45. Razavi, R., D. L. Hill, S. F. Keevil, M. E. Miquel, V. Muthurangu, S. Hegde, K. Rhode, M. Barnett, J. van Vaals, D. J. Hawkes, and E. Baker, "Cardiac catheterisation guided by mri in children and adults with congenital heart disease," *Lancet*, Vol. 362, no. 9399, pp. 1877–1882, 2003.

46. Choi, H. Y., S. M. Kim, M. Jang, B. L. Yun, S. W. Kim, E. Kang, S. Y. Park, W. K. Moon, and E. S. Ko, "Mri-guided intervention for breast lesions using the freehand technique in a 3.0-t closed-bore mri scanner: feasibility and initial results," *Korean J. Radiol.*, Vol. 14, no. 2, pp. 171–178, 2013.

47. Nitz, W. R., A. Oppelt, W. Renz, C. Manke, M. Lenhart, and J. L. . 2001;13:105-114, "On the heating of linear conductive structures as guide wires and catheters in interventional mri," *J Magn Reson Imaging*, Vol. 13, pp. 105–114, 2001.

48. Zamecnik, P., M. G. Schouten, A. J. Krafft, F. Maier, H. P. Schlemmer, J. O. Barentsz, M. Bock, and J. J. FÃ¼tterer, "Automated real-time needle-guide tracking for fast 3-t mr-guided transrectal prostate biopsy: a feasibility study," *Radiology*, Vol. 273, no. 3, pp. 879–886, 2014.

49. Chinzei, K., N. Hata, F. A. Jolesz, and R. Kikinis, "Mri compatible surgical assist robot: System integration and preliminary feasibility study," *Proc. Med. Image Comput. Comput.-Assisted Intervention Conf*, pp. 921–930, 2000.

50. Kaiser, W. A., H. Fischer, J. Vagner, and M. Selig, "Robotic system for biopsy and therapy of breast lesions in a high-field whole-body magnetic resonance tomography unit," *Invest Radiol*, Vol. 35, no. 8, pp. 513–519, 2000.

51. Felden, A., J. Vagner, A. Hinz, H. Fischer, S. Pfleiderer, J. Reichenbach, and W. Kaiser, "Robitom-robot for biopsy and therapy of the mamma," *Biomed Technik, Biomed Eng (Berlin)*, Vol. 47, no. 1, pp. 2–5, 2002.

52. Menard, C., R. C. Susil, P. Choyke, J. Coleman, R. Grubb, A. Gharib, A. Krieger, P. Guion, D. Thomasson, K. Ullman, S. Gupta, V. Espina, L. Liotta, E. Petricoin, G. Fitchtinger, L. L. Whitcomb, E. Atalar, C. N. Coleman, and K. Camphausen, "An interventional magnetic resonance imaging technique for the molecular characterization of intraprostatic dynamic contrast enhancement," *Mol Imaging*, Vol. 4, no. 1, pp. 63–66, 2005.

53. Beyersdorff, D., A. Winkel, B. Hamm, S. Lenk, S. A. Loening, and M. Taupitz, "Mr imaging-guided prostate biopsy with a closed mr unit at 1.5 t: Initial results," *Radiology*, Vol. 234, no. 2, pp. 576–581, 2005.

54. Hushek, S., B. Fetics, and R. Moser, "Initial clinical experience with a passive electromagnetic 3d locator system," *5th Int. MRI Symp. Boston*, 2004.

55. Dumoulin, C. L., S. P. Souza, and R. D. D. R. . M. . 29(3):411â415., "Real-time position monitoring of invasive devices using magnetic resonance," *Magn Reson Med*, Vol. 29, no. 3, pp. 411–415, 1993.

56. Monfaredi, R., K. Cleary, and K. Sharma, "Mri robots for needle-based interventions: Systems and technology," *Ann. Biomed. Eng*, Vol. 46, no. 10, pp. 1479–1497, 2018.

57. Elhawary, H., Z. T. Tse, M. Rea, A. Zivanovic, B. L. Davies, C. Besant, N. M. de Souza, D. McRobbie, I. Young, and M. U. LampÃ©rth, "Robotic system for transrectal biopsy of the prostate: real-time guidance under mri," *IEEE Eng. Med. Biol. Mag.*, Vol. 29, no. 2, pp. 78–86, 2010.

58. Song, S. E., J. Tokuda, K. Tuncali, C. M. Tempany, E. Zhang, and N. Hata, "Development and preliminary evaluation of a motorized needle guide template for mri-guided targeted prostate biopsy," *IEEE Trans. Biomed. Eng.*, Vol. 60, no. 11, pp. 3019–3027, 2013.

59. van den Bosch, M. R., M. R. Moman, M. van Vulpen, J. J. Battermann, E. Duiveman, L. J. van Schelven, H. de Leeuw, J. J. Lagendijk, and M. A. Moerland, "Mri-guided robotic system for transperineal prostate interventions: proof of principle," *Phys. Med. Biol.*, Vol. 55, no. 5, pp. 133–140, 2010.

60. Yakar, D., M. G. Schouten, D. G. Bosboom, J. O. Barentsz, T. W. Scheenen, and J. J. FÃ¼tterer, "Feasibility of a pneumatically actuated mr-compatible robot for transrectal prostate biopsy guidance," *Radiology*, Vol. 260, no. 1, pp. 241–247, 2011.

61. Chinzei, K., R. Kikinis, and A. Jolesz, "Mr compatibility of mechatronic devices: Design criteria.," *Proc Second International Conference on Medical Image Computing and Computer-assisted Interventions (MICCAI)*, pp. 1020–1030, 1999.

62. Hartwig, V., N. Vanello, R. Gassert, D. Chapuis, M. Santarelli, and V. Positano, "A compatibility test for tactile displays designed for fmri studies," *In Proc Euro-Haptics*, pp. 456–458, 2004.

63. Schenck, J., "he role of magnetic susceptibility in magnetic resonance imaging: Mri magnetic compatibility of the first and second kinds," *T. Med Phys*, Vol. 23, no. 6, pp. 815–850, 1996.

64. Koseki, Y., N. Koyachi, T. Arai, and K. Chinzei, "Remote actuation mechanism for mr-compatible manipulator using leverage and parallelogram," *In Proc IEEE International Conference on Robotics and Automation (ICRA)*, pp. 652–657, 2003.

65. Golaszewski, S., C. Siedentopf, E. Baldauf, F. Koppelstaetter, W. Eisner, and J. Unterrainer, "Functional magnetic resonance imaging of the human sensorimotor cortex using a novel vibrotactile stimulator," *Neuroimage*, Vol. 17, pp. 421–430, 2002.

66. Bishop, J., G. Poole, M. Leitch, and D. Plewes, "Magnetic resonance imaging of shear wave propagation in excised tissue," *J Magn Reson Imaging*, Vol. 8, pp. 1257–1265, 1998.

67. Stippich, C., P. Freitag, J. Kassubek, K. Soros, P. Kamada, H. Kober, and K. Scheffler, "Motor, somatosensory and auditory cortex localization by fmri and meg.," *Neuroreport*, Vol. 9, no. 9, pp. 1953–1957, 1998.

68. Golaszewski, S., F. Zschiegner, C. Siedentopf, J. Unterrainer, R. Sweeney, and W. Eisner, "A new pneumatic vibrator for functional magnetic resonance imaging of the human sensorimotor cortex," *J Neurosci Lett*, Vol. 324, no. 2, pp. 125–128, 2002.

69. Zappe, A., T. Maucher, K. Meier, and C. Scheiber, "valuation of a pneumatically driven tactile stimulator device for vision substitution during fmri studies," *Magn Reson Med*, Vol. 51, no. 4, pp. 828–834, 2004.

70. Diedrichsen, J., Y. Hashambhoy, T. Rane, and R. Shadmehr, "Neural correlates of reach errors," *J Neurosci*, Vol. 25, no. 43, pp. 9919–9931, 2005.

71. Bosgiraud, T., J. Thiran, H. Bleuler, and Y. Popowski, "An mr compatible delta arm for brachytherapy applied to prostate cancer treatment," *In Bioengineering Day Conference of the EPFL Biomedical Engineering Society*, 2005.

72. Stoianovici, D., "Multi-imager compatible actuation principles in surgical robotics," *Int J Medical Robotics and Computer Assisted Surgery*, Vol. 1, no. 2, pp. 86–100, 2005.

73. Ganesh, G., R. Gassert, E. Burdet, and H. Bleuler, "Dynamics and control of an mri compatible master-slave system with hydrostatic transmission," *Proc. IEEE Int. Conf. Robot. Autom.*, Vol. 2, pp. 1288–1294, 2004.

74. Hogan, A., "Mri compatible wrist robot," *Available at: http://web.mit.edu/hogan/www/Projects/MRI$_W$rist$_R$obot.htm.*

75. Masamune, K., E. K. adn Y Masutani, M. Suzuki, T. Dohi, and H. Iseki, "Development of an mricompatible needle insertion manipulator for stereotactic neurosurgery," *J Image Guid Surg*, Vol. 1, no. 4, pp. 242–248, 1995.

76. Tajima, F., K. Kishi, K. Nishizawa, K. Kan, H. Ishii, and K. Sudo, "A prototype master-slave system consisting of two mr-compatible manipulators with interchangeable surgical tools," *In Proc IEEE International Conference on Robotics and Automation (ICRA)*, pp. 2505–2510, 2004.

77. Uffmann, K., C. Abicht, W. Grote, H. Quick, and M. Ladd, "Design of an mr-compatible piezoelectric actuator for mr elastography," *Concepts Magn Reson*, Vol. 15, pp. 239–254, 2002.

78. Harada, K., K. Tsubouchi, M. Fujie, and T. Chiba, "Micro manipulators for intrauterine fetal surgery in an open mri," *In Proc IEEE International Conference on Robotics and Automation (ICRA)*, pp. 504–509, 2005.

79. Hata, N., R. Hashimoto, and J. Tokuda, "Needle guiding robot for mr-guided microwave thermotherapy of liver tumor using motorized remote-center-of-motion constraint," *In Proc IEEE International Conference on Robotics and Automation (ICRA)*, pp. 1664–1668, 2005.

80. Harrington, G., C. Wright, and J. Downs, "A new vibrotactile stimulator for functional mri," *Hum Brain Mapp*, Vol. 10, no. 3, pp. 140–145, 2000.

81. Gassert, R., N. Vanello, D. Chapuis, H. Hartwig, E. Scilingo, and A. Bicchi, "Active mechatronic interface for haptic perception studies with functional magnetic resonance imaging: Compatibility and design criteria," *In Proc IEEE International Conference on Robotics and Automation (ICRA)*, pp. 3832–3837, 2006.

82. Yamamoto, A., K. Ichiyanagi, T. Higuchi, H. Imamizu, R. Gassert, and M. I. . . I. p 3658â3663., "Evaluation of mr compatibility of electrostatic linear motor," *In Proc IEEE International Conference on Robotics and Automation (ICRA)*, pp. 3658–3663, 2005.

83. Niino, T., S. Egawa, and T. Higuchi, "Dual excitation multiphase electrostatic drive," *In Proc IEEE Industry Applications Society Annual Meeting (IAS)*, pp. 1318–1325, 1995.

84. Mazzone, A., R. Zhang, A. Kunz, G. Kovacs, and S. Michel, "Novel actuators for haptic displays based on electroactive polymers," *n Proc ACM Symposium on Virtual Reality Software and Technology.*, pp. 196–204, 2003.

85. Malone, E., "Freeform fabrication of electroactive polymer actuators and electromechanical devices," *Proc 15th Solid Freeform Fabrication Symposium*, pp. 697–708, 2004.

86. Choi, H., K. Jung, J. Kwak, S. Lee, H. Kim, and J. Jeon, "Digital polymer motor for robotic applications," *In Proc IEEE International Conference on Robotics and Automation (ICRA)*, pp. 1857–1862, 2003.

87. Nakano, M., A. Mazzone, F. Piffaretti, R. Gassert, M. Nakao, and v. . p. . H Bleuler 2005. ., "Ipmc actuator array as 3-d haptic display," *In Proc SPIE, Smart Structures and Materials: Electroactive Polymer Actuators and Devices (EAPAD)*, Vol. 5759, pp. 339–347, 2005.

88. Graham, S., W. Staines, A. Nelson, D. Plewes, and W. McIlroy, "New devices to deliver somatosensory stimuli during functional mri," *Magn Reson Me*, Vol. 46, pp. 436–442, 2001.

89. Roberts, T., W. Hassenzahl, and R. A. . . . 1095., "Remote control of catheter tip deflection: an opportunity for interventional mri," *J Magn Reson Med*, Vol. 48, no. 6, pp. 1091–1095, 2002.

90. Riener, R., T. Villgrattner, R. Kleiser, T. Nef, and S. Kollias, "fmri-compatible electromagnetic haptic interface," *roc 27th Annual International Conference of the IEEE Engineering in Medicine and Biology Society (EMBC)*, 2005.

91. Rossnagel, S. M., "Thin film deposition with physical vapor deposition and related technologies," *Journal of Vacuum Science Technology A*, Vol. 21, pp. S74–S87, 2003.

92. Lindenroth, L., J. Back, A. Schoisengeier, Y. Noh, H. Wurdemann, K. Althoefer, and H. Liu, "Stiffness-based modelling of a hydraulically actuated soft robotics manipulator," *Proc. IEEE/RSJ Int. Conf. Intell. Robots Syst.*, pp. 2458–2463, 2016.

93. Whitney, J. P., T. Chen, J. Mars, and J. K. Hodgins, "A hybrid hydrostatic transmission and human-safe haptic telepresence robot," *Proc. IEEE Int. Conf. Robot. Autom.*, pp. 690–695, 2016.

94. Guo, Z., Z. Dong, K. H. Lee, C. L. Cheung, H. C. Fu, J. D. L. Ho, H. He, W. S. Poon, D. T. M. Chan, and K. W. Kwok, "Compact design of a hydraulic driving robot for intra- operative mri-guided bilateral stereotactic neurosurgery," *IEEE Robot. Autom. Lett.*, Vol. 3, pp. 2515–2522, 2018.

95. Dong, Z., Z. Guo, K. H. Lee, G. Fang, W. L. Tang, H. C. Chang, D. T. M. Chan, and K. W. Kwok, "High-performance continuous hydraulic motor for mr safe robotic teleoperation," *IEEE Robotics and Automation Letters*, Vol. 4, pp. 1964–1971, 2019.

96. Xiao, Q., R. Monfaredi, M. Musa, K. Cleary, and Y. Chen, "Mr-conditional actuations: A review," *Ann Biomed Eng.*, Vol. 48, no. 12, pp. 2707–2733, 2020.

97. Burkhard, N., S. Frishman, A. Gruebele, J. P. Whitney, R. Goldman, B. Daniel, and M. Cutkosky, "A rolling-diaphragm hydrostatic transmission for remote mr-guided needle insertion," *IEEE International Conference on Robotics and Automation (ICRA)*, pp. 1148–1153, 2017.

98. NEMA, "Determination of signal-to-noise ratio (snr) in diagnostic magnetic resonance imaging," *NEMA Standards Pub., MS 1, N. E. M. Association.*, 2008.

99. Mahcicek, D. I., D. K. Yildirim, G. Kasaci, and O. Kocaturk, "Phantom study of novel biopsy needle and assisted robotic system designed for prostate biopsy procedure under mri," *The International Society for Magnetic Resonance in Medicine (ISMRM) 27th Annual Meeting and Exhibition*, 2019.

100. derKwasta, T. H. V., T. Wolters, A. Evans, and M. Robobol, "Single prostatic cancer foci on prostate biopsy," *Eur. Urol. Suppl.*, Vol. 7, no. 8, pp. 549–556, 2008.

101. Kokes, R., K. Lister, R. Gullapalli, B. Zhang, A. MacMillan, H. Richard, and J. P. Desai, "Towards a teleoperated needle driver robot with haptic feedback for rfa of breast tumors under continuous mri," *Medical image analysis*, Vol. 13, no. 3, pp. 445–455, 2009.

102. He, Z., Z. Dong, G. Fang, J. D. Ho, C. Cheung, H. Chang, C. C. Chong, J. Y. Chan, D. T. M. Chan, and K. Kwok, "Design of a percutaneous mri-guided needle robot with soft fluid-driven actuator," *IEEE Robotics and Automation Letters*, Vol. 5, no. 2, pp. 2100–2107, 2020.